HEAT TRANSFER EXPERIMENTS ON A PULSE DETONATION DRIVEN COMBUSTOR

THESIS

Nicholas C. Longo, Captain, USAF

AFIT/GAE/ENY/11-M18

DEPARTMENT OF THE AIR FORCE
AIR UNIVERSITY

AIR FORCE INSTITUTE OF TECHNOLOGY

Wright-Patterson Air Force Base, Ohio

AFIT/GAE/ENY/11-M18

HEAT TRANSFER EXPERIMENTS ON A PULSE DETONATION DRIVEN COMBUSTOR

THESIS

Presented to the Faculty

Department of Aeronautics and Astronautics

Graduate School of Engineering and Management

Air Force Institute of Technology

Air University

Air Education and Training Command

In Partial Fulfillment of the Requirements for the

Degree of Master of Science in Aeronautical Engineering

Nicholas C. Longo

Captain, USAF

March 2011

AFIT/GAE/ENY/11-M18

HEAT TRANSFER EXPERIMENTS ON A PULSE DETONATION DRIVEN COMBUSTOR

Nicholas C. Longo

Captain, USAF

March 2011

Approved:

_____	_____
Paul I. King (Chairman)	date
_____	_____
Frederick R. Schauer (Member)	date
_____	_____
Robert B. Greendyke (Member)	date

Abstract

Heat transfer experiments were conducted using a heat exchanger behind a pulse detonation combustor and a Garrett automotive turbocharger at the Air Force Research Lab (AFRL). The equivalence ratio and purge fraction were held at 1.0 and 0.9, respectively, while the frequency of operation was varied from 10 to 12 Hz in 1 Hz movements, and the fill fraction was varied from 0.5 to 0.8 in 0.1 increments. Temperatures were calculated using an energy balance and used to determine turbine exit enthalpy. The representative turbine inlet enthalpy was calculated using compressor work and radiation from the turbine. Turbine inlet and exit temperatures were also measured directly using J-type and K-type thermocouples and compared to calculated values using the heat exchanger approach. Compressor and turbine work was computed and compared with recently attained values. Efficiency was presented for varying pressure ratios. The efficiency measurements were compared with time accurate efficiency measurements from on-going work.

Acknowledgements

First I would be remiss if I did not thank my wife. Her daily sacrifices were crucial. Her support, understanding and patience were invaluable through the entirety of this program. I also thank my parents for pushing me to work hard and believing in me throughout everything I have done.

I would like to thank Dr. King for all of his pep talks and the hours he spent with me analyzing data and designs. Thanks to Dr. Schauer for explaining everything to me over and over, and never making me feel the lesser for it. Thanks to Lt Col Rouser for guiding and encouraging me every step of the way. Thanks to Dr. Hoke for helping me troubleshoot and work through all of my experimental issues. I also would like to thank Chris Stevens for staying late to run my experiment, setting up the Schlieren optics and always letting me bounce ideas off of him.

I also appreciate the help of and would like to thank Rich Ryman for welding my heat exchanger together before it was a heat exchanger and Curt Rice for doing pretty much everything else.

Thank you all so very much!

Nick Longo

Table of Contents

Page

List of Figures

Page

List of Tables

Page

List of Symbols

Symbol

A	=	area
C_D	=	nozzle discharge coefficient
C_p	=	specific heat at constant pressure
D	=	diameter
e	=	error (total uncertainty)
E	=	energy
f	=	friction factor
g	=	gravitational constant
h	=	specific enthalpy
H	=	enthalpy
h	=	heat transfer coefficient
J	=	Joules
K	=	Kelvin
kg	=	kilogram
k	=	thermal conductivity
L	=	length
Ln	=	natural logarithm
m	=	meters
$\dot{m}$	=	mass flow rate
M	=	Mach number
Nu	=	Nusselt number
p	=	precision uncertainty
P	=	pressure
Pa	=	Pascals
Pr	=	Prandtl number
q	=	heat transfer rate
R	=	specific gas constant
Ra	=	Rayleigh number
Re	=	Reynolds number
s	=	seconds
T	=	temperature
U	=	internal energy
U	=	overall heat transfer coefficient
V	=	velocity
V	=	volume
w	=	bias uncertainty
W	=	watts
W	=	work
z	=	altitude

Greek Letters

γ	ratio of specific heats	ν	dynamic viscosity
ε	emissivity	ρ	density
η	efficiency	σ	Boltzmann's constant
μ	viscosity	φ	equivalence ratio

List of Abbreviations

Abbreviations

AFIT	Air Force Institute of Technology	Hz	hertz
		MHz	megahertz
AFRL	Air Force Research Laboratory	min	minute
		ms	millisecond
avg	average	mV	millivolts
dB	decibels	PDRF	Pulsed Detonation Research Facility
FC	free convection		
FF	fill fraction	PF	purge fraction
freq	frequency	psia	pounds per square inch absolute
gal	gallon		

rad	radiation	T-s	temperature –entropy
sec	second	V	volts

ENTHALPY MEASUREMENTS OF A PULSE DETONATION DRIVEN COMBUSTOR

I. Introduction

I.1 Motivation

In recent years, Pulse Detonation Engines have gained attention for the promise of improved performance over conventional turbine engines and ramjets (Dyer 2002). More recently, government agencies have pushed for a Pressure Gain Combustion (PGC) engine to be integrated into a production worthy aircraft. The end goal of this program is to design, build and test an engine capable of powering an aircraft through various flight regimes. Due to their promise to provide increased specific thrust and decreased fuel consumption at higher speeds than conventional Gas Turbine Engines (GTEs), PDEs prove to be a promising portion of the solution.

The solution will likely take the form of a hybrid engine that will incorporate the standard elements of a GTE (compressor, turbine and nozzle) and replace the combustion chamber, where deflagration of fuel would normally occur, and replace it with a detonation chamber. There are a number of steps that need to take place before such a hybrid is successfully developed.

PDEs obtain their increased efficiency by means of detonation, a pressure gain, near constant volume combustion process. Conventional gas turbine engines burn, or deflagrate, fuel through approximately constant pressure combustion in the Brayton cycle. A PDE utilizes detonations, which offer much higher pressures at the site of fuel ignition, generating less entropy in the process and ultimately translating into more

energy being extracted from the fuel-air mixture. The PDE cycle is often associated with the Humphrey cycle. The Brayton and Humphrey cycle are compared in Figure I-1 later on.

A simplified model of PDE operation breaks the process into three main phases: fill fire and purge. During the fill phase fuel and air is premixed at a specific equivalence ratio and injected into a tube which is immediately sealed at one end upon completion. In the fire phase an ignition source initiates deflagration, or burning, of the fuel at the closed end. As the flame passes through the fuel air mixture pressure inside the tube builds until the deflagration to detonation transition (DDT) occurs. At this point a coupled shock wave and flame front travel through the remainder of the fuel/air mixture. This detonation wave of combustion gasses is allowed to exit the tube producing thrust. In the purge phase, the tube is filled with air alone to provide a buffer between fire phases and to aid in cooling. This process is repeated in a cyclic fashion, often at high frequency.

At AFRL testing has shown that a PDE is capable of powering a turbocharger as a means to self-aspirate (Hoke, et al. 2002), a critical step in the process of producing an airworthy engine. It has also been shown that a Pulse Detonation Combustion (PDC) powered turbo-charger will produce more specific power than a Steady Deflagration Combustor (SDC) given similar operating conditions (K. P. Rouser, P. I. King and F. R. Schauer, et al., Unsteady Performance of a Turbine Driven by a Pulse Detonation Engine 2010). However, there is still a need to determine the efficiency of a PDC driven turbine compared to a SDC or GTE. In order to make this comparison the PDC exhaust flow must be further characterized, to include measurement of the turbine inlet and exit temperatures, and pressures.

I.2 Problem Statement

The primary parameters that are necessary to determine enthalpy and efficiency across a turbine are turbine inlet and exit temperatures, pressures and mass flow rates. Due to the extreme and unsteady temperatures, pressures and velocities of the flow in a PDC driven turbocharger, acquiring experimental measurements of the combustion products as they leave a radial turbine can be difficult. Observed detonation wave speeds for hydrogen-air (Schauer, et al. 2005) average 1800 m/sec, and detonation temperatures average above 2000 K. Purge air is typically subsonic and at ambient temperatures. Reliable measurement techniques have not been established for such a regime; therefore, a method must be developed. A one-dimensional, constant volume thermodynamic analysis will therefore be used as a means for comparison to a one-dimensional, time accurate method being developed in parallel (K. P. Rouser, P. I. King and F. I. Schauer, et al. 2011).

I.3 Research Objectives

The ultimate goal of this research was to gain an understanding of the efficiency of a PDC driven turbocharger and to enable comparison against other (Ramjet, Gas Turbine Engine) cycles. This research specifically focused on the flow downstream of a turbocharger or a PDC when the turbocharger was not present.

The first objective was to build a heat exchanger capable of cooling the turbine exhaust to a temperature that could be measured accurately on a time averaged basis using thermocouples. Currently it is not possible to measure the temperature of PDC exhaust flow while operating at high frequencies and mass flow rates directly using a thermocouple or similar probe-like device. Other non-intrusive temperature

measurement techniques, like optical pyrometry, have been applied with some success, but are limited to higher temperatures. These limitations do not allow for the flow temperature to be captured over an entire PDC cycle. The exit temperature of the heat exchanger exhaust gas along with the energy removed from the gas by the heat exchanger were added together to provide an average temperature of the flow over a complete cycle.

The second objective is to determine the pressure at the inlet and exit of the heat exchanger. Ideally two state variables, temperature and pressure, will be obtained, which will then allow enthalpy to be calculated. Sonntag (Sonntag 1991) defines enthalpy as

$$\mathrm{H} = U + \mathrm{P}V \qquad \text{Eq. 2.2.1}$$

or the combination of the internal energy with the pressure multiplied by the volume of the system. For an ideal gas, P*V* can be restated as RT, or the ideal gas constant multiplied by the temperature. Therefore for an ideal gas, enthalpy becomes solely a function of temperature. The enthalpy gives the measure of the total energy of the thermodynamic system. This simplification is not applicable to efficiency, therefore the pressure at the inlet and exit of the turbine is still necessary. The third objective was to determine the efficiency of the PDC driven turbocharger.

I.4 Methodology

This experiment employed an application of the first law of thermodynamics, utilizing a quasi-steady approach. A heat exchanger, situated downstream of the turbine reduces the temperature, and to some degree the pressure, of the flow to the point where measurements may be made. The assumption was that the flow exiting the turbine from both the detonation and purge phases were able to mix in the heat exchanger, and the

mixed outlet temperature was measured. The mass flow rate and temperature of this colder exhaust flow and the coolant used in the heat exchanger were combined to determine the inlet energy of the flow and consequently the temperature of the PDC exhaust turbine gases.

Starting with a general form the conservation of energy equation:

$$\dot{E}_{stored} = \dot{E}_{in} - \dot{E}_{out} + \dot{E}_{generated} \qquad \text{Eq. 2.3.1}$$

The system is defined as the heat exchanger itself. The system does not generate energy and it is allowed to achieve steady state in this experiment, so the net change in energy stored is zero:

$$\dot{E}_{in} = \dot{E}_{out} \qquad \text{Eq. 2.3.2}$$

Furthermore, for a counter-flow heat exchanger, the total energy change into and out of the system is the sum of the energy change in the coolant and exhaust gas:

$$\dot{E}_{\substack{coolant \\ in}} + \dot{E}_{\substack{gas \\ in}} = \dot{E}_{\substack{coolant \\ out}} + \dot{E}_{\substack{gas \\ out}} \qquad \text{Eq. 2.3.3}$$

The time rate of change of energy term for any system:

$$\Delta\dot{E}=\dot{m}\left(h+\frac{1}{2}\mathrm{V}^2+\mathrm{gz}\right)_{\mathrm{out}}-\dot{m}\left(h+\frac{1}{2}\mathrm{V}^2+\mathrm{gz}\right)_{\mathrm{in}}+\mathrm{q}+\dot{W} \qquad \text{Eq. 2.3.4}$$

The heat exchanger is not doing any work, so the $\dot{W}$ term becomes 0. The specific enthalpy is a combination of the thermal energy and flow work. The flow is not moving vertically so the potential term is removed. The average velocity at the entrance and exit of the heat exchanger are assumed to be the same for the coolant, so the V^2 term also is removed. At steady state conditions, the rate of change of energy is zero. For ideal turbine gases, the change in specific enthalpy can be approximated by:

$$\Delta h = C_p \Delta T_{total} \qquad \text{Eq. 2.3.5}$$

The energy rate removed by the coolant water, q, can be determined by:

$$\mathrm{q} = \Delta\mathrm{H} = \dot{m}\left(C_{p,in}\mathrm{T}_{in,coolant} - C_{p,out}\mathrm{T}_{out,coolant}\right) \qquad \text{Eq. 2.3.6}$$

In Eq. 2.3.7, T_{in} was determined using the temperature of the coolant entering and exiting the heat exchanger, and the temperature of the exiting combustion gases. This calculated inlet temperature provides an indicator of the energy in the flow at the turbine exit. The T-s diagram in Figure I-1 further illustrates this approach. The process (1-2) is isentropic compression, (2-3H) is constant volume heat addition or detonation, (3H-4H) is isentropic expansion.

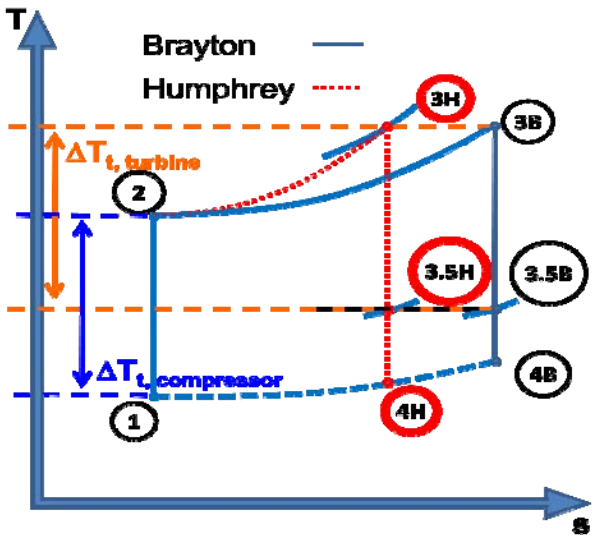

Figure I-1: T-s diagram for Humphrey cycle and Brayton cycle

For the purpose of this experiment process (1-2) takes place in the facility compressor, (2-3H) in the detonation tube, (3H-3.5H) across the turbine and (3.5H-4H) across the heat exchanger.

This study focused on 3H where the combustion products have exited the PDC tube and 3.5H where the combustion products have exited the radial turbine. The fuel/air mixture will not have returned to ambient conditions and will still have retained residual energy. The heat exchanger exhausted into the test cell so pressure at 4H was approximately equal to pressure at 1 (ambient). The energy transferred from the exhaust gases into the coolant was measured in the process.

The temperature of the coolant was measured at the inlet and outlet of the heat exchanger. The PDC exhaust temperature was measured at the outlet of the heat exchanger. The inlet temperature of the heat exchanger is a function of the change in energy of the coolant added to the residual energy left in the gas:

$$T_{in,gas} = \frac{\left(\dot{m} C_p \Delta T\right)_{water} + \dot{m}_{gas} C_{p,gas,out} T_{gas,out}}{\dot{m}_{gas} C_{p,gas,in}} \qquad \text{Eq. 2.3.7}$$

II. Background and Literature Review

Research on extracting energy from the flow of a PDC has been ongoing at the Air Force Research Labs for almost ten years. In 2002 it was demonstrated that a turbocharger is a viable method for self-aspirating a PDC (Hoke, et al. 2002). During this experiment the PDC driven turbocharger was able to run for 25 minutes without any noticeable performance reduction or visible signs of damage. Further experimentation showed the ability of a turbocharger to aspirate a PDC while still producing thrust under varying subsonic conditions to include; varying frequencies (20, 30 and 40 Hz), fill fractions (1.0, 1.5 and 2.0), compressor flow rates (10-20 lb/min) and compressor pressure ratios (1.05-1.73) (Schauer, Bradley and Hoke 2003). In this work a series of high speed pressure transducers were used to determine the effect of the addition of a turbine on the detonation and blow down process. It was shown that the turbine has a damping effect on the shock that is driven by a detonation wave.

More recent work conducted at the Air Force Research Lab has showed that when powered by a PDC, a turbocharger extracts more power than when driven by constant pressure combustion (K. P. Rouser, P. I. King and F. R. Schauer, et al., Unsteady Performance of a Turbine Driven by a Pulse Detonation Engine 2010). Furthermore, this work also showed a 41.3% improvement in specific power and 27.8% improvement in Break Specific Fuel Consumption (BSFC) with a PDC in comparison to constant pressure combustion. It is important to note that this increased power was attained at low pressure ratios. This magnitude of improvement in specific power is not expected to be duplicated at higher pressure ratios, however the trend of increased specific power from a PDC driven turbocharger versus one powered by SDC is still anticipated. To reach the

conclusions on improved performance high speed (5 MHz) compressor pressure, mass flow rate and tachometer data was used. Later work (K. P. Rouser, P. I. King, et al., Parametric Study of Unsteady Turbine Performance Driven by a Pulse Detonation Combustor 2010) at the Air Force Research Lab used similar measurement devices to show that the average specific work performed by a PDC driven turbocharger increased directly as a result of higher operating frequencies. At those higher frequencies rotor speed response approached quasi-steady behavior, or the variation between the peak and minimum rotor speed decreased as frequency increased.

Rouser et al. also evaluated a number of other approaches to acquiring flow field data of a PDC driven turbine (K. P. Rouser, P. I. King and F. I. Schauer, et al. 2011). More specifically, this work measured turbine rotor speeds, turbine pressure ratios and flow temperatures, velocities and densities of the unsteady exhaust leaving a PDC powered turbocharger. Future applications of this work include determining unsteady turbine efficiency. Rouser et al. also noted the need for other formulations for unsteady turbine efficiency, a requirement which this experiment hopes to satisfy.

PDC-turbine integration work has also been performed incorporating axial flow turbines and an array of PDC tubes with a bypass ratio of 7 (Glaser, Caldwell and Gutmark 2006), vice a radial turbine powered by one PDC tube as in previously discussed works. Recorded turbine inlet temperatures were considerably less than will be reported in this work, mainly due to the quantity of bypass air that was used. According to this study increasing fill fraction had the effect of increasing turbine inlet temperature, specific power and efficiency.

In further investigations in 2007, Glaser et al. compared the efficiency of a PDC driven turbine with a steady flow combustor driven turbine(Glaser, Caldwell and Gutmark 2007). This work was very similar to that of Rouser et al. with the exception that the radial turbine is replaced with an axial turbine. Bypass flow was added and an array of six tubes was used. Glaser et al. compared the turbine efficiencies of the two arrangements by using turbine inlet temperature and pressure ratio across the turbine. Direct measurements were possible due to the cooling effect of the bypass flow. Results showed that the efficiency of the PDC driven axial turbine was comparable to the steady combustor driven turbine.

Rasheed et al. also experimented with a single stage axial turbine using 60 % bypass flow in 2005(Rasheed, Furman and Dean 2005). This work reported compressor work of 100 hp with a primary mass flow rate of 2 lb/sec (this includes fill and purge for eight tubes) and a bypass flow rate of 3 lb/sec. A maximum of 350 hp was calculated with a primary mass flow rate of 3 lb/sec and a bypass flow rate of 5 lb/sec while operating at 20 Hz.

Further analytical work has included resolving the efficiency for a turbine under unsteady and periodic flow conditions(Suresh, Hofer and Tangirala 2009). The flow behind a PDC would match this description. Suresh et al. recognized several formulations for this efficiency, one variant involving no averaging and another involving averaging of an equivalent steady flow. In both formulas, the main question lies in the development of the ideal case (the denominator in the efficiency formula). In the non-averaged efficiency, the ideal change in enthalpy is determined by assuming the mass flow through the turbine is expanded instantaneously. The second variant works by

averaging the mass flow over a cycle and mass averaging the total temperature. The total pressure is then work averaged. This work notes that the latter formulation is sensitive to form that the averaging takes. Using CFD, Suresh et al. determined that the work averaged efficiency produces a result that is approximately 10% higher than the efficiency provided by the non-averaged equation.

III. Test Setup

III.1 Preparation

The first goal in this experiment was to determine the design for the heat exchanger. Utilizing heat transfer principals (Incropera, et al. 2007) a spreadsheet was developed to iterate on heat exchanger design parameters. The formulas used and a copy of the spreadsheet can be found in Appendix A. This spreadsheet provided the initial estimates for heat exchanger dimensions given the following inputs:

Table III-1: Heat exchanger spreadsheet inputs and outputs

Inputs		
Temp, hot gas in	1450 K	2150 F
Temp, hot gas out	900 K	1160 F
Temp, liquid in	293 K	68 F
Mass flow, hot gas	.04 Kg/s	5.3 lb/min
Mass flow, liquid	.35 Kg/s	5.5 gal/min
Inner pipe diameter	.089 m	3.5 inch
Outer pipe diameter	.162 m	6.35 inch
Outputs		
Temp, liquid out	313.75 K	105.35 F
Heat exchanger length	5.97 m	19.6 ft
Overall heat transfer coefficient	26.7 W/m^2K	

III.2 Data Collection Instrumentation

Over the course of this experiment, the test setup varied significantly. For a detailed description of the previous designs that led to the final experimental setup, see Appendix D. The following is a description of the final setup that was used to produce the results discussed in Chapters IV and V this paper.

A counter flow heat exchanger design was chosen due to its increased heat transfer rate, q, per unit of surface area. Schedule 10 (1/8th inch thick) 6061-T6 aluminum was selected as the primary building material for its favorable conductive properties (180 W/m K). It was eventually determined during the course of experimentation that one, ten foot section would be sufficient to reduce the temperature of the exhaust products to a point where it could be directly measured with thermocouples. The three inch diameter pipe was set inside of a six inch diameter pipe and a ring of aluminum was welded to each end enclosing an annulus. ¾ inch diameter holes were cut in opposite ends of the enclosure facing opposite directions and ¾ inch pipe fittings were welded to each hole to allow for coolant flow.

Figure III-1: Aluminum heat exchanger section before addition of pipe nipple

Aluminum pipe nipples were welded to each end of the heat exchanger so that it could be secured to the exhaust pipe of the turbine. Water flowed first through a low-flow liquid flow meter upstream of the heat exchanger shown in Figure III-2:

Figure III-2: Low-flow liquid flow meter

The coolant then flows through a ¾ inch diameter Swagelok fitting and across a T-type thermocouple which measures the inlet temperature. Next the water flows into the annulus. Flow is directed vertically into and out of the heat exchanger in order to reduce the likelihood that air pockets form. Water flows in on the same side that hot gas exits and flows out where the exhaust products enter the heat exchanger (counter flow design), at approximately 5.5 gallons per minute. The water flows out through a similar Swagelok fitting where another T-type thermocouple measures temperature. Coolant temperature measurements are taken six inches prior to entering and six inches after exiting the heat exchanger. A simplified schematic of the heat exchanger from a top view is pictured in Figure III-3:

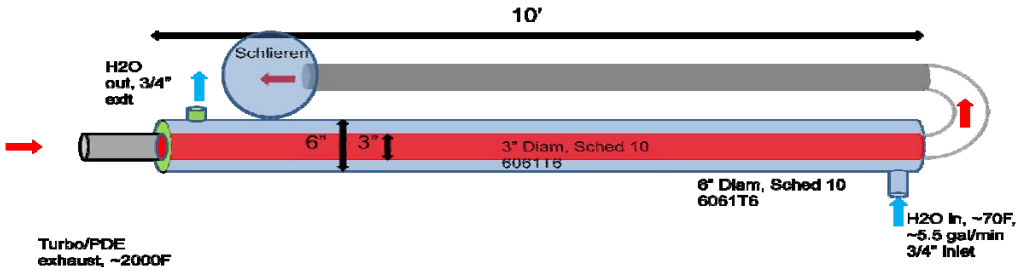

Figure III-3: Top view of heat exchanger

Pressure was measured six inches upstream and downstream of the heat exchanger using 725 psi static pressure transducers with a one foot standoff distance. This standoff distance was necessary to reduce the heating of the pressure transducer and the possibility of a shock wave hitting the sensor and destroying it. Due to their sensitivity, the static pressure transducers were only set in place for short runs (less than ten seconds) to further reduce the risk of damage.

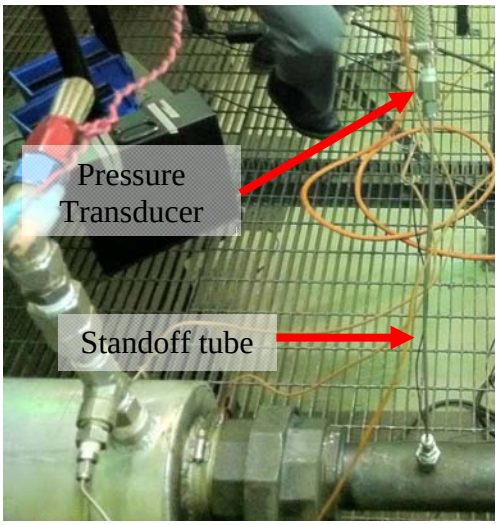

Figure III-4: Sensotec 725 psia pressure transducer fixed to detonation tube via one foot standoff tube

For comparison of the calculated heat exchanger inlet temperature, during extended runs to equilibrium a J-type thermocouple was inserted into the turbine exhaust flow at the location where the pressure transducer was during the shorter runs. J-type thermocouples are attached on the exterior of the heat exchanger three inches from the inlet and the exit to provide temperature measurements used in calculation of the amount of heat escaping or entering the heat exchanger via radiation and or natural convection.

J-type thermocouples were also fixed to the exterior of the PDC tube at 25.5 inches and 48 inches from the engine head for the same purpose.

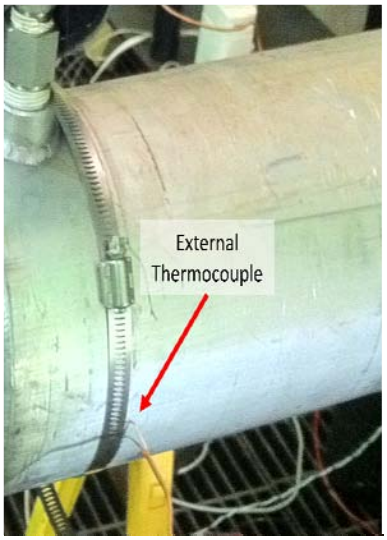

Figure III-5: External thermocouple fixed to heat exchanger

An additional J-type thermocouple is located on the surface of the aluminum nipple used to attach the heat exchanger to either the turbocharger or the PDC tube in order to monitor structural integrity. Figure III-6 and Figure III-7 identify the locations of thermocouples.

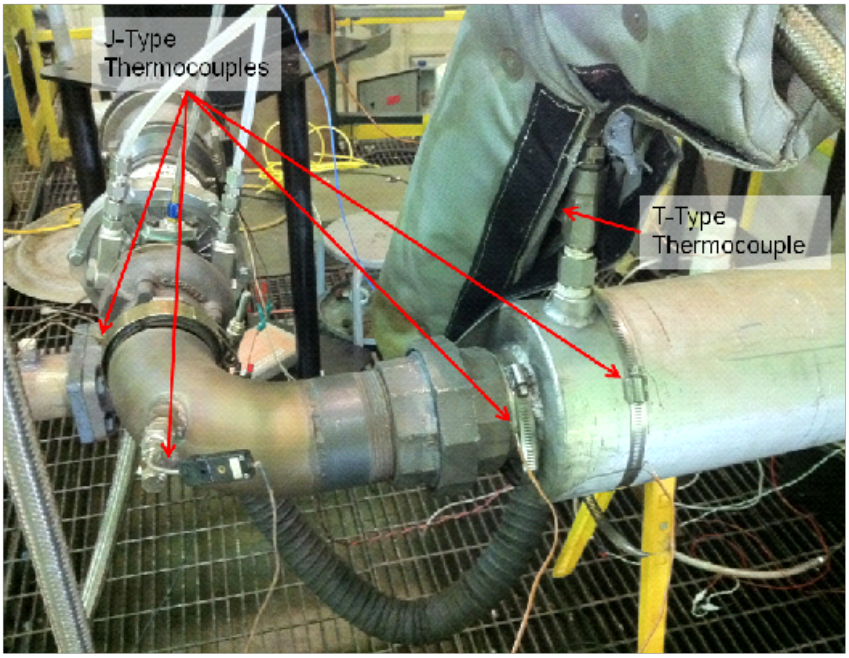

Figure III-6: Heat exchanger instrumentation, head end

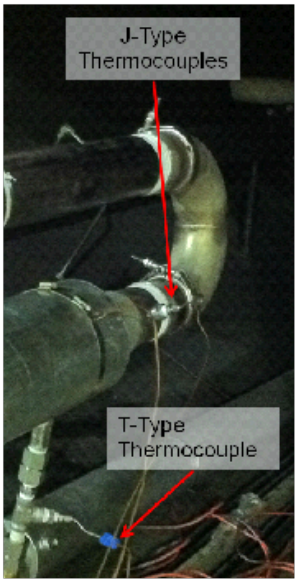

Figure III-7: Heat exchanger instrumentation, tail end

The experiment was carried out in the Pulsed Detonation Research Facility of the Air Force Research Laboratory, using a similar configuration as previous work (K. P. Rouser, P. I. King and F. R. Schauer, et al., Unsteady Performance of a Turbine Driven by a Pulse Detonation Engine 2010). The facility supplies compressed air to the main

and purge manifolds as seen in Figure III-8. The PDRF uses Ingersoll-Rand facility air compressors to provide compressed air to the manifolds. Each of the three compressors is capable of supplying up to 1412 ft^3/min air mass flow at pressures up to 100 psi. Compressed air flows into a 159 ft^3 receiver tank, and then is routed into the test cell, where it is separated into two streams for the main and purge manifolds. Each air stream is controlled by Tescom electromagnetic controllers that actuate pressure regulators and are metered through calibrated converging-diverging nozzles. Fuel is mixed at the entrance to the main manifold. Fill distribution and ignition takes place using an automotive engine head and cam to operate intake and exhaust valves for a desired operating frequency. The engine head is taken from a four-cylinder engine however, for this experiment only one cylinder head was used. The intake valves are used to supply the main fill fuel-air mixture, and the exhaust valves are used to inject purge air. During the fire phase, intake and exhaust valves are closed. The turbocharger and heat exchanger are attached downstream of the engine head, or to the right in Figure III-8.

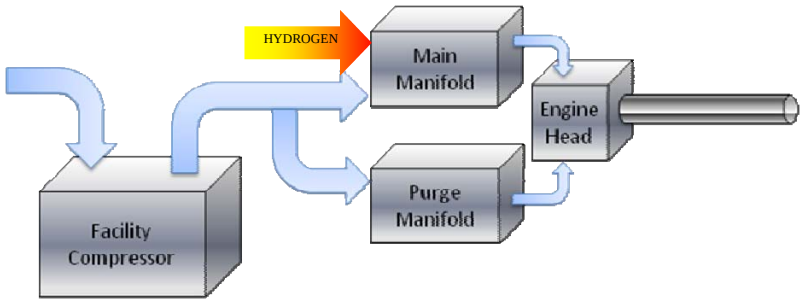

Figure III-8: AFRL Pulse Detonation Research Facility engine test block diagram

A two-inch diameter, four foot long steel pipe with an s-curve was used for a detonation tube. A 16 inch Schelkin-like spiral assisted the DDT process by increasing

the turbulence and mixing of the fuel and air (Schauer, et al. 2005). The s-curve was necessary to bring the exhaust products to an appropriate height to make Schlieren imaging possible. Three ion probes are installed in the detonation tube to verify Chapman-Jouget velocities. The probes short-circuit when the flame front arrives, and velocity is determined from the transition time between probes.

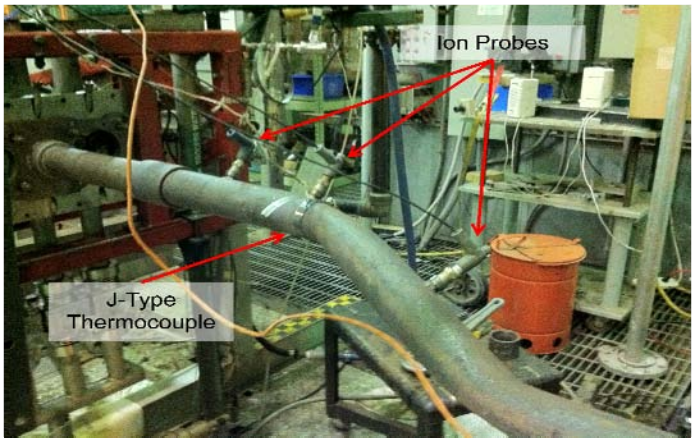

Figure III-9: Two inch diameter s-curve detonation tube attached to engine head

Before the first detonation, the turbocharger turbine is driven by the fill and purge phases associated with the start-up sequence. "Soft starts" were used for all runs to prevent detonating a larger than anticipated volume of fuel and oxidizer. In the soft start process the ignition source, in this case an automotive spark plug, is initiated prior to fuel being added. Fuel is gradually added to the main air until the desired equivalence ratio is achieved. PDC operation is attained by first setting desired operating frequency, equivalence ratio and fill fraction. Lab View software determines the required pressure to achieve the given fill fraction at that operating frequency.

For the final results published in this experiment a Garrett GT2860RS ball bearing turbocharger was used. This turbocharger uses a nine-blade, radial turbine. The GT2860RS is also equipped with a radial compressor having six primary impeller blades and six splitter blades. The GT2860RS uses a 76 trim turbine wheel with 0.63 A/R turbine housing and a 62 trim compressor wheel with a 0.60 A/R. It also uses a T25 turbine inlet flange and has a dual ball bearing, oil and water cooled CHRA (Center Housing Rotating Assembly).

Figure III-10: Garrett GT-2860RS ball bearing turbocharger

The turbine inlet of the turbocharger is coupled to the PDC exit as shown in Figure III-11 and the wastegate is disabled so that all of the mass flow from the PDC enters the turbine.

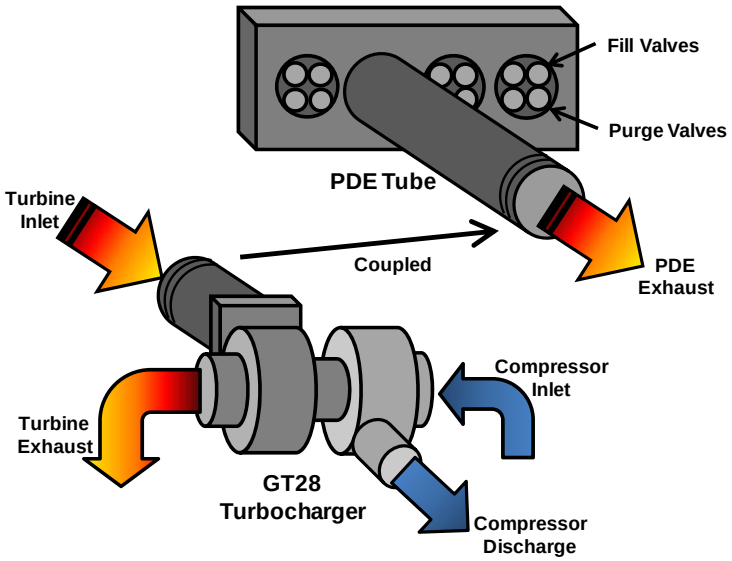

Figure III-11: PDC and turbocharger test rig

The compressor side of the turbocharger received ambient air through a mass air flow (MAF) sensor. The compressor exhaust pipe consisted of a two inch diameter pipe and a ball valve to back-pressure the compressor with a 50 psi static pressure transducer and J-type thermocouple, as seen in Figure III-12. Several different compressor operating conditions are obtained by adjusting the PDC operating frequency. J-type thermocouples are attached to the turbine housing to monitor structural integrity of the turbine. All temperature data is sampled once per second. The mass air flow sensor used was a Pro-M 92mm High Flow Mass Air Meter.

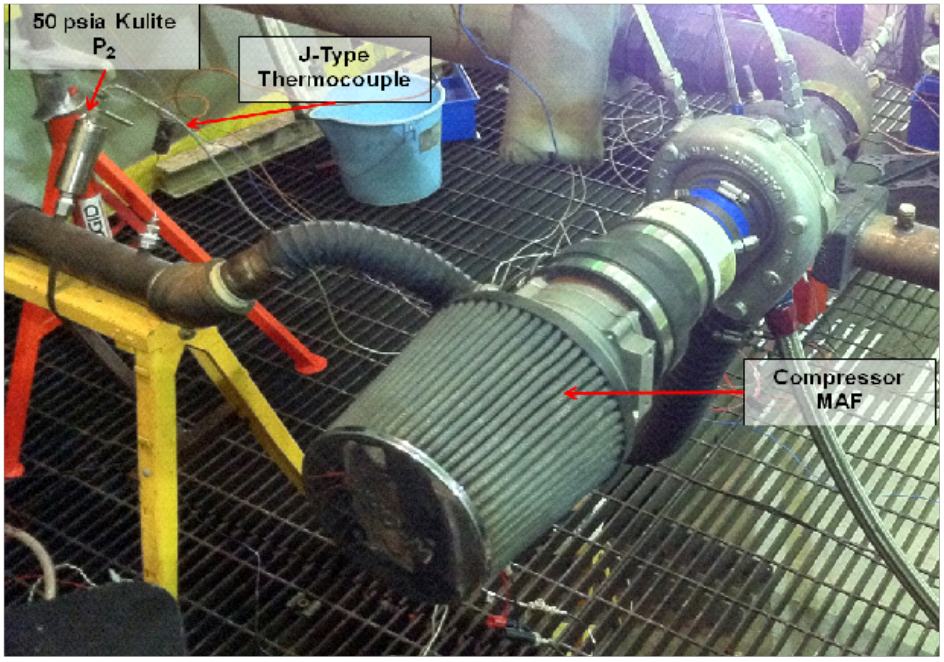

Figure III-12: Turbocharger compressor instrumentation and control valve

Figure III-13 illustrates the GT-2860RS compressor operating map where target compressor operating conditions run down the center of the efficiency islands. Operating frequencies of the PDC ranged up to 20 Hz in this experiment, with fill fractions of 0.5 through 0.8 and purge fraction fixed at 0.9. The fuel being detonated was hydrogen with air as the oxidizer at stoichiometric conditions.

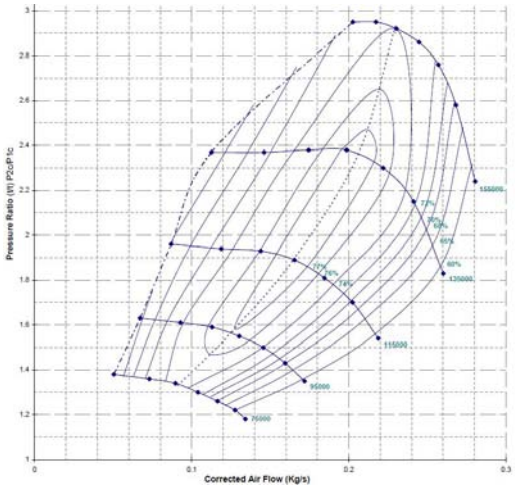

Figure III-13: Garrett GT2860 compressor operating map

The exhaust flow of the heat exchanger needed to be redirected to allow for Schlieren imaging. To accomplish this, a six inch radius, three inch diameter 180º mild-steel elbow turned the flow back towards the engine head. To orient the flow in the frame of the Schlieren camera, an additional eight feet of steel pipe was used for the setup without the turbocharger and nine and a half feet was used for the configuration with the turbocharger.

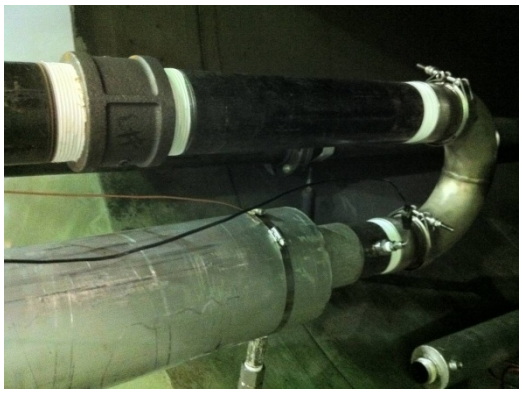

Figure III-14: 180º mild steel elbow and steel pipe extension for Schlieren imaging

A wooden block was positioned under the steel extension pipe to prevent the elbow from yielding. The heat exchanger water outlet was insulated to prevent exhaust gases from affecting the measured water temperature.

Figure III-15: Ten foot heat exchanger with turbocharger

Schlieren imaging took place at the exit of the heat exchanger, with the purpose of determining the density gradients in the exhaust gases. This information helped to quantify the steadiness of the flow as well as to determine relative velocities of the exiting flow. The Schlieren system in Figure III-18 was a folded z-type arrangement consisting of 12.5” (31.7 cm) diameter mirrors. The light source was made up of four pieces: a FSI 250W halogen illuminator, two 50.8 mm diameter 50 mm focal length lenses, and a 25 mm by 25 mm adjustable slit. The camera table contained a vertical knife-edge:

Figure III-16: Phantom camera aimed at vertical knife (razor blade) edge

and a Phantom ® V7.1 high-speed camera with a 1-2.8x zoom lens:

Figure III-17: Phantom ® V7.1 high-speed camera with a 1-2.8x zoom lens

The zoom lens allowed focusing onto the test section.

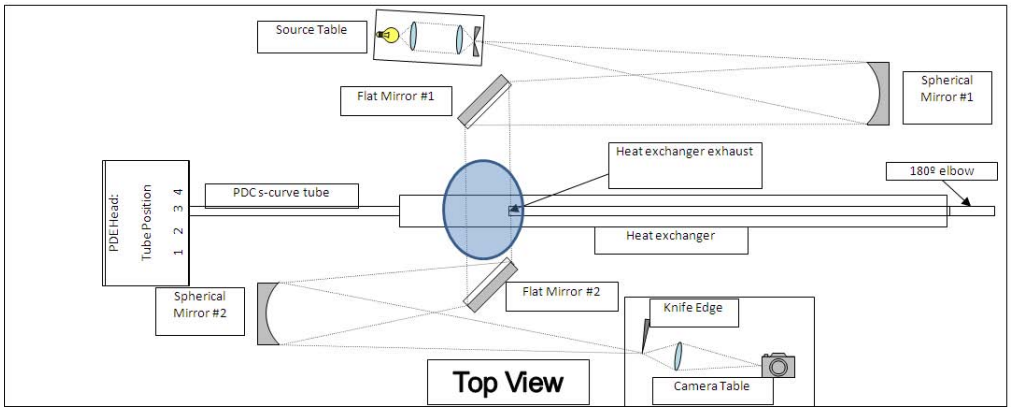

Figure III-18: Schematic of Schlieren setup

The Phantom camera could record a maximum of 75000 frames per second at 256 pixels by 64 pixels resolution. The camera is capable of higher frame rates, and higher resolutions, but not both at the same time. The settings used are a compromise between spatial and temporal resolution.

Schlieren video was captured at 10, 15 and 20 Hz operation with and without the turbocharger at a fill fraction of 0.5 and a purge fraction of 0.9 with a frame rate of 16000 fps, exposure of 2 us, resolution of 256 by 256 pixels, and pixel depth (number of shades of gray) of 8 bit (128 shades). The spatial resolution of the test section was 0.024 inches per pixel (.60 mm per pixel).

III.3 Data Collection Procedure

The experiment began as water first ran through the heat exchanger. A standard gate valve controlled the flow rate of water. The water passed from the gate valve to the low flow liquid flow meter. This flow meter used a 12V AC power source and outputs a

sine wave with a K factor of 330 pulses per gallon. The flow meter output is connected to an oscilloscope. The frequency (in pulses per second) is recorded and then multiplied by the K factor and converted to minutes to determine liquid flow rate in gallons per minute.

$$\frac{\text{gallons}}{\text{min}} = \text{freq}\left(\frac{\text{pulses}}{\text{sec}}\right) \times \frac{1}{\text{K factor}}\left(\frac{\text{gallons}}{\text{pulse}}\right) \times \frac{60\text{sec}}{\text{min}} \qquad \text{Eq. 4.2.1}$$

The gate valve was manipulated until the liquid flow rate was determined to be approximately 5.5 gallons per minute via Eq. 4.2.1. The actual flow rate was recorded by hand.

As previously mentioned the PDC was “soft started” during all experiments. During the soft start procedure the spark was started and fuel is gradually added to the main mixture until the desired equivalence ratio was achieved. The detonations are then verified using the ion probes. “Soft starts” were necessary to prevent fuel and air from accumulating in the heat exchanger and turbine and then being detonated, possibly damaging both.

One of the key test parameters that were varied in this experiment was fill fraction of the detonation tube. Fill fraction is the fraction of the tube that is filled with the fuel-air mixture prior to detonation. Lab View software in the test facility determines the correct pressure and mass flow rate necessary to provide the demanded fill fraction. It starts by determining the volume of tube to be filled by multiplying a fill fraction by the tube volume, both of which are input by the user. It then determines mass of the fill by dividing the fill volume by density. The fill air and fuel are assumed to be ideal gases

and density is considered to be atmospheric pressure divided by the gas constant and the manifold temperature. The mass flow rate then becomes the mass multiplied by the frequency.

$$V_{fill} = (V_{tube})(FF)$$
$$m_{fill} = \frac{V_{fill}}{\rho} = \frac{V_{fill}}{\left(\frac{P_{atm}}{RT_{man}}\right)}$$
$$\dot{m}_{fill} = (m_{fill})(freq)$$

The software calculates mass flow rate the same way, regardless of obstructions or manifold pressures. In this experiment the turbine and heat exchanger act to back pressure the system, thus increasing the amount of pressure necessary to fill the tube to the appropriate volume. Therefore, without further adjustment the software would under fill the tube when obstructions were present downstream of the engine head. For this reason the ion probes are oriented so that they straddle the cross section of the tube corresponding to a fill fraction of 0.5. The length corresponding to a fill fraction of 0.5 was approximately 24 inches, given that the tube was 48 inches long. The estimated tube volume was entered and the tube was filled to what was thought to be a fill fraction of 0.5. A short run was performed (just long enough to record ion probe data). If the actual fill fraction was too large then a sharp drop was noted on the voltages of both ion probes. If the fill fraction was too small, voltage drops were not observed. To correct either issue, the tube volume parameter in the Lab View software is manipulated until a sharp drop was noted on the first ion probe and no voltage drop was indicated on the second. Using this technique, it is possible to determine fill fraction to within six inches

(or whatever the distance is between ion probes). This tube volume was used for both configurations (with and without the turbocharger) in order to ensure that a similar mass flow rate of air and fuel was achieved. This fill fraction test was performed before the run starts to ensure the appropriate tube volume is filled. Fill fraction dissimilarities are noted in section IV.4 due to tube heating, which caused actual fill fraction to increase. The tube volume used for this experiment was 168 cubic inches.

Two separate runs were used to gather all of the measurements necessary for each set point (frequency and fill fraction), a short duration run to collect pressure data and Schlieren imagery and a long duration run to thermal equilibrium to collect temperature measurements. For the short duration runs, the PDC was only pulsing for approximately 10 seconds, just enough time to allow for pressure measurements to be captured by the transducers and for the camera to record at least one cycle of main flow and purge air leaving the heat exchanger. The pressure data could not be collected continuously up to thermal equilibrium along with the temperature measurements due to the sensitivity of the pressure transducers. Ideally the pressures would have been recorded at thermal equilibrium as well as the temperatures. After the pressure data and Schlieren imagery were collected for the given test condition the pressure transducers were removed and the port was filled with a bolt and/or a thermocouple, to prevent any flow from escaping.

The high speed data consisted of only pressure measurements which were sampled at 5 MHz while the rest of the data, to include mass flow rate and temperature, was sampled at 1 Hz. The high speed measurements were triggered manually, while the low speed measurements were recorded continuously for the duration of the run. Each run was recorded electronically on a hard drive and analyzed at a later time. The pressure

transducer output was collected via a Lab View program, a sample of which can be seen here:

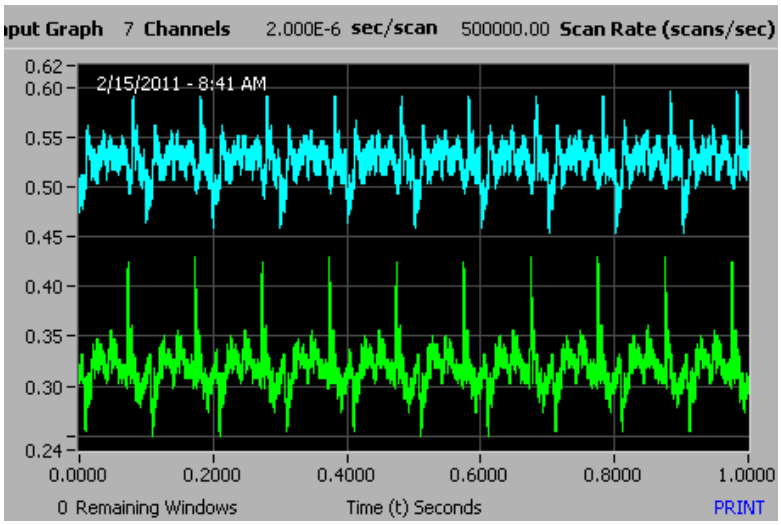

Figure III-19: 1 second data collection at 10 Hz, 0.5 fill fraction and 0.9 purge fraction of pressure downstream of turbocharger (green) and downstream of heat exchanger (blue)

This "high speed" data was then converted to a text file. During the conversion, sampling rate was reduced by ten times, to .5 MHz. This was done to reduce file size and to reduce the load placed on the computer in manipulating and processing data with Microsoft Excel. The one half second long pressure file was then converted from voltage to pressure in pounds per square inch absolute via the formula:

$$psia=\left(\frac{Voltage_{recorded}}{gain}\right)\left(\frac{1psia}{0.139mV}\right)\left(\frac{10V}{Voltage_{excitation}}\right) \qquad \text{Eq. 4.2.2}$$

When the pressure data downstream of the turbine and the heat exchanger were collected with the 725 psia pressure transducers, it was necessary to put a gain on the output so the variations in pressure are noticeable. In this case a gain of 40 dB (voltage-ratio of 100) was used, which corresponds to the "gain" term in Eq. 4.2.2. The second fraction is the amount of voltage generated by one psi and the last fraction takes into account that the voltage used to power the transducer was higher than the reference voltage of 10 volts and the pressure transducer was not regulated.

The low speed data which was sampled at 1 Hz was output from the Lab View software directly to a spreadsheet:

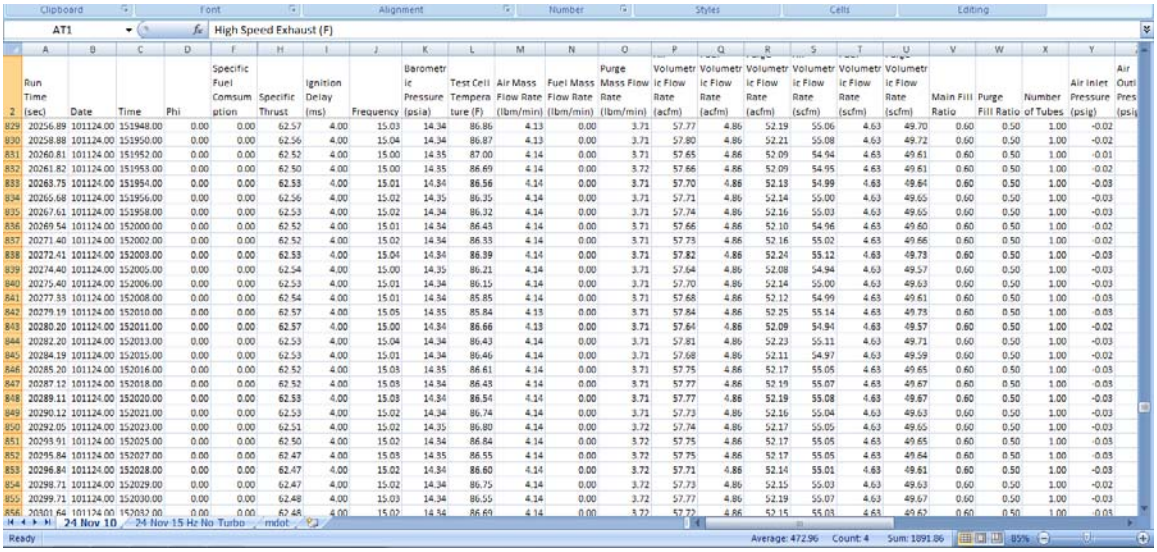

Figure III-20: Low speed data collection spreadsheet

For extended PDC operation to thermal equilibrium, the PDC was allowed to run until the water temperature of the heat exchanger and the exhaust temperature of the heat exchanger remained constant (within three degrees) for approximately 30 seconds, the PDC set point was then changed. Such a condition was considered thermal equilibrium.

Times to reach thermal equilibrium varied from seven to ten minutes after initial start up and approximately five minutes when changing between set points. In either case, the data used for the analysis consisted of the average of the final ten seconds of each run to thermal equilibrium.

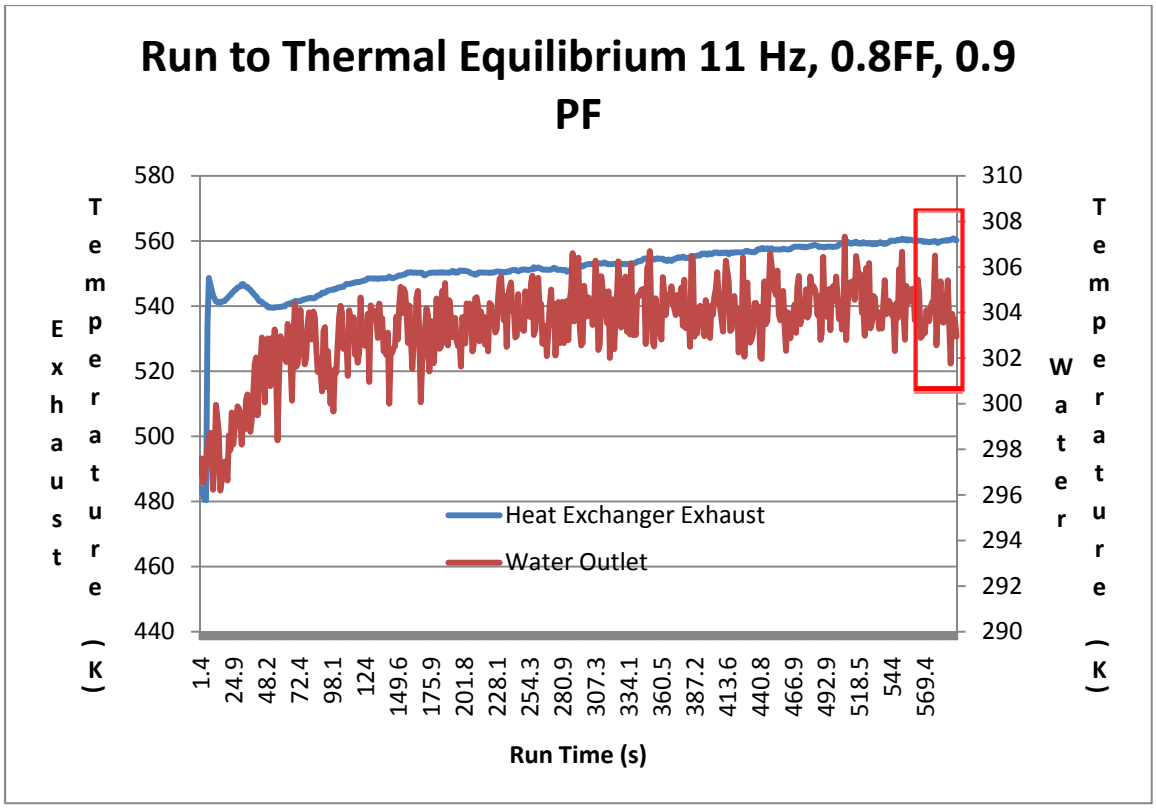

Figure III-21: Data collected during run to thermal equilibrium when changing from previous set point

During initial experimentation of extended runs to equilibrium, the heat exchanger and PDC tube were allowed to cool back down to the water inlet temperature and room temperature respectively. During this cool down period the PDC was still running as it would during an actual test, however fuel was no longer being dispensed and the spark was discontinued. This process allowed the PDC tubes and the turbocharger housing to

cool as they tend to reach temperatures in excess of 1200 °F during extended runs. After cooling down the PDC was started again and this process was repeated for another set point.

Later the PDC was run without allowing for cooling between set points. The water temperatures and heat exchanger exhaust gas rose to the same value (within 3 degrees) as when cooling was allowed. The data analyzed in this experiment was collected without allowing for the system to completely cool in between runs, except where it was necessary to change frequency. When changing frequency it was necessary to turn of the ignition source and fuel otherwise the PDC would backfire. This shutdown interval was minimized as much as possible to avoid cooling and increasing the time necessary to reach equilibrium.

During all experimentation the test cell door was sealed for safety and the status of the experiment was observed via remote cameras and measurement devices. Table III-2 summarizes the operating conditions of the experiment for both configurations:

Table III-2: Experiment operating parameters

Freq. (Hz)	10, 11, 12
Fill fraction	0.5, 0.6, 0.7, 0.8
Purge fraction	0.9
φ (eq. ratio)	1.0
Ignition delay (ms)	3.0
water flow rate (gal/min)	5.6

24 test runs were necessary to collect all of the data for the configuration with the turbocharger, half of which were to thermal equilibrium and half to determine pressures.

Another 24 test runs were used to collect the data for the configuration without the turbocharger.

III.4 Data Analysis

The experiment was run with a ten foot long heat exchanger to reduce the likelihood for condensation inside the heat exchanger. When water was not condensing, the gas leaving the heat exchanger was considered to be the combination of both the main and purge flows. Similar to Eq. 2.3.7, the energy conservation equation can be solved for the average gas inlet temperature:

$$\left(\mathrm{T}\right)_{\substack{\text{main+purge}\\ \text{in}}} = \frac{\left[\left(\dot{m}C_p\mathrm{T}\right)_{\text{main+purge}} + \left(\dot{m}C_p\mathrm{T}\right)_{\text{cool}} + \mathrm{q}_{\text{rad}} + \mathrm{q}_{\text{fc}}\right]_{\text{out}} - \left(\dot{m}C_p\mathrm{T}\right)_{\substack{\text{cool}\\ \text{in}}}}{\left(\dot{m}C_p\right)_{\substack{\text{main+purge}\\ \text{in}}}} \quad \text{Eq. 4.2.3}$$

where

$$\left(\dot{m}C_p\right)_{\substack{main+\,purge\\ in}} = \dot{m}_{total}\left(\frac{\dot{m}_{purge}}{\dot{m}_{total}}C_{p_{purge}} + \frac{\dot{m}_{main}}{\dot{m}_{total}}C_{p_{main}}\right) \quad \text{Eq. 4.2.4}$$

Note that the radiation (q_{rad}) and free convection (q_{fc}) from the heat exchanger was also accounted for. Work on the compressor side of the turbocharger can be used to calculate turbine work:

$$\dot{W}_c = \mathrm{H}_2\text{-}\mathrm{H}_1 = \dot{m}\left(C_p \mathrm{T}_2 - C_p \mathrm{T}_1\right) \qquad \text{Eq. 4.2.5}$$

The temperature change across the compressor actually lags behind the pressure change. To derive the work performed by the compressor more accurately, the isentropic relations for an ideal gas are used:

$$\mathrm{T}_2 = \mathrm{T}_1\left(\frac{\mathrm{P}_2}{\mathrm{P}_1}\right)^{\frac{\gamma-1}{\gamma}} \qquad \text{Eq. 4.2.6}$$

where T_1 and P_1 are room temperature and pressure for this experiment. Substituting Eq. 4.2.6 into Eq. 4.2.5 produces the formula used to calculate compressor work:

$$\dot{W}_c = \dot{m}\left\{C_p\left[\mathrm{T}_1\left(\frac{\mathrm{P}_2}{\mathrm{P}_1}\right)^{\frac{\gamma\text{-}1}{\gamma}}\right] - C_p \mathrm{T}_1\right\} \qquad \text{Eq. 4.2.7}$$

Over the course of this experiment it was found that the turbine housing reaches temperatures in excess of 800 K depending on the set point of the PDC. Due to the significant heating of the turbocharger, it is necessary to account for radiation. To estimate radiation, the turbine was approximated to be a six inch radius sphere, with an emissivity of 0.8. The following equation was used to calculate radiation:

$$\mathrm{q}_{rad} = \varepsilon\sigma A(\mathrm{T}_s^{\,4} - \mathrm{T}_\infty^{\,4}) \qquad \text{Eq. 4.2.8}$$

This analysis was performed at each set of conditions (frequency and fill fraction). The resulting average inlet temperature to the heat exchanger was considered to be the turbine exit temperature. This value was compared to the measured temperature at the exit of the turbine. The turbine inlet temperature was determined by adding the work of the turbine and the radiated energy from the turbine:

$$T_{\substack{turb \\ in}} = \frac{\dot{m}C_p T_{\substack{turb \\ out}} + \dot{W}_{comp} + q_{rad}}{\dot{m}C_p} \text{ or}$$
$$T_3 = \frac{\dot{m}C_p T_4 + \dot{W}_{comp} + q_{rad}}{\dot{m}C_p} \qquad \text{Eq. 4.2.9}$$

The compressor work and mechanical efficiency are used to approximate turbine work:

$$\dot{W}_{turb} = \frac{\dot{W}_{comp}}{\eta_{mech}} \qquad \text{Eq. 4.2.10}$$

The efficiency of the turbine was the ultimate target of this experiment. The efficiency of the turbine describes how well the turbine performs when compared with an ideal turbine. An ideal turbine is one that does work reversibly and does not generate any entropy, or energy that is not available to perform useful work. The actual work performed by the turbine will be less than what would be performed by an ideal turbine due to mechanical, frictional and other losses. Formulations for efficiency exist for

turbine efficiency in a steady flow that have not been applied to unsteady flows such as those resulting from a PDC. The following formulation uses the ratio of the actual work performed by the turbine to the ideal work performed if the flow was expanded isentropically:

$$\eta_t = \frac{H_3 - H_4}{H_3 - H_{4s}} = \frac{\dot{m}_{avg}\left(C_{p3}T_3 - C_{p4}T_4\right)}{\dot{m}_{avg}\left(C_{p3}T_3 - C_{p4s}T_{4s}\right)} \qquad \text{Eq. 4.2.11}$$

where T_{4s} is the temperature at the exit of the turbine after isentropic expansion and C_{p4s} is the corresponding specific heat. For an ideal gas with constant specific heat, T_{4s} may be found by noticing that the temperature ratio across the turbine is a function of the isentropic compression ratio:

$$\left(\frac{P_3}{P_4}\right)^{\frac{\gamma-1}{\gamma}} = \frac{T_3}{T_{4_s}} \qquad \text{Eq. 4.2.12}$$

This equation can then be solved for T_{4s} producing:

$$T_{4s} = T_3\left(\frac{P_4}{P_3}\right)^{\frac{\gamma-1}{\gamma}} \qquad \text{Eq. 4.2.13}$$

When Eq. 4.2.11 is combined with Eq. 4.2.13, the final efficiency equation used for calculations in this experiment results:

$$\eta_t = \frac{\dot{W}_{turb}}{\dot{m}_{avg}\left(C_{p3}T_3 - C_{p4s}T_3\frac{P_3}{P_4}^{\frac{\gamma-1}{\gamma}}\right)} \qquad \text{Eq. 4.2.14}$$

Figure III-22 helps to display the points in temperature and pressure that are being pursued in this experiment on a temperature-entropy diagram.

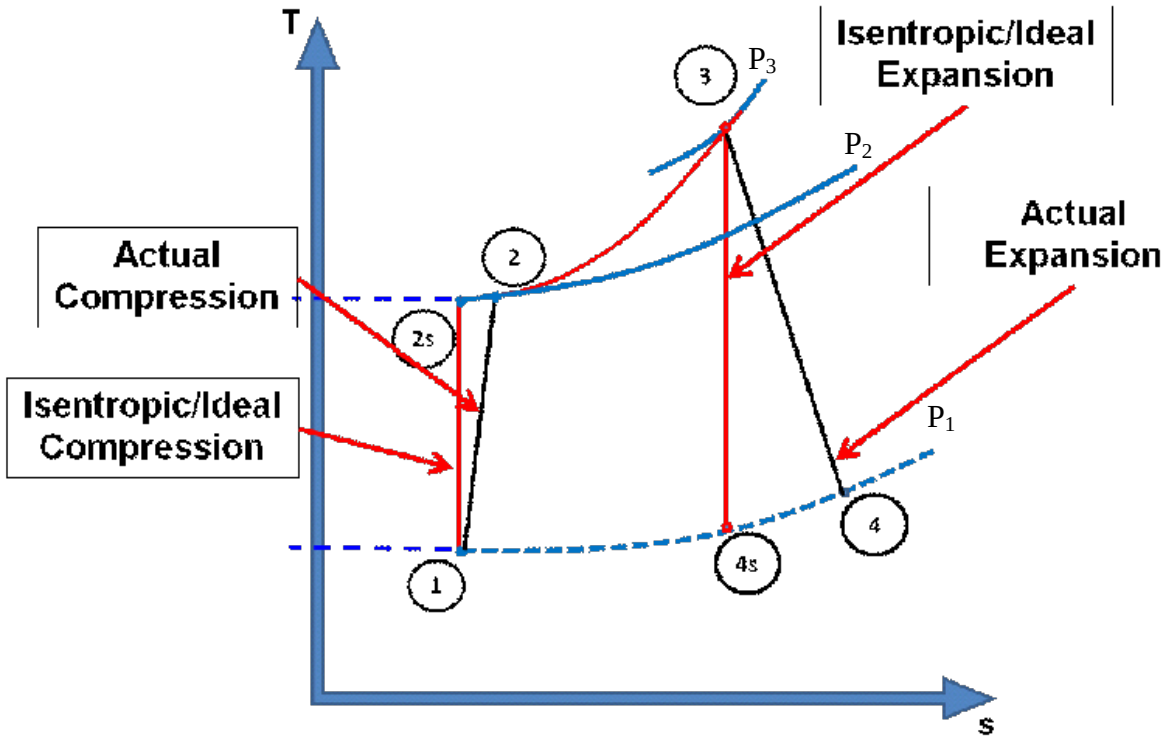

Figure III-22: T-s diagram for compressor and turbine

III.5 Uncertainty Analysis

An uncertainty analysis is necessary to determine the degree of accuracy of the data provided by an experiment. The total uncertainty is the square root of the sum of the bias uncertainty squared and the precision uncertainty squared:

$$e_{Total} = \sqrt{w^2 + p^2} \qquad \text{Eq. 4.2.15}$$

The bias uncertainty can be thought of as how far off a measurement is from the actual value. Holman presents the following formula to determine bias uncertainty:

$$w_R = \left[\left(\frac{\partial R}{\partial x_1} w_1 \right)^2 + \left(\frac{\partial R}{\partial x_2} w_2 \right)^2 + \ldots + \left(\frac{\partial R}{\partial x_n} w_n \right)^2 \right]^{1/2} \quad \text{(Holman 1989)} \qquad \text{Eq. 4.2.16}$$

where w_R is the uncertainty and w_1, w_2, w_n are the uncertainties of each element. Due to the complexity of the formulas used in this analysis, the bias uncertainty will be broken down into parts for ease of calculation.

Representative values were used to calculate the bias uncertainty for this experiment. These representative values are similar to the data that was taken in the experiment, and have a slightly higher error value so that the error reported is conservative.

To determine w_R from Eq. 4.2.16, all of the elemental uncertainties from the system must be addressed. Detailed calculations of the uncertainty values can be found in Appendix F.

The precision error can be thought of as how well the measurement agrees with itself when the actual value being measured is not changing or the randomness of the measurement. For measurements that were recorded electronically with multiple points this is the standard deviation of the samples multiplied by the inverse of the t distribution.

The following table summarizes the uncertainty values for each variable that was analyzed:

Table III-3: Uncertainty values

	bias uncertainty original units (percentage)	precision uncertainty original units (percentage)
Kulite 725 psia pressure transducer	± 36 psia (250)	±0.2 psia (1.4)
Water outlet thermocouple	±1.0 K (5.0)	±1.4 K (7.0)
turbocharger housing thermocouple	±2.5 K (.75)	±7.8 K (2.3)
turbocharger exhaust thermocouple	±4.7 K (.75)	±1.4 K (0.22)
compressor outlet thermocouple	±2.2 K (0.67)	±0.1 K (0.1)
heat exchanger exit thermocouple	±2.2 K (0.4)	±1.8 K (0.7)
water mass flow rate	±.06 gpm (1.0)	±.25 gpm (4.5)
mass flow rate, gas ($\dot{m}_{gas}$)	±1.17E^{-4} kg/sec (0.4)	N/A*
Reynolds number (Re)	±113.6 (0.7)	N/A*
friction factor (f)	±5.5E^{-5} (0.2)	N/A*
Nusselt number (internal) (Nu)	±0.089 (0.2)	N/A*
convection heat transfer coefficient (internal) (h)	±.429 (1.6)	N/A*
heat exchanger purge inlet temperature ($T_{purge\ in}$)	±4.06 K (0.7)	N/A*
Rayleigh number (Ra)	±55300 (1.6)	N/A*
Nusselt number (external) (Nu)	±0.332 (1.1)	N/A*
convection heat transfer coefficient (free convection) (h)	±0.052 W/m K (1.1)	N/A*
heat transfer, convection ($q_{free\ conv}$)	±23.3 (4.6)	N/A*
heat transfer, radiation (q_{rad})	±192 (1400)	N/A*
heat transferred to water (q_{water})	±25.5 W (0.1)	N/A*
average specific heat ($C_{p,avg}$)	±12.2 J/kg K (1.1)	N/A*
turbine inlet temperature (T_{3corr})	±15 K (1.5)	N/A*
ideal turbine exit temperature (T_{4s})	±24 K (1.9)	N/A*
enthalpy gas, out ($h_{gas\ out}$)	±714 W (1.0)	N/A*
heat exchanger inlet temperature ($T_{main+purge,in}$)	±49 K (3.7)	N/A*
compressor work (W_{comp})	±60 W (4.7)	N/A*
turbine work (w_t)	±1408 W (60)	N/A*
turbine efficiency	±.44 (44)	N/A*
* Indicates an extremely small value or does not apply		

IV. Discussion and Results

The data was compiled and analyzed as described in Chapter III and the following trends were noted.

IV.1 Heat Exchanger Inlet Temperature

Utilizing Eq. 4.2.3 and Eq. 4.2.9 the turbine inlet and exit temperatures were calculated and are displayed on the following graphs:

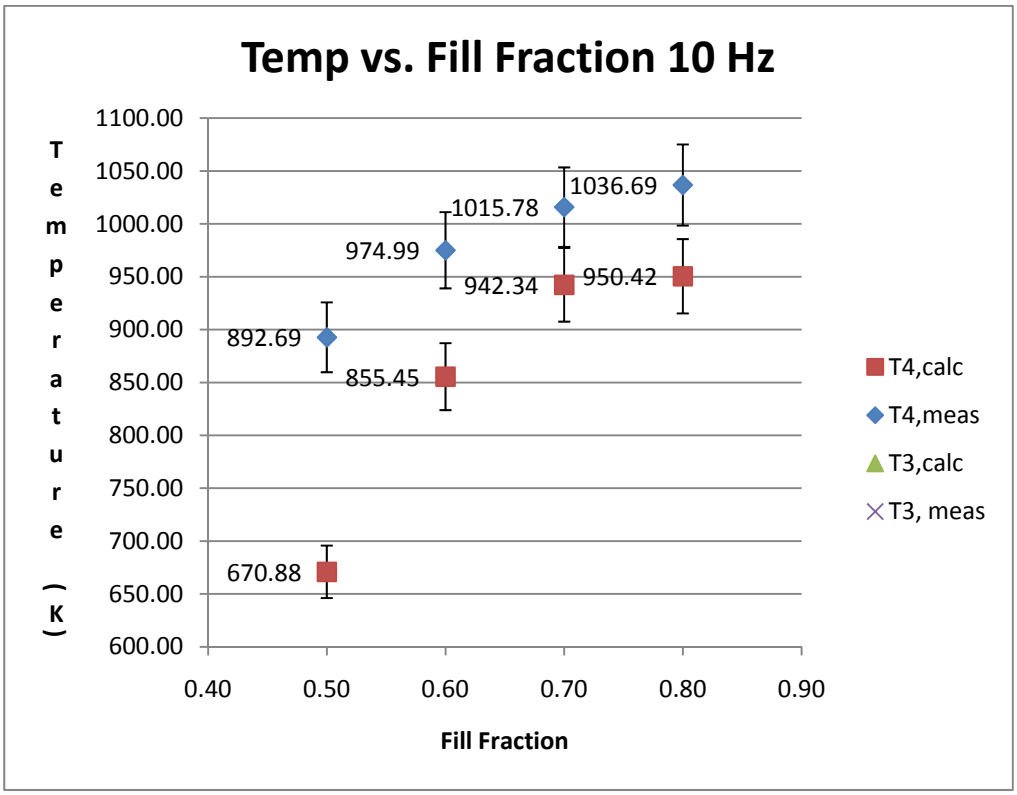

Figure IV-1: Measured and calculated turbine inlet and exit temperature at 10 Hz

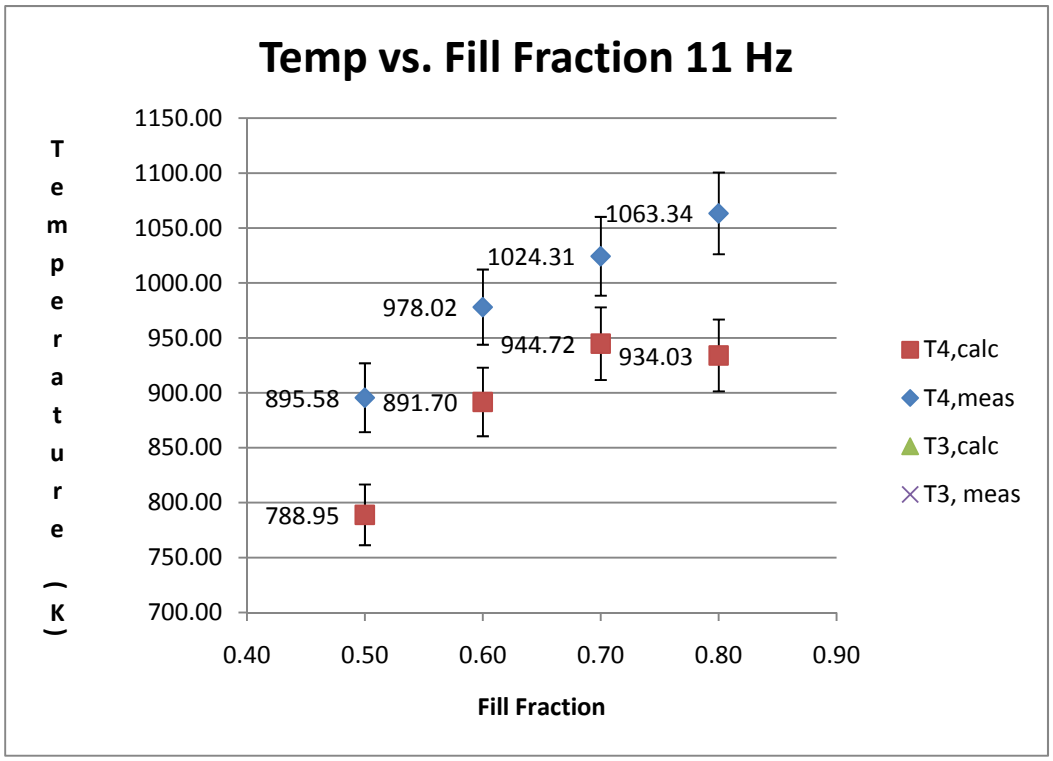

Figure IV-2: Measured and calculated turbine inlet and exit temperature at 11 Hz

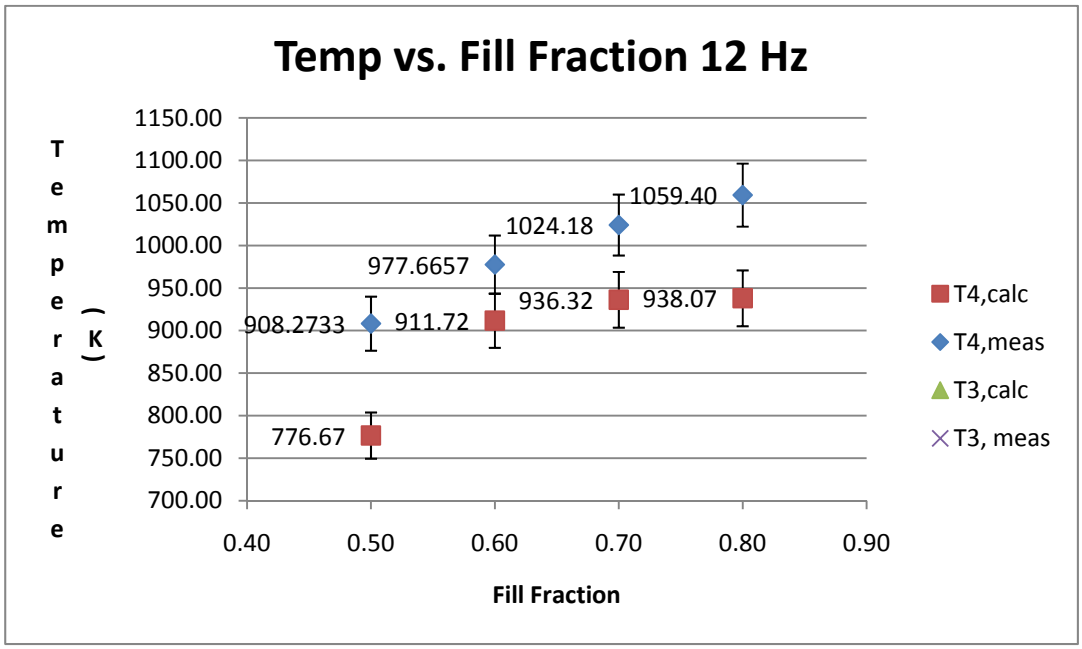

Figure IV-3: Measured and calculated turbine inlet and exit temperature at 12 Hz

In figures IV-1 through IV-3, the $T_{4,meas}$ was the average temperature recorded by the thermocouple at the exit of the turbocharger and $T_{4,calc}$ was the temperature calculated via Eq. 4.2.3. First, it should be noted that for each frequency and fill fraction the turbine inlet temperature was calculated via Eq. 4.2.9, by adding the work performed by the compressor and the heat radiated from the turbine housing. It follows that the changes from T_3 to T_4 measured and calculated are the same for the given frequency and fill fraction.

Due to the lack of data present in the research community in the area of PDC driven turbochargers it was difficult to find a direct comparison to the values derived in this research. Most non-intrusive measurement techniques like optical pyrometry, that capable of resolving temperatures at high speed can only measure temperatures above a certain threshold. For this reason the fire phase of the detonation is the only portion where temperatures were recently found. Based off of available data (K. P. Rouser, P. I. King and F. I. Schauer, et al. 2011) the average temperature at the turbine exit flow during the blowdown phase is approximately 1600 K. This data was recovered at a fill fraction 1.0 and purge fraction of 0.5 at 15 Hz. This average is only over 0.6 milliseconds, which is $1/10^{th}$ of the total time of one cycle at 15 Hz operation. If this data is averaged with a conservative estimate of temperature during the rest of the cycle of 1000 K, the average temperature over a cycle would be 1060 K. This temperature falls very closely in line with what was measured via the thermocouple at the exit of the turbine during the most demanding operating condition (12 Hz, 0.8 fill fraction, 0.9 purge fraction). Using the same approach for the conditions at the inlet of the turbine an average temperature of 1125 K can be estimated. This temperature is also very close to

the turbine inlet temperature calculated based off of the measured exit temperature of 1092 K.

A number of trends are evident in figures IV-1 through IV-3. First, there is an obvious disparity between the measured and calculated inlet temperatures (T3, meas and T3, calc). The measured turbine inlet temperature is expected to be higher than the calculated turbine inlet temperature due to minor energy losses that were not accounted for, but not by such a large margin. This margin is most significant at the lowest fill fraction of 0.5. This margin is mostly due to the relative speeds of the different gases and the fact that they were not well mixed during the runs. As the fill fraction increased the temperature calculated at the inlet of the heat exchanger agreed more with the thermocouple measurement at the inlet. This is due to the fact that as the fill fraction increased, the purge fraction remained the same. At a larger fill fraction the blow down event makes up a larger portion of the exhaust flow. The purge fraction at this larger fill fraction has less time to oscillate and is in contact with the thermocouple for a shorter period of time in comparison to the same purge fraction at the smaller fill fraction. This results in more heat from the blow down gas being transferred to the thermocouple and less from the purge gas and an overall more accurate temperature.

Via the Schlieren imagery produced in this experiment, it was observed that the flow is still segregated at the exit of the heat exchanger. The turbine helps to mix the flow, but even after passing through the turbine , it is evident that the hot gas is moving much faster and is present in the frame for a much shorter period of time (approximately $1/6^{th}$ of the cycle at 10 Hz). The Schlieren videos also showed that cooler, ambient air was actually moving back into the heat exchanger in between fire phases due to the low

pressures in the tube at the exit of the heat exchanger caused by the blow down gas as it exited the heat exchanger. As the pressure in the tube equalizes, the purge flow expanded across the heat exchanger and the extension pipe. This expansion in combination with the faster moving hot gas results in the lower temperature purge flow contacting the thermocouple for a longer period of time in comparison to the blow down gas. This causes the thermocouple to record a lower overall temperature than what is thought to be the average of the two. Figure IV-4 shows the density gradient at the exit of the heat exchanger. From this imagery it is evident that the flow is being pulled in from above and below the pipe as is indicated by the density gradients curving around the edges. From watching the video at reduced speed it also becomes apparent that the hot gas from directly in front of the pipe is also being pulled back in.

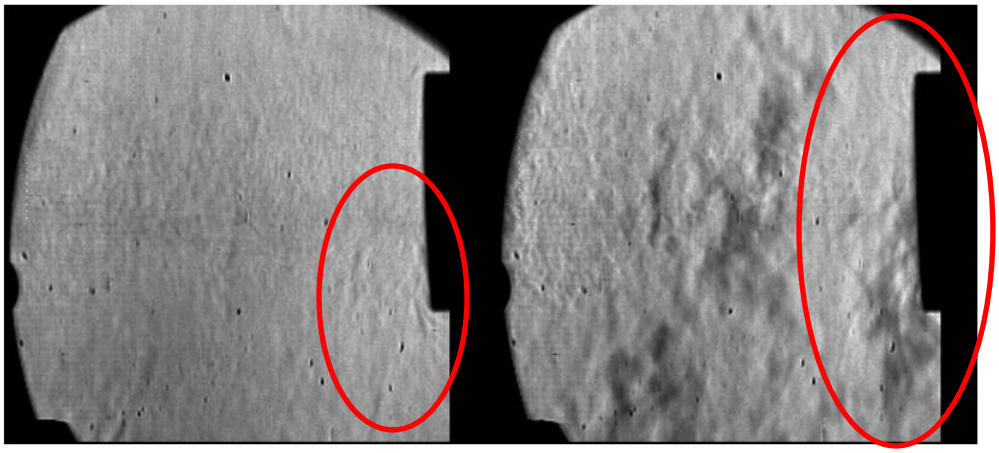

Figure IV-4: Schlieren images indicating suction at exit of heat exchanger while operating at 10 Hz, 0.5 fill fraction and 0.9 purge fraction

Looking at the differences between the calculated and measured temperatures in figures IV-1 through IV-3 it becomes apparent that the higher frequency data produces measurements slightly more in line with what the thermocouple records. The increased

agreement is likely due to the fact that the pressure does not have as much time to oscillate as the next blow down phase arrives faster.

If the pressure oscillation is traveling at the speed of sound, which is approximately 400 m/s at 400 K, it would take it approximately 0.015 seconds to reach the opposite end of the heat exchanger. This means that at 10 Hz, with no obstructions the pressure oscillation would be able to travel up and down the heat exchanger approximately five times before the next fire phase exits. The number of oscillations is actually reduced, as the next mass of exhaust products is moving towards the exit and the pressure equilibration process taking place is interrupted by the next blow down phase. In fact at 10 Hz operation and a fill fraction of 0.5 approximately three pressure oscillations are observed in the Schlieren video. As frequency increases, these oscillations have less of a chance to reach back to the thermocouple located at the exit of the heat exchanger. At approximately 65 Hz operation, the pressure pulse would not be able to travel the length of the steel extension pipe back to the thermocouple in time to beat the next mass of exhaust products. At this elevated frequency the heat exchanger would likely become a more accurate tool for measuring inlet temperature. It is evident from the results above that smaller frequency increases help slightly with accuracy.

The side effect of reduced suction with increasing frequency is also evident in the Schlieren videos. When comparing the 10 Hz operation to the 15 and 20 Hz operation, it becomes immediately apparent that the length of time the flow is retreating into the tube decreases as frequency increases. When comparing the exhaust flow of the PDE driven turbo and the PDE alone, it is evident that the addition of the turbocharger reduces the amount of time the flow reverses direction and moves back into the tube.

The addition of the turbocharger also has the effect of mixing the flow. Originally it was assumed that over the length of the heat exchanger that the hot gas from the fire phase and the cooler flow from the purge phase would mix significantly inside the heat exchanger, however it appears that without the turbocharger, the flow is still considerably segregated. The stratification of the flow is evidenced by the darker lines in the Schlieren video, signifying larger density gradients that follow immediately behind the shock as it exits the exhaust tube. As the suction occurs, the lines become lighter as the tube pulls cooler air back inside. The thick dark lines are not noted again until the next shock wave leaves the tube. Suction was observed at the exit of the heat exchanger for approximately .045 seconds per cycle or 45% of the cycle time at 10 Hz operation with a fill fraction of 0.5.

IV.2 Work Calculations

Compressor work was calculated from Eq. 4.2.7. All values in this calculation were measured directly and turbine work was calculated using Eq. 4.2.10. The change in energy across the turbine was also calculated as:

$$E_{flux} = \dot{m}_{turb}\left(C_p T_{3_{corr}} - C_p T_4\right) \qquad \text{Eq. 5.1.1}$$

where T_3 was calculated using Eq. 4.2.9. The following graphs display the results:

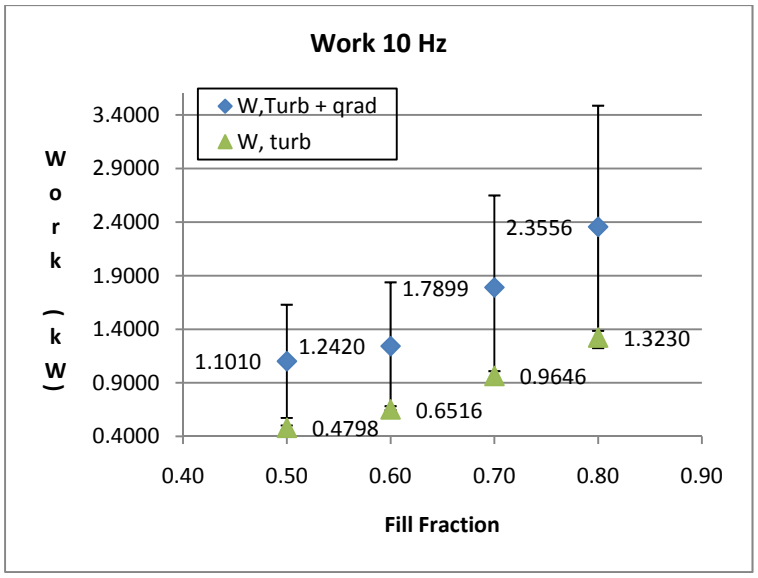

Figure IV-5: Turbine work and radiation at 10 Hz operation

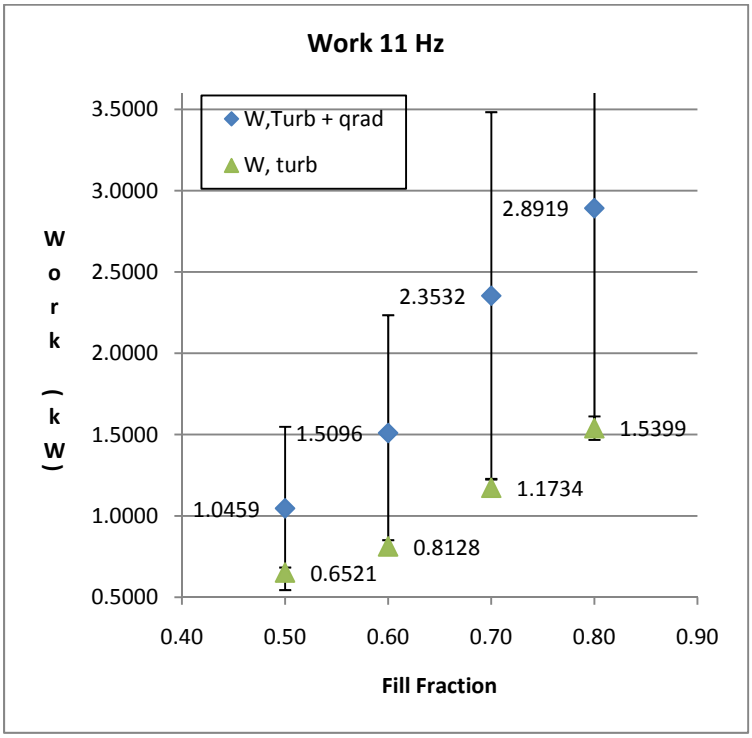

Figure IV-6: Turbine work and radiation at 11 Hz operation

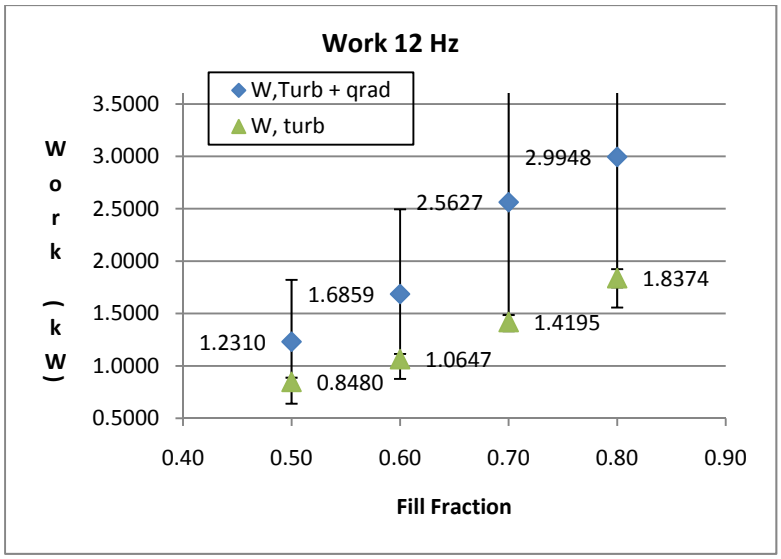

Figure IV-7: Turbine work and radiation at 12 Hz operation

The first trend noted is increasing work with increasing fill fraction and frequency. This trend is consistent with conclusions from other work at AFRL (K. P. Rouser, P. I. King and F. R. Schauer, et al., Unsteady Performance of a Turbine Driven by a Pulse Detonation Engine 2010). Based off of this work it would be reasonable to achieve increased turbine and compressor work as more fuel and air is being combusted at higher fill fractions and frequencies. Using the turbine work numbers and dividing by mass flow provides specific work which is a better unit for comparison:

Table IV-1: Specific work for varying fill fractions and frequencies

Fill Fraction	Purge Fraction	frequency		
		10 Hz	11 Hz	12 Hz
0.5	**0.9**	0.123	0.153	0.179
0.6		0.158	0.179	0.217
0.7		0.222	0.246	0.276
0.8		0.289	0.307	0.336
1.0	**0.5**	0.288*	0.334*	0.368*
*Reported in other work (K. P. Rouser, P. I. King and F. R. Schauer, et al., Unsteady Performance of a Turbine Driven by a Pulse Detonation Engine 2010)				

Comparing the values of specific work with what was reported recently at a fill fraction of 1.0 and purge fraction of 0.5 there is a good agreement. Agreement is expected considered the values were measured in a similar fashion.

One might expect that as fill fraction and frequency increase the specific work would remain relatively constant because the work increases, but the mass flow rate is increasing as well. This increase in specific work is likely due to reduced losses at higher rotor speeds. As the rotor turns faster the momentum becomes larger in proportion to the friction acting against it.

The Eflux term is substantially larger than the work term, and this is mainly due to the added radiation. It would be expected that the radiation term would increase linearly because the temperature of the turbine increases in a fairly linear fashion as fill fraction increases. The nonlinearity of the turbine Eflux term is mainly due to the fact that the radiation equation utilizes the surface temperature raised to the fourth power. After considering this, the fact that the Eflux term always remains approximately 50% above the turbine work term makes more sense.

The large value of the Eflux term would indicate that the turbine cannot be considered as adiabatic or the efficiency term will be artificially inflated as there is a large portion of energy that is being leaving the flow, but isn't generating any work.

IV.3 Efficiency

The overall goal of this experiment was to help determine efficiency for a turbocharger driven by unsteady flow. To that end, both the measured (via the thermocouple at the exit of the turbocharger) and the calculated (via the heat exchanger and first law analysis) turbine exit temperatures and their respective turbine inlet temperatures (calculated based off of turbine work) were used to compute a notional efficiency. To compute efficiency the pressure ratio across the turbocharger was varied and the rest of the variables were held constant in the following analysis. The actual pressure data that was recorded using the 725 psia pressure transducer was not used for this analysis due to the magnitude of its uncertainty value. All efficiencies were calculated using Eq. 4.2.14. For each fill fraction, the same turbine work term was used. The charts below show the effect of turbine pressure ratio on thermal efficiency when turbine temperature ratio and mass flow rate are held constant:

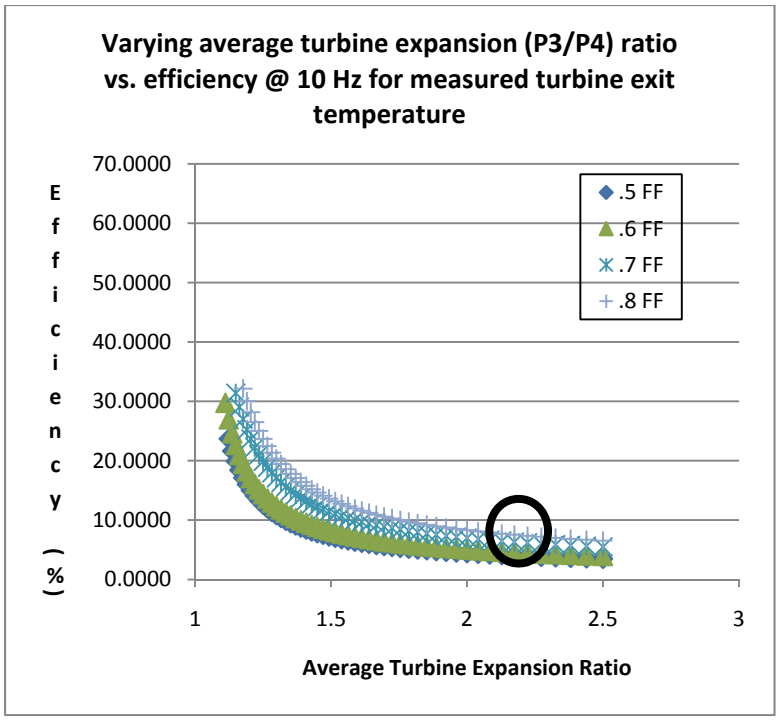

Figure IV-8: Average turbine expansion ratio versus efficiency for 10 Hz operation using measured turbine exit temperature and calculated turbine inlet temperature

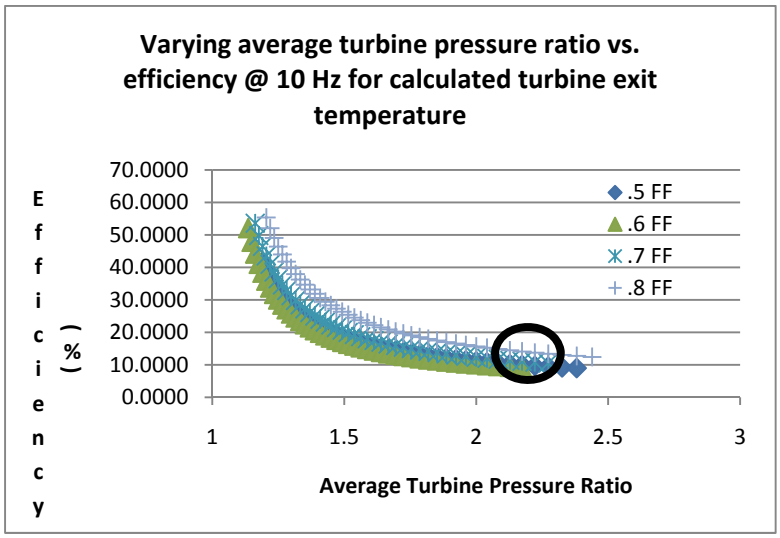

Figure IV-9: Average turbine expansion ratio versus efficiency for 10 Hz operation using calculated turbine exit temperature and calculated turbine inlet temperature

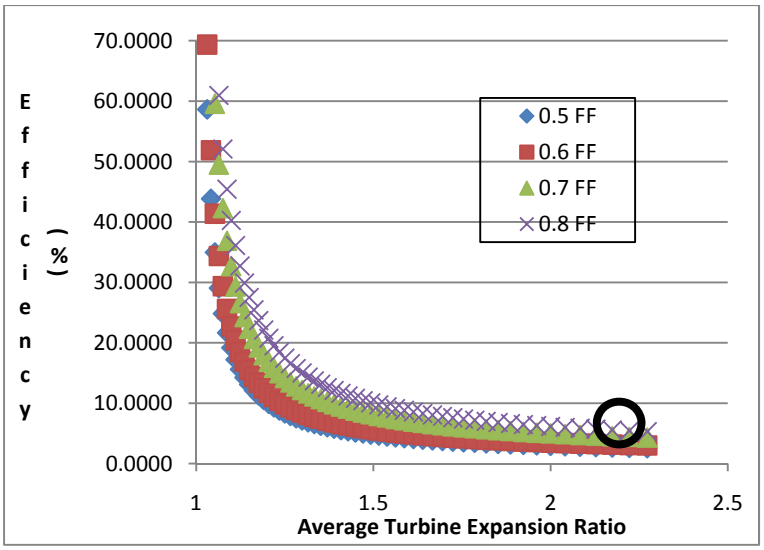

Figure IV-10: Average turbine expansion ratio versus efficiency for 10 Hz operation using measured turbine exit temperature and measured turbine inlet temperature

In Figure IV-8 the turbine inlet temperature (T_3) used to calculate efficiency resulted from Eq. 4.2.3 and adding the turbine work. Figure IV-9 the efficiency was calculated using the turbine inlet temperature from the measured turbine exit temperature and adding the turbine work. Finally in Figure IV-10 the turbine inlet temperature used was measured at the exit of the PDC when the turbine was not present.

The first and most obvious trend in the efficiency calculations was a significant drop in efficiency with increasing pressure ratio. At first this seems counter intuitive and that increasing pressure ratio should increase efficiency. It must be noted that this is for a given turbine inlet and exit temperature. If the turbine inlet and exit temperature corresponded to each pressure ratio, the trend in the charts would be inverted, that is to say that efficiency would increase with increasing pressure ratio.

The next trend observed in Figure IV-9 is that as fill fraction increases from 0.5 to 0.6 the efficiency decreases, but increases from 0.6 to 0.8. It should be noted that this

variation is within the uncertainty of the reported efficiency. The overall trend noted in the three figures increasing efficiency with fill fraction. This trend falls in line with the trend of increasing specific work with increasing fill fraction, noted in the previous section. As the fill fraction increases, the turbine will see an increasing mass flow and as a result will be choked for a larger portion of the cycle. The longer the turbine is choked, the higher the efficiency would become, until it is choked for the entirety of the cycle where efficiency should level off.

Recently, time accurate data was recorded for pressure across a PDC driven turbocharger at 15 Hz with fill and purge fractions of 1.0 and 0.5 respectively. When the inlet and exit pressures were time averaged separately and then divided, the result was an average pressure ratio of 2.22. Extrapolating the trend of increasing fill fraction and applying it to this data would yield an approximate efficiency of 10%.

For a T3 turbine, the maximum efficiency possible is approximately 72% which occurs when the flow is choked. It can be said with certainty that the flow through the turbine is choked at a pressure ratio greater than 2.3. The time accurate data is presented below.

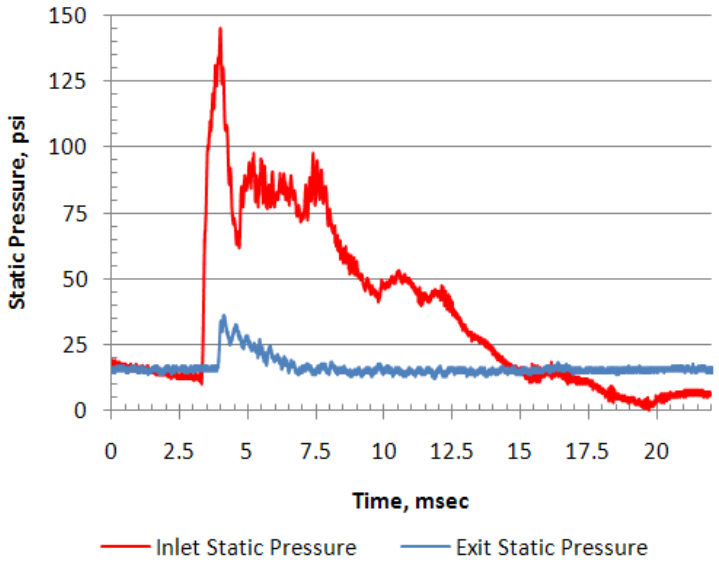

Figure IV-11: Time accurate turbine inlet and exit static pressure at 15 Hz with fill and purge fractions of 1.0 and 0.5 respectively over one cycle (K. P. Rouser, P. I. King and F. I. Schauer, et al. 2011)

The average pressure ratio of the time accurate data indicates that more than 50% of the time the turbine is unchoked, meaning the efficiency of the turbine will be below 72%. It is also apparent from the time accurate data that for a portion of the cycle the pressure ratio is actually negative. Taking into account the portion of time the turbine is unchoked and negative an efficiency of 10% is not unreasonable.

IV.4 Fill Fraction Disparities

As the detonation tube temperature increases, the density of the fuel/air mixture decreases. The decreasing density results in a disparity between perceived and actual fill fraction. At the beginning of a run, a voltage drop over the first ion probe and lack of change in voltage over the successive ion probes were noted which indicated a fill

fraction of approximately 0.5. As the tube temperatures rose, voltage drops across the second and even third ion probes were noted. For example, a test run began and ion probe data shows the fill fraction to be ~0.5:

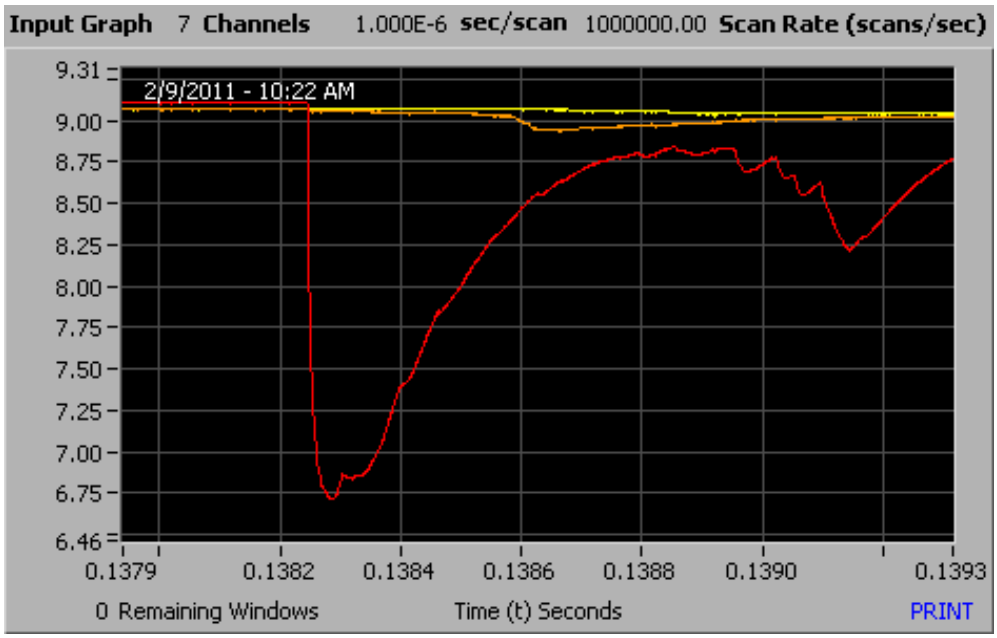

Figure IV-12: Ion traces showing fill fraction of 0.5 at run start

As the detonation tube reaches equilibrium temperature (approximately 680 F for this configuration), the reactants expand at an increasing rate when entering the detonation tube. Therefore, due to the increased temperature, density is reduced and the reactants occupy an increased volume of tube prior to detonation. This increased volume registers on the next ion probe as it detonates, implying an increased fill fraction:

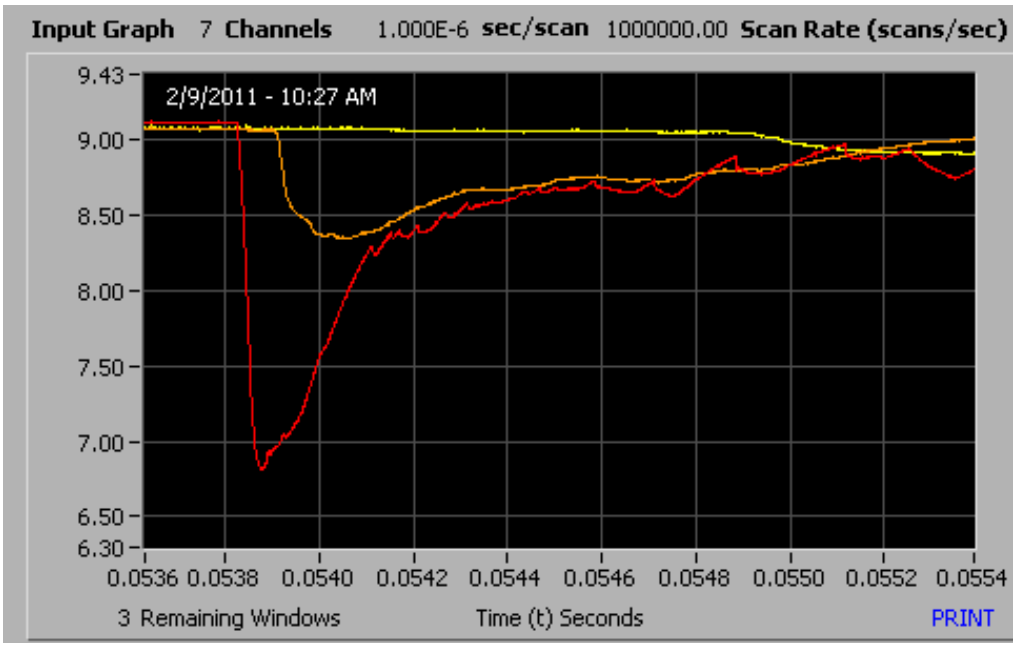

Figure IV-13: Ion traces at equilibrium for the same run showing increased fill fraction

This phenomenon is unavoidable for extended duration runs without changing mass flow rate. In an effort to reduce the variability between configurations, mass flow rate was kept constant. Due to the fact that the Lab View software computes fill fraction based off of the tube volume input by the user, the mass flow rate of the main and purge flows did not change over the course of a given run. Therefore, the user need only to input the measured tube volume, fill fraction, purge fraction and frequency and the software would provide the necessary mass flow rate, regardless of back pressure placed on the system (by the heat exchanger and/or turbocharger).

To ensure that the detonations were still occurring at these equilibrium conditions, wave speed was measured at equilibrium:

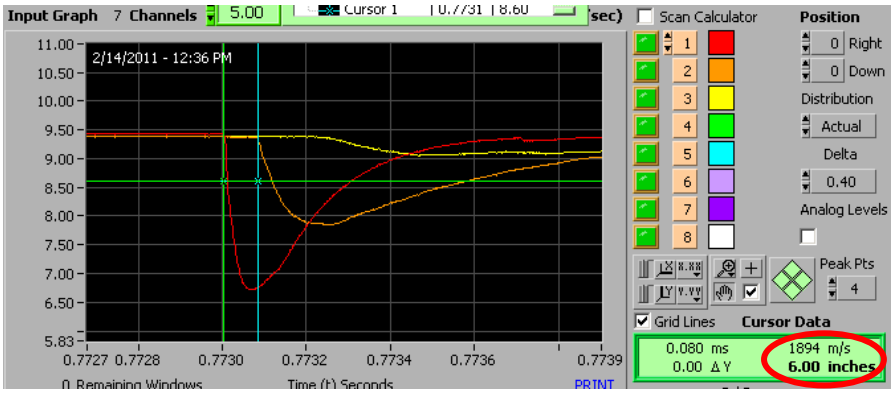

Figure IV-14: Ion traces at equilibrium with wave speed calculated indicating Chapman-Jouget velocity for hydrogen and air at stoichiometric conditions

For hydrogen and air at stoichiometric conditions, typical Chapman-Jouget velocities are approximately 1970 m/s(Schultz 2000). For the drop over the first two ion probes (located at 18.5 and 24.5 inches respectively), the wave speed was approximately 1900 m/s for a fill fraction of 0.5, indicative of detonation. The wave speed calculated between the second pair of ion probes, located at 24.5 and 33 inches respectively was consistently above 1800 m/s. The drop at the third ion probe was not nearly as sharp due to the fact that it was located just behind the s-curve in the detonation tube. As the shock wave traveled around the curve of the tube, it began to round as did the combustion front traveling behind it. As it turned around the s-curve the combustion front and the shock began to decouple, meaning that the detonation was weaker. As the shock rounded, the perceived wave speed decreased slightly and the voltage drop became distorted. The voltage drop across the ion probe was distorted because a decreased number of ionized particles were passing over the probe. This slower wave speed is indicative of a weaker detonation.

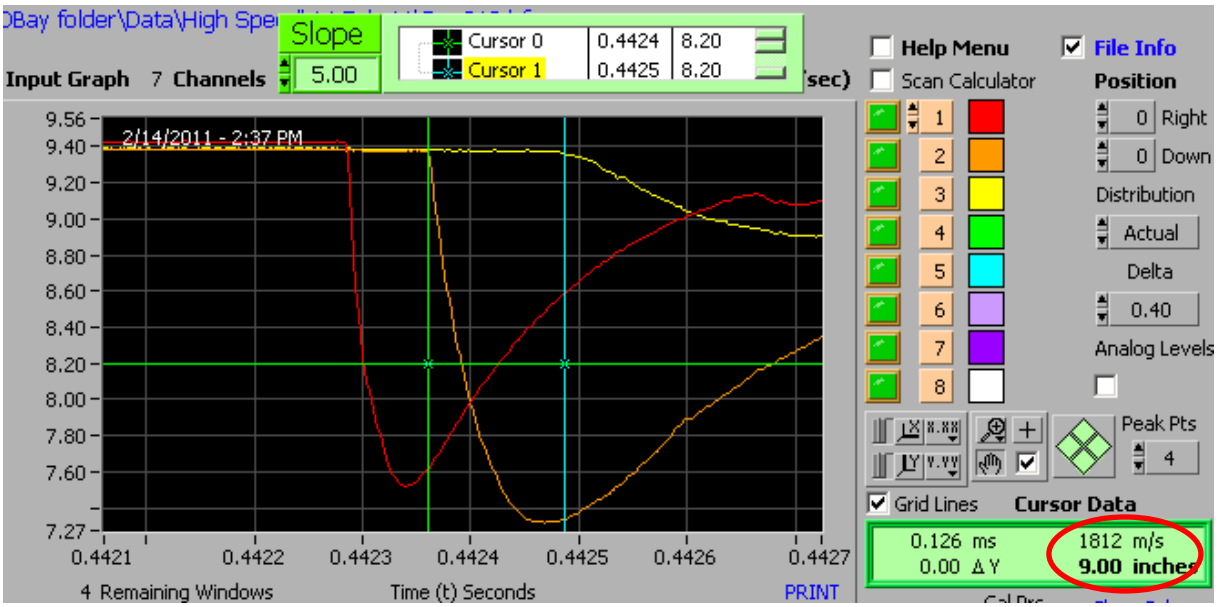

Figure IV-15: Ion probe voltage traces for ten Hz operation at desired fill fraction of 0.5 indicating detonation waves speeds at ~70% of tube length

The phenomenon of tube heating on increasing actual fill fraction has been documented in previous experiments where using a desired fill fraction of 0.34, detonation wave speeds at 70% tube length and combustion events at 80% tube length were documented (Paxson, et al. 2011). From this data it is reasonable to assume that even at a desired fill fraction of 0.5 the actual fill fraction was well over 0.7 and possibly into the turbine.

In this experiment, at a fill fraction of 0.5 the ion probes indicated detonations occurring at a length corresponding to a fill fraction of 0.69. The fact that detonations were still occurring this far down the tube implies the likelihood that combustion and possibly even detonation was occurring in the turbocharger and possibly even the heat exchanger itself. Combustion and or detonations occurring inside and/or past the turbine would have the effect of artificially increasing the measured thermal efficiency if

temperature upstream of the turbine were measured directly. The artificially increased efficiency is due to the combustion taking place after the flow enters the turbine or after it exits. In this scenario it would appear that the temperature at the exit of the turbine is higher than if combustion were complete before the flow entered the turbine. Burning into or past the turbine may even cause the temperature at the exit of the turbine to be higher than the temperature at the turbine inlet, creating efficiencies greater than 100%. To the contrary, such a situation would actually greatly reduce the efficiency of the turbocharger, as the turbine would not have the opportunity to extract energy from the flow as it burns after passing through. To prevent this issue future experiments should include an ion probe at the entrance and possibly even at the exit of the turbine to determine if combustion is still occurring.

IV.5 Phase Change

It was learned over the course of experimentation that during PDC operation, the water in the PDC exhaust products was condensing inside the heat exchanger. The fact that the water was condensing meant that a phase change was taking place inside of the heat exchanger that was previously unaccounted for. As the water vapor in the exhaust gas condenses on the surface of the heat exchanger it releases energy into the surface which is transferred into the coolant in the heat exchanger. This energy released needed to be accounted for in the calculation of the inlet temperature or the condensation needed to be avoided.

Another side effect of the vapor condensing on the heat exchanger walls was a reduction in heat transfer coefficient. The water acts as another barrier between the hot gas and the liquid coolant that serves to remove heat, much like fouling in a heat exchanger, this is due to the relatively low conductivity of water (~.6 W/m K) in comparison to aluminum (~180 W/m K). The fact that the water releases a significant amount of energy (2257 kJ/kg) as it changes phase has the effect of overshadowing the reduced convection coefficient due to the fouling effect.

In an attempt to avoid condensation on the inner wall of the heat exchanger, the length of the heat exchanger was halved. This shorter heat exchanger gave the exhaust gas less surface area to contact and transfer heat over, resulting in increased average exhaust gas temperatures. This hotter flow caused increased temperatures at the heat exchanger wall. The assumption was that the wall temperature would be above the boiling temperature of water (373 K/212 F) so that when the water vapor made contact with the wall it would not condense there.

After multiple runs with the ten foot long heat exchanger over varying set points, no water was observed exiting the heat exchanger during equilibrium. To further justify that water was not collecting inside the heat exchanger a simplified analysis was conducted. Using the knowledge that:

$$q = \dot{m} C_p \Delta T$$

It is possible to calculate the heat removed by the water. This number was calculated at ten Hz for fill fractions of 0.5 and 0.8 without the turbocharger. Due to the relatively

small thickness of the aluminum wall and the high conductivity of the aluminum, the temperature gradient across the wall will be very small, so it can be assumed that the temperature on one side of the wall will be approximately the same as the temperature on the other side of the wall. To determine the change in temperature from the gas flow to the hot wall the following formula was manipulated:

$$q = hA\Delta T$$

where the heat transfer was removed by the water. The following table summarizes the results:

Table IV-2: Heat transfer comparison for fill fractions of 0.5 and 0.8

fill fraction	0.5	0.8
q_{water} (W)	22172	32120
h (W/m^2 K)	350	350
ΔT (K)	87	125
average hot gas temperature (K)	603	791
average hot wall temperature (K)	516	665

Both of the resulting average hot wall temperatures are well above the boiling point of water (373 K).

The temperatures measured at the exit of the heat exchanger via a J-type thermocouple supported this argument. At the exit of the heat exchanger, with the turbine in the flow, exhaust gas temperatures ranged from 394 K to 573 K and pressures measured at the exit of the heat exchanger were slightly below atmospheric ranging from 13.6 psia to 14.2 psia. The temperatures and pressures recorded would not support condensation.

The lowest temperature noted was 394 K at 14.1 psia when the PDC was running at 10 Hz and 0.5 fill fraction. At this pressure the water in the exhaust products would need to drop to 371 K or 23 K below the temperature observed in order to condense. Due to the temperature difference from the gas temperature measured in the centerline of the flow to the wall of the heat exchanger, there may have been water condensing inside the heat exchanger, but the temperatures at the exit of the heat exchanger would still have been high enough to re-evaporate any water that might have condensed on the walls. Due to the control volume approach of this technique, the water condensing and evaporating inside of the heat exchanger should not affect the calculated temperature at the inlet of the heat exchanger.

IV.6 Startup/Shutdown Transient

Another phenomenon that was exposed during experimentation was a significant increase in heat exchanger exhaust gas temperature after detonations were terminated. One example of this occurrence can be seen in Figure IV-16. The temperature rose for 25 seconds after shutdown before it began to cool. Heat exchanger exhaust gas temperature peaked at 231 F, about 52% higher than the maximum temperature measured while detonations were occurring. For all experiments with the original 20’ long heat exchanger, the PDC was allowed to run for more than seven minutes, to allow for a steady measurement to be recorded. Upon shutdown of the PDC, cooling air was still flowing through the detonation tubes at the same temperatures and pressures as it would

if the PDC were operating without a spark. This temperature spike was prevalent in every run 10 and 15 Hz run at a fill fraction of 0.5.

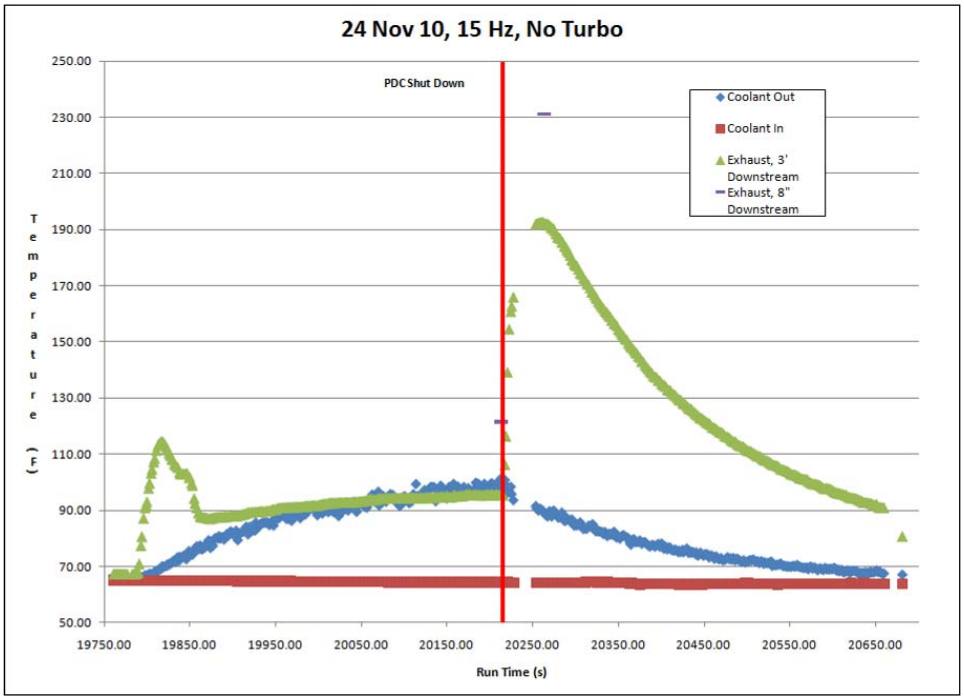

Figure IV-16: Shutdown transient temperature spike

Though the exhaust temperature of the heat exchanger was increasing after detonations ceased, it should be noted that the water temperature did decline as expected, and the overall calculated inlet temperature also recedes. The calculated inlet temperature during the startup and shutdown of the PDC are much less reliable as the experiment has not reached a steady state condition, therefore the energy storage term is changing. However, it is not the value, but the trend that is important. The decline in heat exchanger inlet temperature indicates an overall reduction in the energy into the system.

The higher temperature readings at the exhaust of the heat exchanger after shutdown are unexpected because the flow entering the detonation tube is slightly above ambient conditions and moving at subsonic speeds. The slower, colder flow, that spends more time in contact with the heat exchanger, would be expected to produce lower exhaust temperatures than during PDC operation. This phenomenon is possibly caused by a decreased convective heat transfer coefficient after shutdown. Convective heat transfer coefficient is a function of Nusselt number, which is lower during purge and after shutdown (similar to purge) than during the blow down phase.

There are a number of factors that need to be considered with the convective heat transfer coefficient. The Nusselt number, seen in Eq. 5.1.9, is a function of Reynolds number, Prandtl number and friction factor. The Reynolds number, which is the ratio of inertial forces to viscous forces, can be defined as:

$$\mathrm{Re} = \frac{\rho u_{\infty} L}{\mu} \qquad \text{Eq. 5.1.2}$$

In the transition from blow down to purge, L, the reference length (in this case the length of the wall of the heat exchanger) does not change. The velocity increases by an order of magnitude and the density decreases slightly. The following table illustrates a simple comparison of the two conditions to show why the heat transfer coefficient, and therefore the energy transferred to the heat exchanger would be increased during blow down:

Table IV-3: Simplified comparison of blow down phase and purge phase heat transfer

	blow down	purge
pressure (Pa)	506625	101325
temperature (K)	1200	560
density (kg/m^3)	1.47154932	0.630664
velocity (m/s)	30	5
conductivity (W/m K)	0.078889806	0.04389
viscosity (N s/m^2)	4.79474E-05	2.9E-05
Prandtl number	0.721889856	0.689562
Reynolds Number	1.40E+06	1.66E+05
friction factor	0.01098332	0.016213
Nusselt number	1530.321435	262.9776
convection heat transfer coefficient (W/m K)	1584.3407	151.4709
average convection heat transfer coefficient (W/m K)	356.1665726	
heat transferred (W)	421950.2515	-30393.6
total heat transfer (W)	34226.97906	
actual heat transferred (from water) (W)	~34000	

This comparison simplifies the analysis by assuming a uniform, average temperature of the purge and blow down gas temperatures and the wall temperature. The wall temperature is assumed to be 835 K. The diameter, circumference and surface area used in this calculation were all based off of the ten foot heat exchanger used in later experimentation.

In this simplified comparison the pressure during blow down is assumed to be approximately five atmospheres, which is consistent with previous results (B. H. Schauer et al. 2003), while the purge pressure is estimated to be atmospheric. The temperature during blow down is estimated to be 1200 K (a conservative estimate) when it reaches the heat exchanger, while the purge temperature used is the same as what is calculated in Appendix C. The density is calculated directly assuming the working fluid is an ideal gas (air) with gas constant 286.9 (J/kg K). The velocity during blow down is estimated to be

six times faster than the purge flow. The conductivity, viscosity and Prandtl number are all based off of the associated flow temperature. The Reynolds number, friction factor, Nusselt number and heat transfer numbers are all calculated based off of the previously mentioned values and the equations used in Appendix A. The average heat transfer coefficient and average heat transferred values are velocity averaged, meaning that because the velocity of the blow down is six times higher than the purge velocity, the blow down heat transfer coefficient is multiplied by one seventh and the added to the purge heat transfer coefficient which is multiplied by six sevenths. The total heat transferred is calculated in the same manner, using the heat transferred during each phase and multiplying by the velocity coefficient.

The resulting heat transfer coefficient and heat transfer is significantly increased during the blow down phase. Based off of this analysis, the heat transferred during the purge phase is actually negative, meaning that the purge air is cooling the inner wall of the heat exchanger. It should be noted that the average heat transferred (34.2 kW) is in the range of what was calculated to be removed by the water during testing which was between 22 kW and 35 kW.

It is also hypothesized that the pressure oscillation had a great deal to do with the temperature spike at shutdown. The temperature spike was more prevalent with the twenty foot long heat exchanger. The pressure oscillation was constantly pulling cool air back into the heat exchanger for a larger portion of every cycle during operation, creating a cooling effect over the thermocouple. When the PDC stopped detonating, the pressure oscillation almost completely disappeared and as a result the thermocouple is in contact with a more consistent flow temperature associated with the purge flow that is heated by

the detonation tube. This flow temperature is actually hotter than what the thermocouple at the heat exchanger exit was in contact with on average during operation.

The temperature spike was significantly reduced and observed when operating with the 9.5 foot extension at the exit of the heat exchanger at lower frequencies and fill fractions. In the same configuration at higher frequencies and fill fractions the temperature spike was not observed was not noticeable. The temperature spike was not present because the average flow temperature registered by the thermocouple was greater than the purge flow temperature, even after PDC tube heating.

IV.7 Analytical Errors and Corrections

After stepping back from analysis, it appears that there were four main causes of error in the analysis of data for this experiment: pressure oscillations and flow speeds, water condensing in the heat exchanger, water mass flow rate inaccuracy and water outlet temperature precision. These issues were evaluated at 10 Hz and a fill and purge fraction of 0.5 and 0.9 because this is where the largest disagreement was found between the calculated and measured values. The evaluation looks at a maximum value that would be expected if the error were corrected and possible solutions to correct for the error, either analytically or experimentally. The results of this evaluation are located in the table below:

Table IV-4: Leading causes of error, adjusted values and possible solutions

issue	temperature (K)	change	possible solution
thermocouple contact ratio	932 (+39% from 670 K) (+4.5% from 892 K)	1:1 vs. 1:6 blow down: purge	increase frequency/mass flow rate,
heat exchanger condensation	553 (-18% from 670 K)	0% to 100% relative humidity	increase exhaust gas temperature
water flow rate	688 K to 664 K (+2.7% to -0.9% from 670 K)	+.25 gal/min to -.25 gal/min	increase water flow rate, increase accuracy of meter
water temperature	738 K to 614 K (+10% to -8.4% from 670 K)	+2 K to -2 K	decrease water flow rate
Original calculated heat exchanger inlet temperature was 670 K and the measured value was 892 K			

The first and largest cause of error evaluated was the lack of accounting for the variance in the speed of the flow and the ratio of time each portion of the flow spends in contact with the thermocouple. Due to the determination that the flow is still segregated as it passes over the thermocouple, the blow down and purge flows spend a varying length of time in contact with the thermocouple. Through observation of the Schlieren video it was determined that the blow down gas spends approximately $1/6^{th}$ of the cycle in the frame, while the rest is significantly cooler gases. It is reasonable to assume that the flow at the exit of the heat exchanger exhaust pipe is very similar to what is seen at the thermocouple at the exit of the heat exchanger, therefore this was the assumption. A very simplified analysis was used to determine a corrected value. The evaluation started by estimating the temperature of the blow down gas to be 2500 K based off of recent high speed measurements (K. P. Rouser, P. I. King and F. I. Schauer, et al. 2011). It was also estimated that the purge gas entered the heat exchanger at the temperature approximated by the original calculations of 382 K. At this point it was estimated that all of the energy transferred into the water was done so by the blow down gas. The energy transfer would bring the temperature of the blow down gas to 1945 K. The purge temperature would

likely increase slightly, removing energy from the heat exchanger inner wall, so it is estimated to be 400 K when it reaches the thermocouple. Applying the ratio previously mentioned it is possible to calculate an average heat exchanger exit temperature yields 657 K versus what was measured at 393 K:

$$T_{\substack{avg \\ HX \\ exit}} = \left(T_{blowdown}\right)\left(\frac{1}{6}\right) + \left(T_{purge}\right)\left(\frac{5}{6}\right)$$

$$= \left(1945\ K\right)\left(\frac{1}{6}\right) + \left(400\ K\right)\left(\frac{5}{6}\right) = 657\ K$$

This temperature is now applied to the original heat exchanger analysis via the method described in section III.4. The resulting average heat exchanger inlet temperature after applying this correction is 932 K. This value is approximately 4.5 % higher than the measured temperature, and is in much better agreement with the measured value.

This issue could be corrected analytically as discussed in the previous paragraph or experimentally by increasing the frequency of operation, and/or mass flow rate of the fuel-air mixture. Increasing frequency would increase the speed that the purge gas is pushed through the tube by the blow down, and the ratio would be closer to 1:1. Increasing the mass flow rate of the main fuel-air mixture would increase the volume of the blow down phase and as a result the thermocouple would be in contact with the hot gas for a longer period of time and record an increased temperature. The main fill fraction was varied during the experiment and this increasing temperature was verified.

The next issue that was analyzed was the possibility of water condensing in the heat exchanger. In order to approximate the difference in average heat exchanger inlet temperature if condensation were occurring the worst case scenario was considered if 100% relative humidity were measured at the exit of the heat exchanger. The method for

calculating this temperature is described thoroughly in Appendix E. The resulting temperature if all of the water in the exhaust products condensed into liquid inside of the heat exchanger was 533 K versus the 670 K measured. To correct the issue of water condensing in the heat exchanger, the exhaust gas temperature would need to increased so that the water in the products remains well above 373 K (212 F), the temperature where the water would condense. The experiment was actually modified to correct this issue and the resulting (uncorrected) heat exchanger exit temperatures were above 370 K.

To approximate the error caused by the inaccuracy of the mass flow rate measurement, the original analysis from Section III.4 was conducted, but water mass flow rate was increased and decreased by .25 gallons per minute (the precision error of the meter). The increase in water flow rate yielded an average heat exchanger inlet temperature of 688 K and decreasing it yielded a temperature of 664 K. To reduce this error the mass flow rate of the water could be increased. Increasing the water mass flow rate would serve to reduce the error in proportion to the measured rate. Increasing the mass flow rate would also have the negative side effect of increasing the percentage of precision error of water outlet temperature and as a result, it is recommended that a more accurate water flow meter be acquired.

Finally to quantify the precision error of the water outlet temperature a similar analysis as discussed in the previous paragraph was conducted. Increasing the water temperature by two Kelvin increased the calculated average heat exchanger inlet temperature to 738 K and the opposite reduced the temperature calculated to 614 K. To reduce the percentage of the precision error on water outlet temperature the water flow rate could be reduced. Reducing the water mass flow rate would raise the change in

water temperature from the inlet to the exit of the heat exchanger and decrease, by percentage, the precision error.

V. Conclusions

One of the original assumptions made prior to this experiment was that the temperatures and pressures calculated at the inlet of the heat exchanger when the turbocharger was not present would be representative of the turbine inlet conditions when the turbocharger was present. This analysis also hypothesized that the calculated temperatures and pressures at the inlet of the heat exchanger would be representative of the turbine exit temperature when the turbine was in the flow. It became very clear upon examining the data that this assumption was not accurate for the conditions analyzed. It was found that the pressure oscillations at the exit of the heat exchanger were more pronounced without the turbocharger to act as a damper. The increased pressure oscillations caused for even lower temperature measurements when the turbocharger was not present. The inaccuracy was so extreme in fact that the results produced turbine exit temperatures greater than the turbine inlet temperatures.

The addition of the turbocharger also adds back pressure to the PDC tube and as a result, increased pressures and temperatures are observed. The trend of increasing combustion temperatures with increasing pressure is consistent with analytical results (Schultz 2000). Manifold pressures increased by approximately 10% with the addition of the turbocharger. Combustion occurring in and through the turbine could also have contributed to the increased temperatures measured at the exit of the turbine in comparison to without the turbine.

Significant pressure oscillations were observed during experimentation at the exit of the heat exchanger which was likely the cause for the lack of conformity between the

calculated temperatures and those that were measured directly. It is likely that at higher frequencies, approximately 65 Hz and greater, the pressure oscillations would be attenuated and the calculated inlet temperature of the heat exchanger would be in closer agreement with the mass averaged temperatures at the same location. Operation at higher frequencies is also supported by the fact that at 10 and 15 Hz operation, the turbine remains unchoked for a majority of the cycle. At higher frequencies, the opposite would be true and likely increase efficiency.

Originally the test matrix for this experiment included operation at higher and more varied frequencies (10, 15 and 20 Hz). Unfortunately the PDC began backfiring during extended runs. Backfiring was due to auto-ignition where the spiral used for DDT became so hot that the fuel-air mixture began igniting before the valves closed behind it. This discovery forced extended runs to be conducted at lower frequencies. It was noted that the tube temperatures remained higher when the turbocharger was applied at the exit of the PDC tube. Use of alternate fuels, like ethylene, may allow the PDC to be run for extended periods at higher frequencies.

Prior to this experiment it was hypothesized that the addition of the heat exchanger and turbocharger would serve to help mix and steady the flow. After analyzing the Schlieren high speed videos it was apparent that the flow was still extremely unsteady at the exit of the heat exchanger. The combination of increasing frequency and adding the turbocharger resulted in reduced pressure oscillations at the exit of the heat exchanger, but the flow still pulsed into and out of the exhaust pipe several times over the course of one cycle at 20 Hz.

Though uncertainty values for turbine work, compressor work and efficiency were higher than desired, the resulting values are still reasonable. For a turbine powered by unsteady flow that is unchoked, efficiencies between 10 to 15% are not outlandish. Ideally a time accurate efficiency could be attained and integrated over an entire cycle to provide a comparison.

The process of using compressor mass flow rates, temperatures and pressures to estimate compressor work was found to be consistent. The calculated turbine exit temperatures agree more with those that were measured directly as frequency increased. The temperatures measured using thermocouples at the exit of the PDC and turbine were closer to the mass weighted average temperatures than those calculated however, as PDC frequency increases a thermocouple is not likely to survive, let alone measure temperature accurately. The energy balance approach would be best suited for a scenario where PDC frequency is higher, in order to reduce the likelihood that pressure oscillations allow ambient air to reach the thermocouple at the heat exchanger exit.

A mass averaged temperature is necessary for calculating work and efficiency. The temperature recorded by a thermocouple is actually the result of heat transfer to and from the thermocouple during unsteady flow. This thermocouple measured temperature will fall short of the mass averaged temperature for an unsteady flow.

VI. Recommendations

Future experimentation should include operation at higher frequencies and mass flow rates for reasons mentioned previously. The majority of the error in calculated turbine inlet and exit temperatures was the result of pressure fluctuations at the exit of the heat exchanger. More emphasis should be placed on steadying the flow of the PDC to acquire a more accurate measurement. This could be accomplished by using a larger vessel (on the order of ten times the volume of the heat exchanger used in this experiment) at the exit of the turbine where the shock wave would have room to expand and dissipate. Without steadying the flow there is little hope for measuring a mass averaged temperature. Schlieren or other flow visualization techniques should be used to verify steady flow at the exit of the device. Arrangements should be made to account for any burning in or through the turbine, especially during extended runs. Using ion probes immediately in front of and behind the turbine would help to identify any combustion that may be occurring in the area. Any future approaches to measuring enthalpy at the inlet or exit of the turbocharger would need to steady the flow before a temperature measurement is taken.

VII. Appendices

Appendix A - Heat Exchanger Design

The following formulas and methods were used in combination with Microsoft Excel® in order to produce estimates of heat exchanger parameters (length, diameter, etc.).

First, an initial guess at inlet temperature and desired outlet temperature for PDC the hot gases were necessary. Initial conservative estimates for heat exchanger inlet temperature of 1450 K (2150 F) and outlet temperature of 900 K (1160 F) were used. This inlet temperature was greater than what the expected average inlet temperature would be and the outlet temperature was selected to ensure the exhaust gases would be cold enough to be directly measured with a J-type thermocouple (<1382 F). A total mass flow of 5.3 lb/min was selected and the constant pressure specific heat for the inlet and outlet flow is attained from a source (Incropera, et al. 2007). From these numbers, q is calculated:

$$q = \dot{m}\left(C_{p_{hg,in}} T_{hg,in} - C_{p_{hg,out}} T_{hg,out}\right) \qquad \text{Eq. 5.1.3}$$

All of the heat is assumed to go straight into the water:

$$q_{hg} = q_{water} = q \qquad \text{Eq. 5.1.4}$$

The outlet temperature of the water is calculated in the reverse manner, based off of the water mass flow rate and the water inlet and outlet temperatures and specific heats. The open loop cooling system has a constant liquid inlet temperature. The mass flow rate of the liquid is manipulated to maintain an outlet temperature that is below boiling:

$$T_{liq,out} = \frac{\left(\frac{q}{\dot{m}_{liq}} + C_{p_{liq,in}} T_{liq,in} \right)}{C_{p_{liq,out}}} \qquad \text{Eq. 5.1.5}$$

Next the Reynolds numbers of the hot gas flow and the liquid flow must be determined:

$$\mathrm{Re}_{hg} = \frac{4\dot{m}_{hg}}{\pi \mathrm{D} \mu_{hg}} \qquad \text{Eq. 5.1.6}$$

and

$$\mathrm{Re}_{liq} = \frac{4\dot{m}_{liq}}{\pi \left(\mathrm{D_o} + \mathrm{D}_i \right) \mu_{liq}} \qquad \text{Eq. 5.1.7}$$

Because the coolant flows through the annulus, the same calculation is not used for Reynolds number. The friction factor was calculated using:

$$f = \left(0.790 \ln\left(\mathrm{Re} \right) - 1.64 \right)^{-2} \qquad \text{Eq. 5.1.8}$$

The hot gas Reynolds number is above 10,000 so the correlation for Nusselt number (Nu), the ratio of convection to pure conduction heat transfer, used is:

$$Nu = \frac{\left(f/8 \right)\left(\mathrm{Re} - 1000 \right) \mathrm{Pr}}{1 + 12.7 \left(f/8 \right)^{1/2} \left(\mathrm{Pr}^{2/3} - 1 \right)} \qquad \text{Eq. 5.1.9}$$

Prandtl number, a ratio of the momentum diffusivity (or ν the kinematic viscosity which is the dynamic viscosity divided by density) to thermal diffusivity (α), is assumed to be that of air. The friction factor and Nusselt number of the liquid is calculated in the same fashion. The convective heat transfer coefficient for the hot gas side is then:

$$\mathrm{h}_{hg} = \frac{Nu_{hg} k_{hg}}{D} \qquad \text{Eq. 5.1.10}$$

and the convective heat transfer coefficient for the liquid side is:

$$h_{liq} = \frac{Nu_{liq} k_{liq}}{D_{hyd}} \qquad \text{Eq. 5.1.11}$$

Next the overall heat transfer coefficient is calculated:

$$U = \frac{1}{\frac{1}{h_{hg}} + \frac{1}{h_{liq}}} \qquad \text{Eq. 5.1.12}$$

The next step is to calculate the log mean temperature difference:

$$\Delta T_{lm} = \frac{\left(T_{hg,in} - T_{liq,in}\right) - \left(T_{hg,out} - T_{liq,out}\right)}{Ln\left[\left(T_{hg,in} - T_{liq,in}\right) / \left(T_{hg,out} - T_{liq,out}\right)\right]} \qquad \text{Eq. 5.1.13}$$

Now all of the necessary values have been attained to allow for the calculation of the overall length of the system:

$$L = \frac{q}{U \pi D_i \Delta T_{lm}} \qquad \text{Eq. 5.1.14}$$

A snapshot of the spreadsheet used for this analysis is seen in Figure VII-1:

		Concentric tube counterflow		Input Variables/Fixed Values	Output Variables		
Given	SI Units	US units		Table Lookup	Formula		
T,hg,in (K)	1450	2150.6	deg F				
T,hg,out (K)	900	1160.6	deg F	mdot*Cpout*Tout-mdot*Cpin-T			
mdot,hg (Kg/s)	0.04	5.291066667	lb/min	q,hg (W)	Re,D	Nu,D	h,hg
Cp,in,hg (J/Kg*K) (air)	1225	Pr,avg	0.685	30694	11015.2549	31.86145992	32.4879493
Cp,out,hg (J/Kg*K) (air)	1121					form 8.62 (Incropera)	
					friction factor	Cf	
T,liq,in (K)	293	68	deg F		0.030643519	0.00766088	
T,liq,out (K)	313.75	105.3500615	deg F				
Cp,in,liq (J/Kg*K)	4181			q,liq=q,hg			
Cp,out,liq (J/Kg*K)	4184			q,liq (W)	liquid Re,D	Nu,D	h,liq (W/m^2K)
mdot,liq (Kg/s)	0.35	5.548216645	gal/min	30694	2.73E+03	1.71E+01	1.51E+02
					pi*Dhyd^2/4		
D,tube,in (m)	0.089	3.50393712	inch	deltaT,lm (K)	Ac (m^2)	Ac (in^2)	Length (in)
D,tube,out (m)	0.1615	6.35826792	inch	844.152919	0.014263812	22.10895485	240
Liquid Properties							
D,hyd (m)(liquid)	0.0725	2.8543308	inch				
visc,avg (Ns/m^2) (liqui	0.000651	visc in	visc out	Pr in	Pr out	Kin	Kout
Pr,avg (liq)	4.38	9.59E-04	3.43E-04	6.62	2.14	0.606	0.671
k,avg (W/mK) (liq)	0.6385						
Hot Gas Properties							
visc,avg (Ns/m^2)	5.2E-05	visc in	visc out	Pr in	Pr out	Kin	Kout
Pr,avg	0.7075	5.90E-05	4.49E-05	0.687	0.728	0.11	0.0715
k,avg (W/mK)	0.09075						
			U (Overall Heat Transfer Coefficient) (W/m^2K)		friction factor	Cf	
Process			2.67E+01		4.70E-02	1.18E-02	
Mdot*Cp*(Tin-Tout)=q	qhg=-qliq	qliq=U*A*Tlm					
		A=pi*Din*L	L, pipe length (m)	in feet			
		Dhyd=Dout-Din	5.97E+00	1.96E+01			

Figure VII-1: Sample heat exchanger design spreadsheet

It is notable from Figure VII-1 that the convective heat transfer coefficient for the liquid side is much larger than for the hot gas side. This translates physically into the wall of the heat exchanger being primarily the same temperature as the liquid flowing past the wall.

Table VII-1: Original heat exchanger properties

Annulus Volume	.0895 m^3	3.16 ft^3
Inner diameter volume	.0328 m^3	1.159 ft^3
Volumetric gas flow rate	845.7 m^3/s	147.2 ft^3/s
Volumetric coolant flow rate	3.47 E^{-4} m^3/s	.735 ft^3/s
Average coolant velocity	5.411 E^{-3} m/s	1.775 E^{-2} ft/s
Average air velocity (10 Hz)	13 m/s	9.845 ft/s
Coolant cycle time	1126 s	18.77 min
Hot gas cycle time	0.5 s	.03 min

Appendix B - Free convection and radiation calculations for PDC tube and heat exchanger

The following formulas and methods (Incropera, et al. 2007) were used in combination with Microsoft Excel® in order to produce estimates of heat exchanger losses to include free convection and radiation.

The heat transfer at the boundary of the system (out of the heat exchanger) is:

$$q'=q'_{conv}+q'_{rad}=\bar{h}\pi D\left(T_s-T_\infty\right)+\varepsilon\pi D\sigma\left(T_s^4-T_\infty^4\right) \qquad \text{Eq. 5.1.15}$$

During operation the highest temperature the surface of the heat exchanger reached was 105 F (313 K) so a conservative estimate of 120 F (322 K) is used for T_s, surface temperature, in this analysis. To calculate the heat transfer coefficient for free convection ($\bar{h}$), Rayleigh number (Ra), the ratio of the buoyancy forces to the viscous forces in the fluid, must first be calculated:

$$Ra=\frac{g\beta\left(T_s-T_\infty\right)D^3}{\upsilon\alpha} \qquad \text{Eq. 5.1.16}$$

(Note: in the case of free convection air is assumed to be an ideal gas and an average value of g, β, ν and α is used.) For an ideal gas:

$$\beta=\frac{1}{T_{avg}} \qquad \text{Eq. 5.1.17}$$

The empirical correlation for Nusselt number of a long horizontal cylinder (which the heat exchanger will be approximated as) is:

$$Nu_D = \left\{ 0.60 + \frac{0.387 Ra_D^{1/6}}{\left[1 + \left(0.559/\mathrm{Pr}\right)^{9/16}\right]^{8/27}} \right\}^2 \qquad \text{Eq. 5.1.18}$$

Finally free convection heat transfer coefficient is calculated in the same manner as in Eq. 5.1.10.

The numbers for the radiation calculation q_{rad} were directly inserted into Eq. 5.1.15. It should be noted that q_{total} is the sum of q_{rad} and $q_{nat.conv}$ multiplied by the length of the heat exchanger.

	Heat Transfer from Heat X				
			$Gr_L = \frac{g\beta(T_s - T_\infty)L^3}{\upsilon^2}$ $\beta = \frac{1}{T}(ideal\_gas)$	g (m/s^2)	9.8
	F	K		sigma (W/m^2 K^4)	5.67E-08
Ttube,avg (conservative)	123	323.705556	$Ra_D = \frac{g\beta(T_s - T_\infty)D^3}{\upsilon\alpha}$		
Tamb	65	291.483333			
Tdelta	58	32.2222222	$\overline{Nu}_D = \left\{ 0.60 + \frac{0.387 Ra_D^{1/6}}{\left[1 + (.559/\mathrm{Pr})^{9/16}\right]^{8/27}} \right\}^2$		
Tavg		307.594444			
rho,air,avg (kg/m^3)		1.1614	$\bar{h} = \frac{k}{D}\overline{Nu}_D$ $\beta = \frac{1}{T_s - T_{amb}}$		
Beta (K^-1)		0.03103448			
D (in, m)	6.625	0.168275	$q' = q'_{conv} + q'_{rad} = \bar{h}\pi D(T_s - T_\infty) + \varepsilon\pi D\sigma(T_s^4 - T_\infty^4)$		
L,tube (in,m)	240	6.096			
nu,avg (m^2/s)		1.59E-05			
alpha,avg (m^2/s)		2.25E-05			
Pr,avg		0.707			
k,avg (W/mK)		2.63E-02			
emiss,Al		0.2			
Ra,D		1.31E+08			
Nu,D		61.3771738			
h (W/m^2K)		9.592748			
q',nat.conv. (W/m)		163.405999			
q',rad. (W/m)		22.5487927			
q,total (Hp, W)	1.518998	1133.58041			
	mdot (air)				
	lb/min	kg/s			
	7.84	0.059192			

Figure VII-2: Sample free convection and radiation calculation spreadsheet

Appendix C – Purge gas heat exchanger inlet temperature

As the purge gas travels through the PDC detonation tube, heat is transferred from the tube to the gas in a cooling process. This change in temperature is significant and cannot be ignored. The following process provides an estimate of the purge gas temperature as it enters the heat exchanger.

First the manifold temperature (Tman) is measured directly. This is the temperature of the air as it enters the PDC tube. The PDC tube temperature is also measured at the front and back ends of the tube to determine an average tube surface temperature (Tsurf). The mass flow rate ($\dot{m}$) of the purge flow is directly measured as well. The Reynolds number and friction factors are determined using Eq. 5.1.6 and Eq. 5.1.8. The Nusselt number is found by again using Eq. 5.1.9 for fully developed turbulent flow in a smooth circular tube. Next the convective heat transfer coefficient is calculated with Eq. 5.1.10. Finally the purge gas temperature at the heat exchanger inlet is calculated, assuming a constant surface temperature based off of the average tube surface temperature (Tsurf) and :

$$T_{\substack{purge\\in}} = T_{surf} - e^{-\left(\frac{PL}{\dot{m}C_p}\bar{h}\right)}\left(T_{surf} - T_{man}\right) \qquad \text{Eq. 5.1.19}$$

All properties of air are based off of curve fits from tabular data (Incropera, et al. 2007), to include specific heat, thermal conductivity, Prandtl number and viscosity. An average temperature of the purge gas is used to find the air properties. For the reason that the values of the properties vary with temperature, this is an iterative process.

T,man/T,in (K)	293		
T,surf (K)	1200		
m,dot,purge	0.015787		
visc,purge (N s/m^2)	2.39885E-05		
Tube Length (m)	1.2192		
Tube Diam (m)	0.0547878		
Re	15294.0818		
f	0.028040509		
Pr	0.690646642		
n (.4 heating,.3 cooling)	0.4		
Nu	44.16201946	41.41097	
k(W/mK)	0.036562142		
h (W/(m^2K)	27.63523417		
Cp(air)	1017.765672		
T,purge,out (K)	567.7965566		
T,avg,purge (K)	430.42	430.3983	

Figure VII-3: Sample purge gas inlet temperature calculation spreadsheet

Appendix D – Original Experiment and Modifications

Due to the many lessons learned in the process of conducting this experiment, it was necessary to continually adapt and modify the experiment to attain accurate turbine inlet temperatures. This appendix includes a summary of those changes.

Originally two aluminum pipes were cut from single 20 foot sections into two 10 foot sections for ease of transportation and to prevent the experiment from protruding over the side of the test stand. A ¾ inch diameter bent tube allows water to flow between ten foot sections of the heat exchanger. A 180º mild steel elbow turned the exhaust products back into the second section of the heat exchanger. At this point the exhaust products are aimed back at the PDC rig, so a 90º steel elbow turns the flow again where the temperature of the gas was measured eight inches downstream of the heat exchanger exit. A simplified schematic of the heat exchanger from a top view is pictured in Figure VII-4:

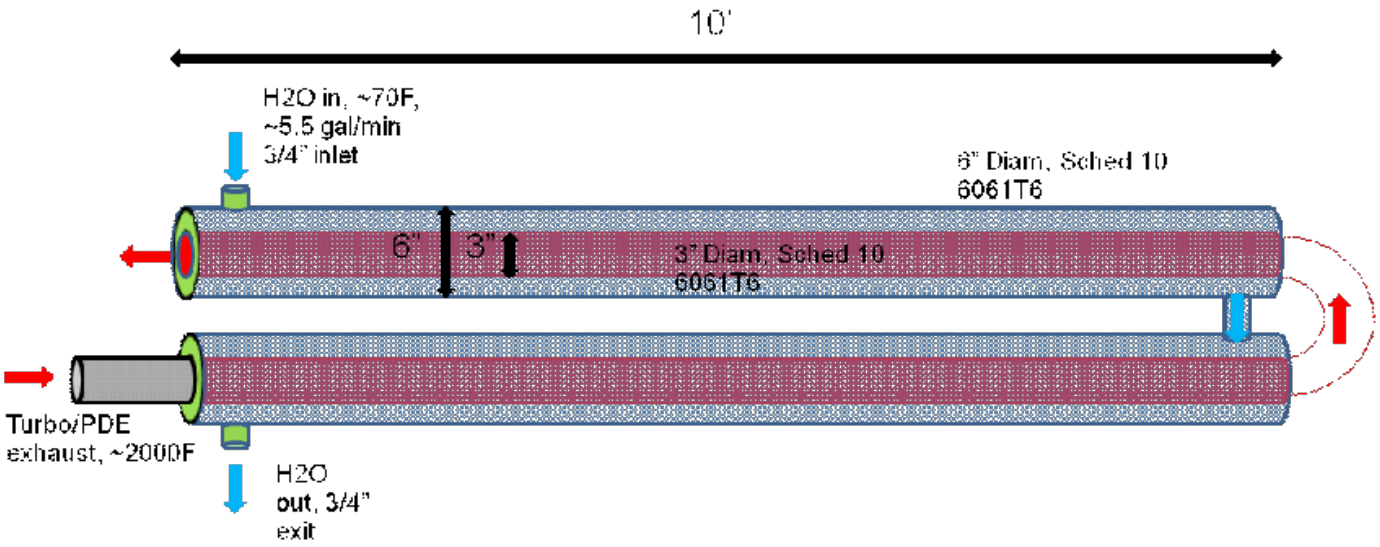

Figure VII-4: Top view of heat exchanger

Figure VII-5 shows the flow direction for both hot gas and coolant through the heat exchanger and Figure VII-6 identifies the locations of thermocouples.

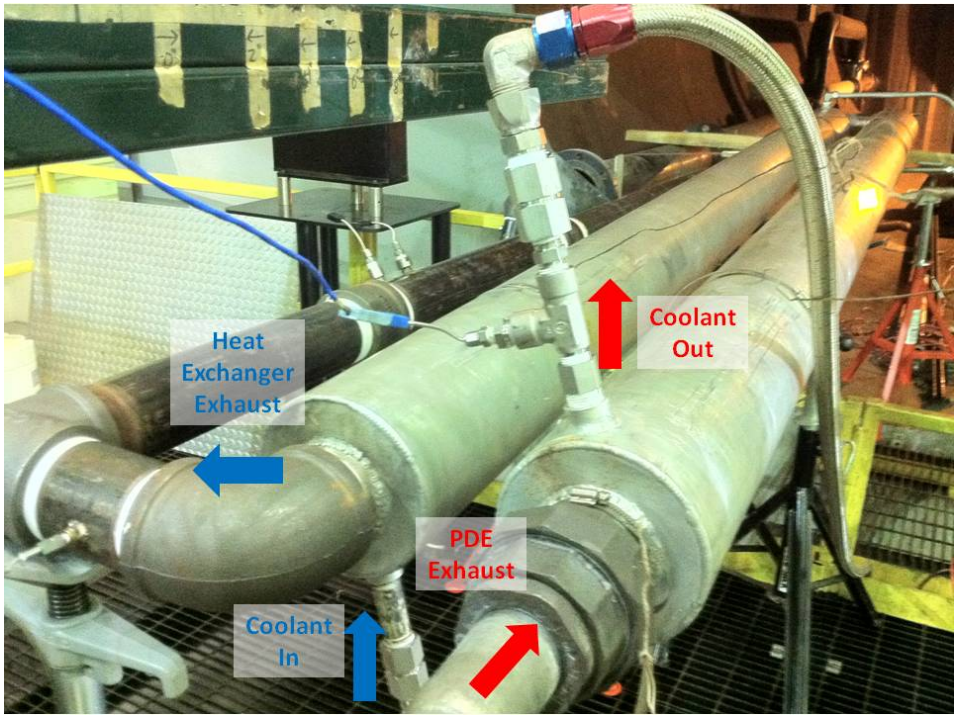

Figure VII-5: Counter flow heat exchanger attached directly to PDC

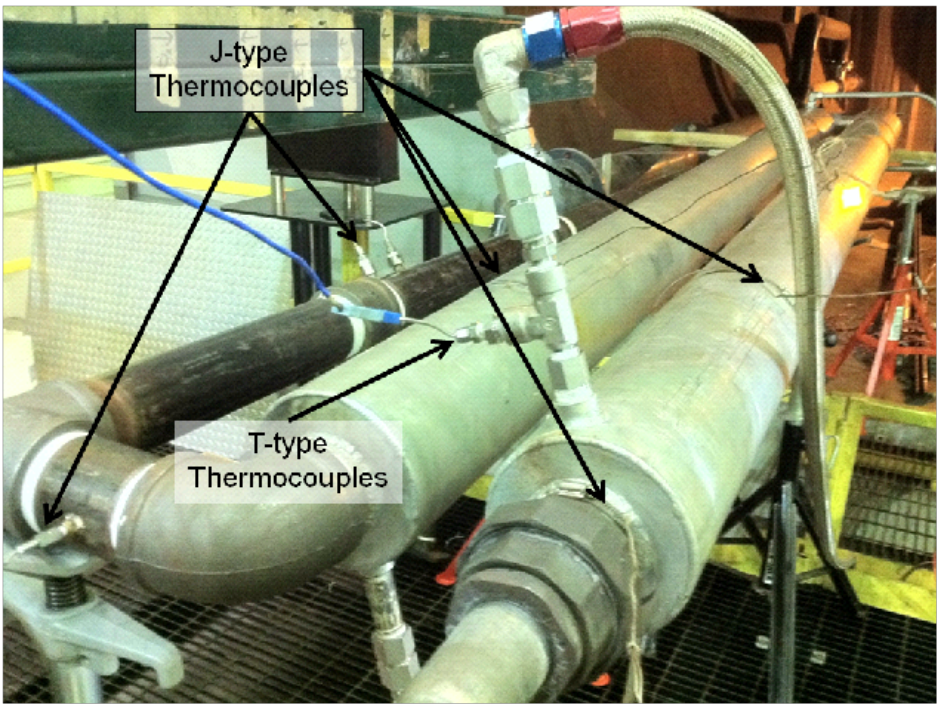

Figure VII-6: Heat exchanger instrumentation

The eleven-blade, radial turbine used in initial experimentation was a Garrett T3 automotive turbocharger, pictured in Figure VII-7. The turbine wastegate was capped so that all combustor exhaust passes through the turbine. The T3 was also equipped with a radial compressor having six primary impeller blades and six splitter blades. The water-cooled, center housing contains the shaft and dual journal bearing assemblies. The T3 has a 0.58 A/R, 45 trim compressor, a T3 4-Bolt inlet and T3 5-bolt discharge exhaust.

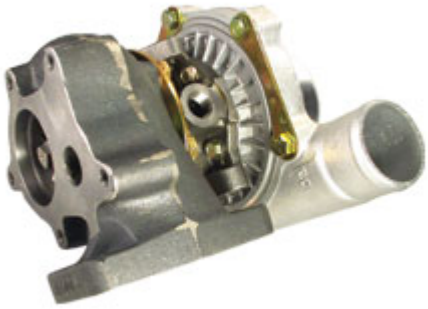

Figure VII-7: Garrett T3/T4E automotive turbocharger

Figure VII-8 illustrates the T3 compressor operating map where target compressor operating conditions run down the center of the efficiency islands.

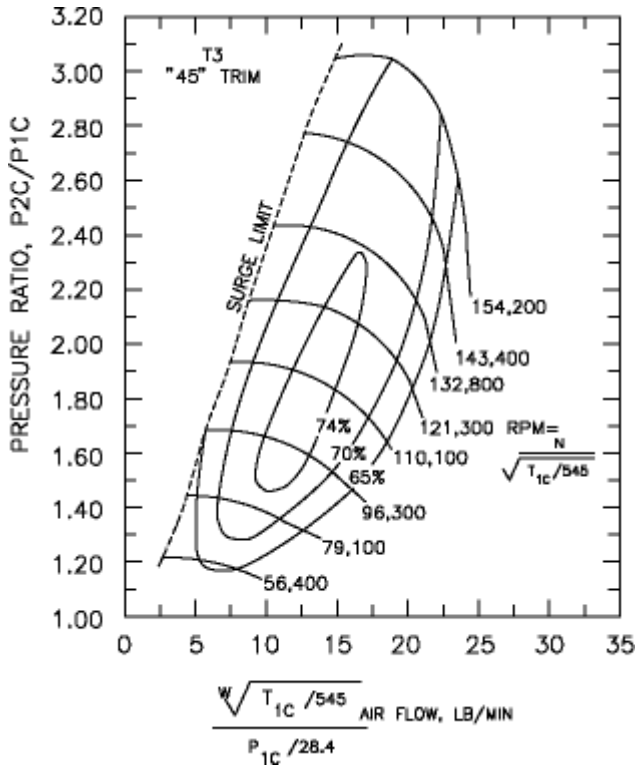

Figure VII-8: Garrett T3 compressor operating map

Originally the experiment was run in two different configurations: configuration 1, without a turbocharger seen in Figure VII-9 and configuration 2, with a turbocharger seen in Figure VII-10. Both configurations used a 20 foot long heat exchanger.

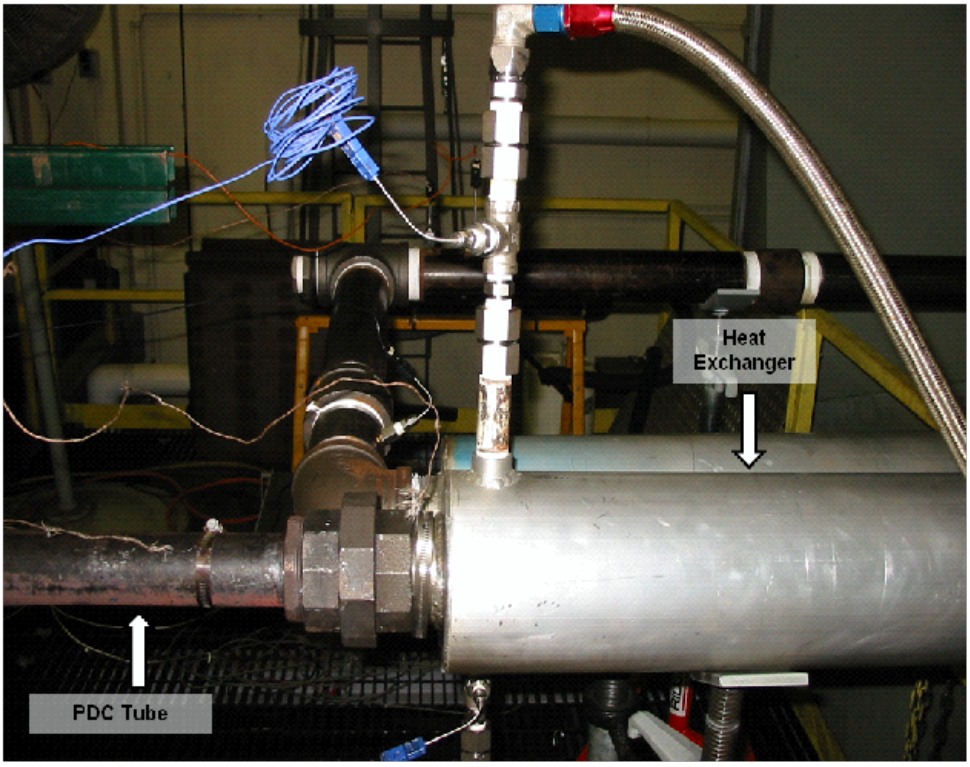

Figure VII-9: Configuration 1-PDC and heat exchanger

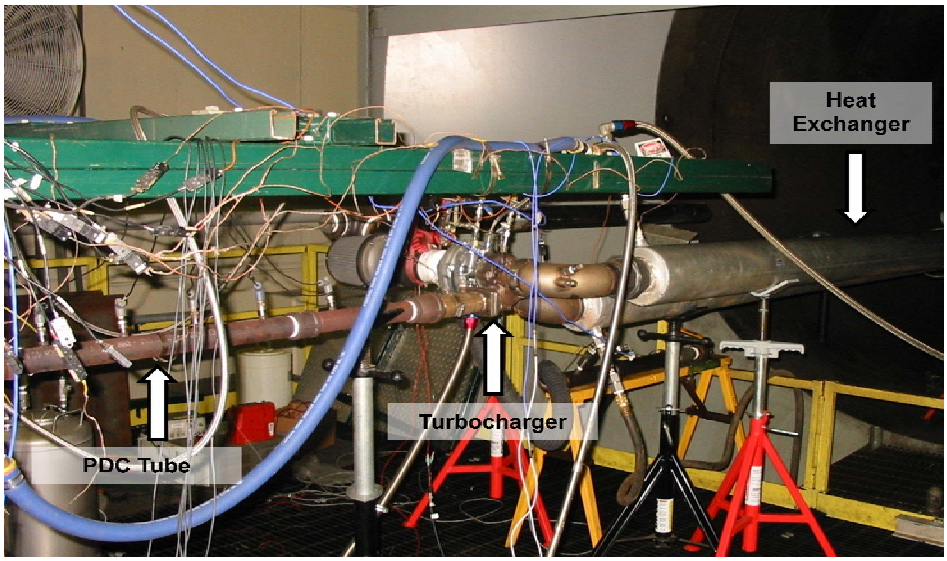

Figure VII-10: Configuration 2-PDC, turbocharger and heat exchanger

Preliminary results showed that due to low heat exchanger exhaust temperatures that the water in the exhaust products was able to condense inside the heat exchanger. To reduce the amount of energy removed from the exhaust and prevent water from condensing the heat exchanger length was reduced to ten feet.

The majority of the results derived in this paper are the result of configuration two, with a ten foot heat exchanger. It was determined that the data produced without the turbocharger did not mimic accurately the conditions at the inlet of the turbocharger. The increased pressure oscillations noted upon removing the turbocharger we the most likely cause of the reduced accuracy of this approach.

Appendix E– Data analysis with water condensing

During the experiment using a 20 foot long heat exchanger it was noted that water condenses inside the heat exchanger. Condensing water signifies a phase change is taking place. The phase change suggested additional energy was being released into the wall of the heat exchanger which was not accounted for in previous calculations. Starting from Eq. 2.3.3, a latent heat term must be added to account for the phase change:

$$\dot{E}_{\substack{coolant\\in}} + \dot{E}_{\substack{gas\\in}} = \dot{E}_{\substack{coolant\\out}} + \dot{E}_{\substack{gas\\out}} + \dot{E}_{\substack{phase\\change}} \qquad \text{Eq. 5.1.20}$$

where the energy released during phase change is a function of the mass rate of fluid condensing in the heat exchanger and the latent heat of water:

$$\Delta\dot{E}_{\substack{phase\\change}} = \dot{m}L \qquad \text{Eq. 5.1.21}$$

Further expansion of Eq. 5.1.20 yields:

$$\left[\left(\dot{m}C_p\mathrm{T}\right)_{main+purge} + \left(\dot{m}C_p\mathrm{T}\right)_{cool}\right]_{in} = \left[\begin{matrix}\left(\dot{m}C_p\mathrm{T}\right)_{purge} + \left(\dot{m}C_p\mathrm{T}\right)_{N_2} + \left(\dot{m}C_p\mathrm{T}\right)_{H_2O(g)} \\ + \left(\dot{m}C_p\mathrm{T}\right)_{H_2O(l)} + \left(\dot{m}C_p\mathrm{T}\right)_{cool} + \mathrm{q}_{rad} + \mathrm{q}_{fc}\end{matrix}\right]_{out} - \dot{m}L \qquad \text{Eq. 5.1.22}$$

where the main flow (combustion products) and purge flow (air) are separated in the latter half of the equation. The main flow is subdivided into nitrogen, gaseous water and liquid water so that the water can be accounted for separately. This separation is possible because the experiment was always run with an equivalence ratio of one and the fuel used was hydrogen, so the only products should have been nitrogen and water.

This equation is manipulated to solve for $T_{avg,in}$ or the average temperature of the gas as it enters the heat exchanger:

$$T_{avg,in} = \frac{\begin{bmatrix} \left(\dot{m}C_p T\right)_{purge} + \left(\dot{m}C_p T\right)_{N_2} + \left(\dot{m}C_p T\right)_{H_2O(g)} \\ + \left(\dot{m}C_p T\right)_{H_2O(l)} + \left(\dot{m}C_p T\right)_{cool} + q_{rad} + q_{fc} \end{bmatrix}_{out} - \dot{m}L - \left(\dot{m}C_p T\right)_{\substack{cool \\ in}}}{\left(\dot{m}C_p\right)_{\substack{avg \\ in}}} \quad \text{Eq. 5.1.23}$$

where

$$\left(\dot{m}C_p\right)_{\substack{avg \\ in}} = \dot{m}_{total}\left(\frac{\dot{m}_{purge}}{\dot{m}_{total}}C_{p_{purge}} + \frac{\dot{m}_{main}}{\dot{m}_{total}}C_{p_{main}}\right) \quad \text{Eq. 5.1.24}$$

It should be noted that the specific heat for both purge and main flow gases vary significantly, due to their dependence on temperature. For this reason it is necessary to estimate the purge temperature as it enters the heat exchanger, so that an accurate specific heat may be calculated. This process is displayed in Appendix C.

The mass flow rate of the purge and main flow is measured in the purge and main manifolds respectively. It is assumed that the mass flows are conserved and do not change from the manifolds to the exit of the heat exchanger. The gaseous specific heats are attained via curve fit coefficients (Turns 2006) and the liquid specific heats are looked up form a table (Incropera, et al. 2007). The temperatures for the exiting gases (purge air, N_2 and H_2O (g)) are measured from the J-type thermocouples at the exit of the heat exchanger while the temperature of the exiting condensing liquid (H_2O (l)) is assumed to be the same as the coolant temperature as it leaves the heat exchanger.

To determine the mass rate of liquid water condensing in the heat exchanger an equilibrium reaction is assumed (Eq. 5.1.25).

$$H_2 + \frac{1}{2}\left(O_2 + 3.76N_2\right) \rightleftarrows H_2O_{(g)} + \frac{3.76N_2}{2} \quad \text{Eq. 5.1.25}$$

This assumption lies on the fact that the reaction is taking place at stoichiometric conditions, which is believed to be the case. It is also assumed that the purge flow is completely composed of air (O_2+3.76N_2). Next the mole fractions for the main exhaust products are determined to be:

$$\chi_{H_2O} = \frac{N_{H_2O}}{N_{mix}} = .347 \qquad \text{Eq. 5.1.26}$$

$$\chi_{N_2} = \frac{N_{N_2}}{N_{mix}} = .653 \qquad \text{Eq. 5.1.27}$$

Using the mole fraction of water, the total mass flow of water (gaseous and liquid) that enters the heat exchanger may be calculated:

$$\dot{m}_{H_2O(total)} = \dot{m}_{main}\chi_{H_2O} \qquad \text{Eq. 5.1.28}$$

Next, steam tables (Sonntag 1991) are used with pressure and temperature measurements of the gaseous water as it exits the heat exchanger to approximate its density ($\rho_{H_2O(g)}$). This density is used to determine the mass flow rate of gaseous water with Eq. 5.1.29.

$$\dot{m} = \rho AV \qquad \text{Eq. 5.1.29}$$

The area is based off of the inner diameter of the heat exchanger and the velocity is determined by coherent structure velocimetry provided by Schlieren. Coherent structure velocimetry determines the velocity of the large and small scale structures present in Schlieren imagery. It accomplishes this by tracking the structures, depicted by the density gradients, from one frame to the next. The frame rate and the frame size or the spacial resolution (physical area represented by each pixel) are both known. By calculating the distance that the structure travels over each frame and dividing by the amount of time elapsed from one frame to the next, velocity is produced.

The result of Eq. 5.1.29 is the mass flow rate of the gaseous H_2O, which is subtracted from the total mass flow rate to determine the rate of liquid water being produced at the exit of the heat exchanger:

$$\dot{m}_{H_2O(l)} = \dot{m}_{H_2O(total)} - \dot{m}_{H_2O(g)} \qquad \text{Eq. 5.1.30}$$

The radiation (q_{rad}) and natural convection (q_{nc}) terms, if found to be significant are included. These calculations can be found in Appendix B. With this information it is possible to return to Eq. 5.1.23 and calculate the average temperature at the inlet of the heat exchanger ($T_{avg,in}$). It is necessary to iterate on this temperature because the inlet temperature is dependent on the specific heat of the inlet gases, which is also temperature dependent.

When the analysis was performed for the configuration without the turbocharger in the flow, the result of Eq. 5.1.23 or Eq. 4.2.3 was considered the average turbine inlet temperature and when performed for the configuration with the turbocharger, turbine exit temperature was calculated.

The inlet temperature calculated during these experiments using Eq. 5.1.22 was 1139 K (1591 F) with the turbocharger and 1262 K (1812 F) without the turbocharger. For 20 Hz at a fill and purge fraction of 0.5 and 0.5 respectively. Looking at specific work, this translates to 177 kW/kg (1.79 hp/lb/min). It is possible to convert the specific work to average work by multiplying the specific work by the mass flow rate. Doing so yields 4.45 kJ/s (5.95 hp). The work provided in the initial results is higher than expected. This approach may provide inflated results because it assumes that all of the energy removed from the flow by the turbine is completely converted into work. In reality a portion of the

energy in the flow is heating the turbine. The turbine housing temperature rose above 800 K (1000 F) during extended runs.

Appendix F– Uncertainty Calculations

The first sensor to be examined is the water flow meter. The water flow meter was used to determine the mass flow rate of coolant through the heat exchanger. The meter used was a FTB4707 low flow liquid flow meter was used which has an accuracy of $\pm$ 1.0% (Omega, Omega.com 2010). The temperature of the coolant was measured using T-type Omega, mini quick disconnect thermocouple probes, both at the entrance and exit of the heat exchanger. These thermocouples have a tolerance of 1 K or 0.75% (Omega, ANSI and IEC Color Codes for Thermocouples, Wire and Connectors 2010).

Looking at the heat removed from the system by the coolant:

$$\mathrm{q}_{water} = \Delta \mathrm{H} = \dot{m}\left(C_{p,in}\mathrm{T}_{in,coolant} - C_{p,out}\mathrm{T}_{out,coolant}\right) = R \qquad \text{Eq. 5.1.31}$$

Based off of representative values a nominal heat removed by water is calculated:

$$\begin{aligned}\mathrm{q} &= (.347)\left[(4178)(310)-(4184)(292)\right]\\ &= 25487.8\ \mathrm{W}\end{aligned}$$

It is necessary to determine all of the terms in the equation before solving:

$$\frac{\partial \mathrm{q}}{\partial \dot{m}} = C_{\underset{out}{p}}T_{out} - C_{\underset{in}{p}}T_{in} = \left[(4178)(310)-(4184)(292)\right] = 73452$$

$$\frac{\partial \mathrm{q}}{\partial \mathrm{T}} = \dot{m}\left(C_{\underset{out}{p}} - C_{\underset{in}{p}}\right) = .347(4178-4184) = 2.082$$

$$w_{\dot{m}} = (.347)(.001) = \pm .000347\ \mathrm{kg/s}$$

$$w_{\mathrm{T}} = \pm 1\ \mathrm{K}$$

Now applying Eq. 4.2.16 to the equation for heat removed by the water yields:

$$\begin{aligned}w_{\mathrm{q}} &= \left[(73452)^2(.000347)^2 + (2.082)^2(1)^2\right]^{1/2}\\ &= \pm 25.5\ \mathrm{W}\ \textit{or}\ 0.10\%\end{aligned}$$

The air mass flow rate through the manifolds is governed by the equation:

$$\dot{m} = c_D P_0 \left(\frac{D}{2}\right)^2 \left(\frac{\gamma+1}{2}\right)^{-\left(\frac{\gamma+1}{2(\gamma-1)}\right)} \sqrt{\frac{\gamma g_c}{RT_0}} = .0267\ kg/s \qquad \text{Eq. 5.1.32}$$

where P_0 and T_0 are the stagnation pressure and temperature, C_D is the nozzle discharge coefficient, D is the nozzle throat diameter of the converging–diverging nozzle, γ is the ratio of specific heats, R is the gas constant, and g_c is the gravitational proportionality constant. The nozzle throat diameter is measured to the nearest .001 inches, resulting in an uncertainty of $\pm$.0005 inches or 1.27 E^{-5} meters (Engineering 2011). The nozzle throat diameter used for this analysis is .252 inches or .0064 meters. The discharge coefficient for the nozzle is 0.991 with an uncertainty of $\pm$1%. The thermocouples used to measure the temperature in both manifolds were Omega J-type thermocouples with a published accuracy of 1 K or $\pm$ 0.75% (Omega, ANSI and IEC Color Codes for Thermocouples, Wire and Connectors 2010). Sensotec model TJE pressure transducers measure the pressure in each of the manifolds to within $\pm$ 0.1% accuracy (Honeywell 2005).

Using the same methodology as before, the components of the equation are:

$$\frac{\partial \dot{m}}{\partial c_D} = P_0\left(\frac{D}{2}\right)^2\left(\frac{\gamma+1}{2}\right)^{-\left(\frac{\gamma+1}{2(\gamma-1)}\right)}\sqrt{\frac{\gamma g_c}{RT_0}}$$

$$= (360511)\left(\frac{.0064}{2}\right)^2\left(\frac{1.4+1}{2}\right)^{-\frac{1.4+1}{2(1.4-1)}}\sqrt{\frac{(1.4)(9.8)}{(286.9)(292)}}$$

$$= .0273 \qquad w_{C_D} = (.991)(.01) = \pm.00991$$

$$\frac{\partial \dot{m}}{\partial P_0} = c_D\left(\frac{D}{2}\right)^2\left(\frac{\gamma+1}{2}\right)^{-\left(\frac{\gamma+1}{2(\gamma-1)}\right)}\sqrt{\frac{\gamma g_c}{RT_0}} = 7.51\,E^{-8} \qquad W_{P_0} = \pm 84\,Pa$$

$$\frac{\partial \dot{m}}{\partial D} = c_D P_0\left(\frac{D}{2}\right)\left(\frac{\gamma+1}{2}\right)^{-\left(\frac{\gamma+1}{2(\gamma-1)}\right)}\sqrt{\frac{\gamma g_c}{RT_0}} = 8.47 \qquad W_{P_0} = \pm 84\,Pa$$

$$\frac{\partial \dot{m}}{\partial T_0} = -c_D P_0\left(\frac{D}{2}\right)^2\left(\frac{\gamma+1}{2}\right)^{-\left(\frac{\gamma+1}{2(\gamma-1)}\right)}\frac{\gamma g_c}{2\sqrt{\frac{\gamma g_c}{RT_0}T_0{}^2 R}} = -4.64\,E^5 \quad W_{T_0} = \pm 1\,K$$

$$w_{\dot{m}} = \left[\begin{array}{l}(.0273)^2(.00991)^2 + (7.51\,E^{-8})^2(84)^2 \\ +(8.47)^2(1.27\,E^{-5})^2 + (-4.64\,E^5)^2(-1)^2\end{array}\right]$$

$$= \pm.000117 \text{ kg/s or } 0.433\%$$

Next the purge gas temperature as it enters the heat exchanger will be analyzed starting with the Reynolds Number. The tube diameter is measured to the nearest 1/16 inches, so the uncertainty is $\pm$1/32 inches or 0.00079 m:

$$\mathrm{Re} = \frac{4\dot{m}}{\pi \mathrm{D}\mu} = 15294$$

$$\frac{\partial \mathrm{Re}}{\partial \dot{m}} = \frac{4}{\pi \mathrm{D}\mu} = \frac{4}{\pi(.055)\left(2.40\times10^{-5}\right)} = 965467$$

$$\frac{\partial \mathrm{Re}}{\partial \mathrm{D}} = \frac{-4\dot{m}}{\pi \mathrm{D}^2\mu} = \frac{(-4)(.0158)}{\pi(.055)^2\left(2.40\times10^{-5}\right)} = 277212$$

$$w_{\dot{m}} = \pm.000117 \text{ kg/s}$$

$$w_{\mathrm{D}} = (.055)(.00079) = \pm.000043 \ m$$

$$w_{\mathrm{Re}} = \left[(965467)^2(.000117)^2 + (277212)^2(.000043)^2\right]^{1/2}$$

$$= \pm 113.587 \ \textit{or}\ 0.74\%$$

Friction factor uncertainty is:

$$f = \left(0.790 Ln(\mathrm{Re}) - 1.64\right)^{-2} = .028$$

$$\frac{\partial f}{\partial \mathrm{Re}} = \frac{-3.20461}{\mathrm{Re}\left(Ln(\mathrm{Re}) - 2.07595\right)^3} = -4.85 \ E^{-7}$$

$$w_{\mathrm{Re}} = \pm 113.587$$

$$w_f = \left[\left(4.85 \ E^{-7}\right)^2(113.587)^2\right]^{1/2} = \pm 5.5 \ E^{-5} \ \textit{or}\ 0.20\%$$

Nusselt number (note: this formula is valid for a wide range of internal flows) uncertainty is:

$$Nu = \frac{(f/8)(\mathrm{Re}-1000)\mathrm{Pr}}{1+12.7(f/8)^{1/2}\left(\mathrm{Pr}^{2/3}-1\right)} = 44$$

$$\frac{\partial Nu}{\partial f} = \frac{\left(.0139 f^{1/2}\left(\mathrm{Pr}^{2/3}-1\right)+.445\right)(\mathrm{Re}-1000)\mathrm{Pr}}{\left(f^{1/2}\left(\mathrm{Pr}^{2/3}-1\right)+.223\right)^2} = 1622$$

$$\frac{\partial Nu}{\partial \mathrm{Re}} = \frac{.0278 f \ \mathrm{Pr}}{f^{1/2}\left(\mathrm{Pr}^{2/3}-1\right)+.223} = .002893$$

$$w_f = \pm 5.5 \ E^{-5}$$

$$w_{\mathrm{Re}} = \pm 113.587$$

$$w_{Nu} = \left[(1622)^2\left(5.5 \ E^{-5}\right)^2 + (.002893)^2(113.587)^2\right]^{1/2}$$

$$= \pm .089 \ \textit{or}\ 0.20\%$$

Next convection coefficient uncertainty is calculated:

$$h = \frac{Nu\ k}{\mathrm{D}} = 27.6$$

$$\frac{\partial h}{\partial Nu} = \frac{k}{\mathrm{D}} = \frac{.037}{.055} = .673 \qquad w_{Nu} = \pm .089$$

$$\frac{\partial h}{\partial \mathrm{D}} = -\frac{Nu\ k}{\mathrm{D}^2} = -\frac{(44)(.037)}{.055^2} = -538 \qquad w_D = \pm 0.00079\ m$$

$$w_h = \left[(.673)^2 (.089)^2 + (538)^2 (.00079)^2 \right]^{1/2}$$

$$= \pm .429\ \frac{\mathrm{W}}{m\ \mathrm{K}}\ or\ 1.56\%$$

The last portion of the purge temperature uncertainty examines the purge temperature formula itself, Eq. 5.1.19:

$$\mathrm{T}_{\substack{\mathrm{purge} \\ \mathrm{in}}} = \mathrm{T}_{surf} - e^{-\left(\frac{PL}{\dot{m}C_p}h\right)} (\mathrm{T}_{\mathrm{surf}} - \mathrm{T}_{\mathrm{man}}) = 567.8\ \mathrm{K}$$

$$\frac{\partial \mathrm{T}_{\mathrm{purge}}}{\partial \mathrm{T}_{\mathrm{surf}}} = \left(e^{\left(\frac{PL}{\dot{m}C_p}h\right)} - 1 \right) e^{-\left(\frac{PL}{\dot{m}C_p}h\right)} = 0.305 \qquad w_{\mathrm{Tsurf}} = \pm 7.5\ \mathrm{K}$$

$$\frac{\partial T_{purge}}{\partial \mathrm{T}_{man}} = e^{-\left(\frac{PL}{\dot{m}C_p}h\right)} = 0.701 \qquad w_{\mathrm{Tman}} = \pm 7.5\ \mathrm{K}$$

$$\frac{\partial \mathrm{T}_{\mathrm{purge}}}{\partial h} = \frac{e^{-\left(\frac{PL}{\dot{m}C_p}h\right)} (T_{surf} - T_{man})(PL)}{C_p \dot{m}} = 8.39 \qquad w_h = \pm .4292$$

$$\frac{\partial \mathrm{T}_{\mathrm{purge}}}{\partial \dot{m}} = \frac{-e^{-\left(\frac{PL}{\dot{m}C_p}h\right)} (T_{surf} - T_{man})(hPL)}{C_p \dot{m}^2} = -14681 \qquad w_{\dot{m}} = \pm .000117\ \mathrm{kg/s}$$

$$w_{\mathrm{Tpurge}} = \left[(.305)^2 (7.5)^2 + (.701)^2 (7.5)^2 + (8.39)^2 (.4292)^2 + (14681)^2 (.000117)^2 \right]^{1/2}$$

$$= \pm 7.0\ \mathrm{K}\ or\ 1.2\%$$

Moving on to the radiation and free convection of the heat exchanger, because β for an ideal gas is only a function of temperature (1/temperature):

$$\beta = \frac{1}{T_{avg}} = .0033 \text{ K}^{-1}$$

$$\frac{\partial \beta}{\partial T_{avg}} = -\frac{1}{T_{avg}^{\ 2}} = .000011$$

$$w_{Tavg} = \pm 7.5 \text{ K}$$

$$w_{Ra} = \left[(.000011)^2 (1)^2 \right]^{1/2}$$

$$= \pm .00008 \text{ K}^{-1} \textit{ or } 2.5\%$$

$$Ra = \frac{g\beta (T_s - T_\infty) D^3}{\upsilon \alpha} = 1.37 \ E^7$$

$$\frac{\partial Ra}{\partial D} = \frac{3g\beta (T_s - T_\infty) D^2}{\upsilon \alpha} = \frac{3(9.8)(0.003)(324-292)0.168^2}{(1.59 \ E^{-5})(2.25 \ E^{-5})} = 2.23 \ E^8$$

$$w_D = \pm 1.27 \ E^{-5} \ m$$

$$\frac{\partial Ra}{\partial T_s} = \frac{g\beta D^3}{\upsilon \alpha} = 389669 \qquad w_{Ts} = \pm 7.5 \text{ K}$$

$$\frac{\partial Ra}{\partial T_\infty} = \frac{-g\beta D^3}{\upsilon \alpha} = -389669 \qquad w_{T\infty} = \pm 1 \text{ K}$$

$$\frac{\partial Ra}{\partial \beta} = \frac{g (T_s - T_\infty) D^3}{\upsilon \alpha} = 4.16 \ E^9 \qquad w_\beta = \pm .00001 \text{ K}^{-1}$$

$$w_{Ra} = \left[\begin{array}{l} (2.23 \ E^8)^2 (1.27 \ E^{-5})^2 + (389669)^2 (7.5)^2 + \\ (-389669)^2 (-1)^2 + (4.29 \ E^9)^2 (.00001) \end{array} \right]^{1/2}$$

$$= \pm 2.94 \ E^6 \textit{or } 21.5\%$$

Next the uncertainty of the Nusselt number for a long horizontal cylinder is addressed:

$$Nu = \left\{ 0.60 + \frac{0.387 Ra_D^{1/6}}{\left[1 + \left(0.559/\mathrm{Pr}\right)^{9/16}\right]^{8/27}} \right\}^2 = 31$$

$$\frac{\partial Nu}{\partial Ra} = \frac{0.061}{\left(\left(1/\mathrm{Pr}\right)^{9/16} + 1.387\right)^{16/27} Ra_D^{2/3}} = 6.01\ E^{-7}$$

$$w_{Ra} = \pm 2.94\ E^{6}$$

$$w_{Nu} = \left[\left(6.01\ E^{-7}\right)^2 \left(2.94\ E^{6}\right)^2\right]^{1/2} = \pm 1.766\ or\ 5.7\%$$

Once the uncertainty of the Nusselt number is known, the convection coefficient uncertainty may be determined:

$$h = \frac{Nu\ k}{\mathrm{D}} = 4.84\ \frac{\mathrm{W}}{m\mathrm{K}}$$

$$\frac{\partial h}{\partial Nu} = \frac{k}{\mathrm{D}} = \frac{0.0263}{0.168} = 0.157 \qquad w_{Nu} = \pm 1.76$$

$$\frac{\partial h}{\partial \mathrm{D}} = -\frac{Nu\ k}{\mathrm{D}^2} = 28.9 \qquad w_D = \pm 1.27E^{-5}\ m$$

$$w_h = \left[\left(0.157\right)^2 \left(1.76\right)^2 + \left(28.9\right)^2 \left(1.27E^{-5}\right)^2\right]^{1/2}$$

$$= \pm .27\ \frac{\mathrm{W}}{m\ \mathrm{K}} or\ 5.7\%$$

The uncertainty for the radiation and free convection are also evaluated:

$$q_{conv} = h\pi DL\left(T_s - T_\infty\right) = 503\ W$$

$$\frac{\partial q_{conv}}{\partial h} = \pi DL\left(T_s - T_\infty\right) = 104 \qquad w_h = \pm.27\ \frac{W}{m\ K}$$

$$\frac{\partial q_{conv}}{\partial D} = h\pi L\left(T_s - T_\infty\right) = 2989 \qquad w_D = \pm 1.27\ E-5\ m$$

$$\frac{\partial q_{conv}}{\partial L} = h\pi D\left(T_s - T_\infty\right) = 83 \qquad w_L = \pm.00079\ m$$

$$\frac{\partial q_{conv}}{\partial T_s} = h\pi DL = 16 \qquad w_{Ts} = \pm 7.5\ K$$

$$\frac{\partial q_{conv}}{\partial T_\infty} = -h\pi DL = -16 \qquad w_{Ts} = \pm 7.5\ K$$

$$w_{qconv} = \left[\begin{matrix}(104)^2(.27)^2 + (2989)^2\left(1.27\ E^{-5}\right)^2 + (83)^2(.00079)^2 \\ +(16)^2(7.5)^2 + (-16)^2(-7.5)^2\end{matrix}\right]^{1/2}$$

$$= \pm 172\ W\ or\ 34\%$$

The emissivity of 6061-T6 aluminum was found to be .02 with an uncertainty of ±.01 (Technology 2011).

$$q_{rad} = \varepsilon\pi DL\sigma\left(T_s^4 - T_\infty^4\right) = (.02)\pi(.168)(6.096)\left(5.67\ E^{-8}\right)\left(324^4 - 292^4\right)$$

$$= 13.7\ W$$

$$\frac{\partial q_{rad}}{\partial \varepsilon} = \pi DL\sigma\left(T_s^4 - T_\infty^4\right) = 684 \qquad w_\varepsilon = \pm.01$$

$$\frac{\partial q_{rad}}{\partial D} = \varepsilon\pi L\sigma\left(T_s^4 - T_\infty^4\right) = 81.4 \qquad w_D = \pm 1.27\ E^{-5}\ m$$

$$\frac{\partial q_{rad}}{\partial L} = \varepsilon\pi D\sigma\left(T_s^4 - T_\infty^4\right) = 2.24 \qquad w_L = \pm.00079\ m$$

$$\frac{\partial q_{rad}}{\partial T_s} = 4\varepsilon\pi DL\sigma T_s^3 = 160 \qquad w_{Ts} = \pm 7.5\ K$$

$$\frac{\partial q_{rad}}{\partial T_\infty} = -4\varepsilon\pi DL\sigma T_\infty^3 = -106 \qquad w_{Ts} = \pm 7.5\ K$$

$$w_{qrad} = \left[\begin{matrix}(684)^2(.01)^2 + (81.4)^2\left(1.27\ E^{-5}\right)^2 + (2.24)^2(.00079)^2 \\ +(160)^2(7.5)^2 + (-106)^2(7.5)^2\end{matrix}\right]^{1/2}$$

$$= \pm 1443\ W\ or\ 10500\%$$

Note that the uncertainty values calculated for heat transfer only reflect the error from this analysis. Actual uncertainty values for heat transfer may vary over a much wider range.

The formula for average specific heat at the outlet of the heat exchanger must be analyzed before the uncertainty for the enthalpy at the same location can be determined:

$$C_{\underset{out}{p,main+purge}} = \frac{\dot{m}_{purge}}{\dot{m}_{total}} C_{p_{purge}} + \frac{\dot{m}_{main}}{\dot{m}_{total}} C_{p_{main}} = 1139 \frac{J}{kg\ K}$$

$$\frac{\partial C_p}{\partial \dot{m}_{main}} = \frac{1}{\dot{m}_{total}} C_{p_{main}} = \frac{1}{.027}(1320) = 48889 \qquad w_{\dot{m}_{main}} = \pm .000117\ kg/s$$

$$\frac{\partial C_p}{\partial \dot{m}_{purge}} = \frac{1}{\dot{m}_{total}} C_{p_{purge}} = \frac{1}{.027}(1007) = 37296 \qquad w_{\dot{m}_{purge}} = \pm .000117\ kg/s$$

$$\frac{\partial C_p}{\partial \dot{m}_{main}} = -\frac{\dot{m}_{purge}}{\dot{m}_{total}^{\ 2}} C_{p_{purge}} - \frac{\dot{m}_{main}}{\dot{m}_{total}^{\ 2}} C_{p_{main}} = -\frac{.016}{.027}(1007) - \frac{.011}{.027}(1320) = -42019$$

$$w_{\dot{m}_{total}} = \pm .000234\ kg/s$$

$$w_{\underset{out}{C_{p,main+purge}}} = \left[(48889)^2 (.000117)^2 + (37296)^2 (.000117)^2 + (-42019)^2 (.000234)^2 \right]^{1/2}$$

$$= \pm 12.2\ \frac{\mathrm{J}}{\mathrm{kg\ K}}\ or\ 1.07\%$$

Next, the enthalpy of the exhaust gases is determined:

$$h_{\underset{out}{gas}} = \left(\dot{m}_{total} C_{\underset{out}{p,avg}} \mathrm{T}_{\underset{\text{out}}{\text{avg}}} \right) = (.027)(1139)(314) = 9656\ W$$

$$\frac{\partial h}{\partial \dot{m}} = C_{\underset{out}{p,avg}} \mathrm{T}_{\underset{\text{out}}{\text{avg}}} = 357646 \qquad w_{\dot{m}} = \pm .000234\ kg/s$$

$$\frac{\partial h}{\partial C_p} = \dot{m}_{total} \mathrm{T}_{\underset{\text{out}}{\text{avg}}} = 8.48 \qquad w_{Cp} = \pm 12.2\ \frac{J}{kg\ K}$$

$$\frac{\partial h}{\partial \mathrm{T}} = \dot{m}_{total} C_{\underset{out}{p,avg}} = 30.8 \qquad w_{\mathrm{T}} = \pm 2.2\ K$$

$$w_h = \left[(357646)^2 (.000234)^2 + (8.48)^2 (12.2)^2 + (30.8)^2 (2.2)^2 \right]^{1/2}$$

$$= \pm 150\ W\ or\ 1.5\%$$

Knowing the uncertainty of the mass flow for both the main and purge manifolds, it is possible to calculate the uncertainty of the enthalpy of the gas as it exits the heat exchanger. Again J-type thermocouples are used for the temperature measurement of the gas at the exit of the heat exchanger.

Now that all of the input arguments' uncertainties have been solved for, the inlet temperature uncertainty can be considered:

$$\left(\mathrm{T}\right)_{\underset{\text{in}}{\text{main+purge}}} = \frac{\left[h_{\underset{out}{gas}} + \mathrm{q}_{\text{rad}} + \mathrm{q}_{fc} + \mathrm{q}_{\text{water}} \right]_{out}}{\left(\dot{m} C_p\right)_{\underset{in}{main+purge}}} = 1335\ K$$

$$\frac{\partial \left(\mathrm{T}\right)_{\underset{\text{in}}{\text{main+purge}}}}{\partial h_{\underset{out}{gas}}} = \frac{1}{\left(\dot{m} C_p\right)_{\underset{in}{main+purge}}} = \frac{1}{(.027)(1142)} = .032 \qquad w_{h_{\underset{out}{gas}}} = \pm 150\ W$$

$$\frac{\partial \left(\mathrm{T}\right)_{\underset{\text{in}}{\text{main+purge}}}}{\partial \mathrm{q}_{rad}} = \frac{1}{\left(\dot{m} C_p\right)_{\underset{in}{main+purge}}} = .032 \qquad w_{\mathrm{q}_{rad}} = \pm 1443\ W$$

$$\frac{\partial \left(\mathrm{T}\right)_{\underset{\text{in}}{\text{main+purge}}}}{\partial \mathrm{q}_{fc}} = \frac{1}{\left(\dot{m} C_p\right)_{\underset{in}{main+purge}}} = .032 \qquad w_{\mathrm{q}_{fc}} = \pm 172\ W$$

$$\frac{\partial \left(T\right)_{\underset{in}{main+purge}}}{\partial q_{water}} = \frac{1}{\left(\dot{m} C_p\right)_{\underset{in}{main+purge}}} = .032 \qquad w_{q_{water}} = \pm 25.5\ W$$

$$\frac{\partial \left(T\right)_{\underset{in}{main+purge}}}{\partial \dot{m}} = -\frac{\left[h_{\underset{out}{gas}} + q_{rad} + q_{fc} + q_{water} \right]_{out}}{\left(\dot{m}^2 C_p\right)_{\underset{in}{main+purge}}} = -49965 \qquad w_{\dot{m}} = \pm .000117\ kg/s$$

$$\frac{\partial \left(T\right)_{\underset{in}{main+purge}}}{\partial C_p} = -\frac{\left[h_{\underset{out}{gas}} + q_{rad} + q_{fc} + q_{water} \right]_{out}}{\left(\dot{m} C_p^{\,2}\right)_{\underset{in}{main+purge}}} = 1.02 \qquad w_{C_p} = \pm 12.2\ \frac{J}{kg\ K}$$

$$w_h = \left[\begin{array}{l} (0.032)^2 (150)^2 + (0.032)^2 (1443)^2 + (0.032)^2 (172)^2 \\ + (0.032)^2 (25.5)^2 + (-49965)^2 (.000234)^2 + (1.02)^2 (12.2)^2 \end{array} \right]^{1/2}$$

$$= \pm 49\ K \text{ or } 3.7\%$$

The uncertainty of the compressor work will be addressed next:

$$w_{comp} = \dot{m} C_{p_{avg}} \left(\mathrm{T}_1 \left(\frac{\mathrm{P}_2}{\mathrm{P}_1} \right) \text{-} \mathrm{T}_1 \right) = (.067)(1019) \left((304) \left(\frac{122803}{99739} \right) - (304) \right) = 1270 \ W$$

$$\frac{\partial w_t}{\partial C_{p_{avg}}} = \dot{m} \left(\mathrm{T}_1 \left(\frac{\mathrm{P}_2}{\mathrm{P}_1} \right) \text{-} \mathrm{T}_1 \right) = 4.7 \qquad w_{C_{Pavg}} = \pm 12.2 \ \frac{J}{kg \ K}$$

$$\frac{\partial w_t}{\partial \mathrm{T}_1} = \dot{m} C_{p_{avg}} \left(\left(\frac{\mathrm{P}_2}{\mathrm{P}_1} \right) \text{-} 1 \right) = 15 \qquad w_{T_1} = \pm 1 \ K$$

$$\frac{\partial w_t}{\partial \dot{m}} = C_{p_{avg}} \left(T_1 \left(\frac{\mathrm{P}_2}{\mathrm{P}_1} \right) \text{-} \mathrm{T}_1 \right) = 71663 \qquad w_{\dot{m}} = \pm .000117 \ kg/s$$

$$w_{w_t} = \left[(4.7)^2 (12.2)^2 + (15)^2 (1)^2 + (71663)^2 (.000117)^2 \right]^{1/2}$$

$$= 60 \ W \ or \ 4.7\%$$

Next the uncertainty of the enthalpy at the turbine exit will be addressed:

$$h_4 = \dot{m} C_{p_4} \mathrm{T}_4 = (.055)(1242)(1036) = 70550 \ W$$

$$\frac{\partial h_4}{\partial C_{p_4}} = \dot{m} \mathrm{T}_4 = 57 \qquad w_{C_{Pavg}} = \pm 12.2 \ \frac{J}{kg \ K}$$

$$\frac{\partial w_t}{\partial \mathrm{T}_4} = \dot{m} C_{p_4} = 68 \qquad w_{\mathrm{T}_1} = \pm 1 \ K$$

$$\frac{\partial w_t}{\partial \dot{m}} = C_{p_4} \mathrm{T}_4 = 1.28 \ E^6 \qquad w_{\dot{m}} = \pm .000117 \ kg/s$$

$$w_{w_t} = \left[(57)^2 (12.2)^2 + (68)^2 (1)^2 + \left(1.28 \ E^6\right)^2 (.000117)^2 \right]^{1/2}$$

$$= 714 \ W \ or \ 1.0\%$$

The uncertainty of the corrected turbine inlet temperature was calculated as:

$$\mathrm{T}_{3_{\mathrm{corr}}} = \frac{\dot{W}_{comp} + h_{rad} + h_4}{\dot{m} C_{p_4}} = \frac{1270 + 1090 + 63990}{(.055)(1233)} = 978 \ K$$

$$\frac{\partial \mathrm{T}_{3_{\mathrm{corr}}}}{\partial C_{p_4}} = \frac{-\left(\dot{W}_{comp} + h_{rad} + h_4\right)}{\dot{m} C_{p_4}^{\ 2}} = .79 \qquad w_{C_{P_{avg}}} = \pm 12.2 \ \frac{J}{kg \ K}$$

$$\frac{\partial \mathrm{T}_{3_{\mathrm{corr}}}}{\partial \dot{W}_{comp}} = \frac{1}{\dot{m} C_{p_4}} = .015 \qquad w_{\dot{W}_{comp}} = \pm 60 \ W$$

$$\frac{\partial \mathrm{T}_{3_{\mathrm{corr}}}}{\partial h_{rad}} = \frac{1}{\dot{m} C_{p_4}} = .015 \qquad w_{h_{rad}} = \pm 192 \ W$$

$$\frac{\partial \mathrm{T}_{3_{\mathrm{corr}}}}{\partial h_4} = \frac{1}{\dot{m} C_{p_4}} = .015 \qquad w_{h_4} = \pm 714 \ W$$

$$\frac{\partial \mathrm{T}_{3_{\mathrm{corr}}}}{\partial \dot{m}} = \frac{-\left(\dot{W}_{comp} + h_{rad} + h_4\right)}{\dot{m}^2 C_{p_4}} = -17789 \qquad w_{\dot{m}} = \pm .000117 \ kg/s$$

$$w_{\mathrm{T}_{3_{\mathrm{corr}}}} = \left[\begin{matrix} (.79)^2 (12.2)^2 + (.015)^2 (60)^2 + (.015)^2 (714)^2 \\ + (.015)^2 (192)^2 + (-17789)^2 (.000117)^2 \end{matrix}\right]^{1/2}$$

$$= 15 \ K \ or \ 1.5\%$$

Knowing the uncertainty of the inlet temperature, the work performed by the turbine may be assessed:

$$\dot{W}_t = \dot{m}\left(C_{p_3} \mathrm{T}_{3_{\mathrm{corr}}} - C_{p_4} \mathrm{T}_4\right) = (.055)\left[(1302)(977) - (1294)(950)\right] = 2351 \ W$$

$$\frac{\partial \dot{W}_t}{\partial \mathrm{T}_{3_{\mathrm{corr}}}} = \dot{m} C_{p_3} = 72 \qquad w_{T_{3\ corr}} = \pm 15 \ K$$

$$\frac{\partial \dot{W}_t}{\partial \mathrm{T}_4} = -\dot{m} C_{p_4} = 71 \qquad w_{T_4} = \pm 4.7 \ K$$

$$\frac{\partial \dot{W}_t}{\partial \dot{m}} = \left(C_{p_3} \mathrm{T}_{3_{\mathrm{corr}}} - C_{p_4} \mathrm{T}_4\right) = 42754 \qquad w_{\mathrm{T}_4} = \pm .000117 \ K$$

$$w_{\dot{W}_t} = \left[(72)^2 (19)^2 + (71)^2 (4.7)^2 + (42754)^2 (.000117)^2\right]^{1/2}$$

$$= 1130 \ W \ or \ 48\%$$

The isentropic relation used in Eq. 4.2.13 is probed next:

$$T_{4s} = T_3 \left(\Pr\right)^{\frac{\gamma-1}{\gamma}} = \left(977\right)\left(2.4\right)^{\frac{.4}{1.4}} = 1254\ K$$

$$\frac{\partial T_{4s}}{\partial T_3} = \left(\frac{P_4}{P_3}\right)^{\frac{\gamma-1}{\gamma}} = 1.28 \qquad w_{T_3} = \pm 15\ K$$

$$w_{T_{4s}} = \left[\left(1.28\right)^2\left(15\right)^2\right]^{1/2} = 19.2\ K\ or\ 1.5\%$$

Finally the efficiency for the turbine:

$$\eta_t = \frac{\dot{W}_{turb}}{\dot{m}\left(C_{p3}T_{3_{corr}} - C_{p4s}T_{4s}\right)} = \frac{2356}{.055\left[\left(1302\right)\left(977\right) - \left(1292\right)\left(951\right)\right]} = .987$$

$$\frac{\partial \eta_t}{\partial \dot{W}_{turb}} = \frac{1}{\left(C_{p3}T_3 - C_{p4s}T_{4s}\right)} = .000023 \qquad w_{\dot{W}_{turb}} = \pm 1130\ W$$

$$\frac{\partial \eta_t}{\partial T_{3_{corr}}} = -\frac{C_{p_3}T_{3_{corr}}}{\dot{m}\left(C_{p3}T_3 - C_{p4s}T_{4s}\right)^2} = .012 \qquad w_{T_{3_{corr}}} = \pm 15\ K$$

$$\frac{\partial \eta_t}{\partial T_{4s}} = \frac{T_{4_s}\dot{W}_{turb}}{\dot{m}\left(C_{p4s}T_{4s} - C_{p3}T_{3_{corr}}\right)^2} = .021 \qquad w_{T_{4s}} = \pm 19\ K$$

$$\frac{\partial \eta_t}{\partial \dot{m}} = -\frac{-\dot{W}_{turb}}{\dot{m}^2\left(C_{p3}T_3 - C_{p4s}T_{4s}\right)} = 18 \qquad w_{C_{p3}} = \pm .0001177\ kg/s$$

$$w_{\eta_t} = \left[\left(.000023\right)^2\left(1130\right)^2 + \left(.012\right)^2\left(15\right)^2 + \left(.022\right)^2\left(19\right)^2 + \left(18\right)^2\left(.000117\right)^2\right]^{1/2}$$

$$= .44\ or\ 44\%$$

Bibliography

Dyer, Kaemming. "The Thermodynamic Basis of Pulsed Detonation Engine Thrust Production." *38th AIAA/ASME/SAE/ASEE Joint Propulsion Conference and Exhibit.* 7-10 Jul., Indianapolis, IN: AIAA, 2002. 8.

Engineering, FlowMaxx. *Sonic Nozzles.* January 31, 2011. http://www.flowmaxx.com/sonic.htm (accessed January 31, 2011).

Glaser, Aaron J., Nicholas Caldwell, and Ephraim Gutmark. "Performance Measurements of a Pulse Detonation Combustor Array Integrated with an Axial Flow Turbine." *44th AIAA Aerospace Sciences Meeting and Exhibit.* Reno: AIAA, 2006. 12.

Glaser, Aaron, Nicholas Caldwell, and Ephraim Gutmark. "Performance of an Axial Flow Turbine Driven by Multiple Pulse Detonation Combustors." *45th AIAA Aerospace Sciences Meeting and Exhibit.* 8-11 January. Reno, NV: AIAA, 2007. 10.

Glassman, I. *Combustion, 3rd Ed.* San Diego, CA: Academic Press, 1996.

Hoke, John, Royce Bradley, Jeff Stutrud, and Fred Schauer. "Integration of a Pulsed Detonation Engine with an Ejector Pump and with a Turbo-Charger as Methods to Self-Aspirate." *40th AIAA Aerospace Sciences Meeting and Exhibit.* Reno, NV, 14-17 January 2002: American Institute of Aeronautics and Astronautics, 2002. 8.

Holman, J. P. *Experimental Methods for Engineers.* New York: McGraw-Hill, Inc., 1989.

Honeywell. *Precision Gage/Absolute.* January 3, 2005. http://www.alliedelec.com/Images/Products/Datasheets/BM/HONEYWELL_SENSOTEC/386-0002.PDF (accessed January 31, 2011).

Incropera, DeWitt, Berman, and Lavine. *Fundamentals of Heat and Mass Transfer, 6th Ed.* Hoboken, NJ: John Wiley & Sons, Inc., 2007.

Omega. *ANSI and IEC Color Codes for Thermocouples, Wire and Connectors.* June 29, 2010. http://www.omega.com/toc_asp/frameset.html?book=Temperature&file=TC_GEN_SPECS_REF (accessed January 31, 2011).

—. *Omega.com.* January 31, 2010. http://www.omega.com/ppt/pptsc.asp?ref=FTB4700_FTB4800 (accessed January 31, 2010).

Paxson, Daniel E., Andrew G. Naples, John L. Hoke, and Fred Schauer. "Numerical Analysis of a Pulse Detonation Cross Flow Heat Load Experiment." *ASM 2011*. Orlando: AIAA, 2011. 12.

Rasheed, Adam, Anthony Furman, and Anthony J. Dean. "Experimental Investigations of an Axial Turbine Driven by a Multi-tube Pulsed Detonation Combustor System." *41st AIAA/ASME/SAE/ASEE Joint Propulsion Conference & Exhibit.* 10-13 July. Tucson, AZ: AIAA, 2005. 13.

Rouser, Kurt P., Paul I. King, Frederick I. Schauer, Rolf Sondergaard, Larry P. Goss, and John L. Hoke. "Time-Accurate Flow Field and Rotor Speed Measurements of a Pulsed Detonation Driven Turbine." *Aerospace Sciences Meeting.* Orlando: AIAA, 2011. 16.

Rouser, Kurt P., Paul I. King, Frederick R. Schauer, Rolf Sondergaard, and John L. Hoke. "Parametric Study of Unsteady Turbine Performance Driven by a Pulse Detonation Combustor." *Joint Propulsion Conference and Exhibit.* Nashville, TN 25-28 July 2010: American Institute of Aeronautics and Astronautics, 2010. 12.

—. "Unsteady Performance of a Turbine Driven by a Pulse Detonation Engine." *48th AIAA Aerospace Sciences Meeting.* 4-7 Jan., Orlando Florida: AIAA, 2010. 16.

Schauer, F. R., C. L. Miser, K. C. Tucker, R. P. Bradley, and J. L. Hoke. "Detonation Initiation of Hydrocarbon-Air Mixtures in a Pulse Detonation Engine." *43rd AIAA Aerospace Sciences Meeting and Exhibit.* Jan. 10-13. Reno, NV: AIAA, 2005. 10.

Schauer, Fred, Royce Bradley, and John Hoke. "Interaction of a Pulsed Detonation Engine with a Turbine." *41st Aerospace Sciences Meeting and Exhibit.* 6-9 Jan. Reno, NV: AIAA, 2003. 6.

Schultz, Shephard. *Validation of Detailed Reaction Mechanisms for Detonation Simulation.* Pasadena: California Institute of Technology, 2000.

Sonntag, Van Wylen. *Introduction to Thermodynamics Classical and Statistical.* NY: John Wiley and Sons, Inc., 1991.

Suresh, Ambady, Douglas C. Hofer, and Venkat E. Tangirala. "Turbine Efficiency for Unsteady, Periodic Flows." *47th AIAA Aerospace Sciences Meeting.* 5-8 January. Orlando, FL: AIAA, 2009. 13.

Technology, Epner. *Emissivity Qualification Comparison.* February 4, 2011. http://public.epner.net/default/index.cfm/processes-and-products/laser-gold/tech-data/emissivity/emissivity-qualification-comparison/ (accessed February 4, 2011).

Turns, Stephen R. *An Introduction to Combustion: Concepts and Applications Second Edition.* Boston: McGraw Hill, Inc., 2006.

REPORT DOCUMENTATION PAGE

Form Approved
OMB No. 074-0188

1. REPORT DATE *(DD-MM-YYYY)*	**2. REPORT TYPE**	**3. DATES COVERED** *(From – To)*
24-Mar-2011	Master's Thesis	March 2010 – March 2011

4. TITLE AND SUBTITLE

Heat Transfer Experiments on a Pulse Detonation Driven Combustor

5a. CONTRACT NUMBER

5b. GRANT NUMBER

5c. PROGRAM ELEMENT NUMBER

6. AUTHOR(S)

Longo, Nicholas C., Captain, USAF

5d. PROJECT NUMBER

5e. TASK NUMBER

5f. WORK UNIT NUMBER

7. PERFORMING ORGANIZATION NAMES(S) AND ADDRESS(S)

Air Force Institute of Technology
Graduate School of Engineering and Management (AFIT/ENY)
2950 Hobson Way, Building 640
WPAFB OH 45433-8865

8. PERFORMING ORGANIZATION REPORT NUMBER

AFIT/GAE/ENY/11-M18

9. SPONSORING/MONITORING AGENCY NAME(S) AND ADDRESS(ES)

Air Force Research Laboratory/Combustion Branch
7th Street, Bldg 71a D-bay
Wright-Patterson AFB OH 45433
Voice: 937-255-7266, DSN 785-7266
frederick.schauer@wpafb.af.mil

10. SPONSOR/MONITOR'S ACRONYM(S)

AFRL/RZTC

11. SPONSOR/MONITOR'S REPORT NUMBER(S)

12. DISTRIBUTION/AVAILABILITY STATEMENT

APPROVED FOR PUBLIC RELEASE; DISTRIBUTION UNLIMITED

13. SUPPLEMENTARY NOTES

14. ABSTRACT

Heat transfer experiments were conducted using a heat exchanger behind a pulse detonation combustor and a Garrett automotive turbocharger at the Air Force Research Lab (AFRL). The equivalence ratio and purge fraction were held at 1.0 and 0.9, respectively, while the frequency of operation was varied from 10 to 12 Hz in 1 Hz movements, and the fill fraction was varied from 0.5 to 0.8 in 0.1 increments. Temperature measurements were calculated using an energy balance allowing for the calculation of heat exchanger inlet enthalpy. The heat exchanger inlet enthalpy was estimated to be the exit enthalpy of the turbocharger it was coupled to. The representative turbine inlet enthalpy was calculated using compressor work and radiation from the turbine. Turbine inlet and exit temperatures were also measured directly using J-type and K-type thermocouples and compared to calculated values using the heat exchanger approach. Turbine work was calculated from the change in enthalpy from the inlet to the exit. This data was compared with average values of time accurate data from published work. Compressor and turbine work was also presented and compared with recently attained values. Efficiency was presented for varying pressure ratios. The efficiency measurements were compared with time accurate efficiency measurements from on-going work.

15. SUBJECT TERMS

Pulse Detonation Engine, combustor, turbine, heat transfer, enthalpy, work, efficiency

16. SECURITY CLASSIFICATION OF:			**17. LIMITATION OF ABSTRACT**	**18. NUMBER OF PAGES**	**19a. NAME OF RESPONSIBLE PERSON**
a. REPORT	**b. ABSTRACT**	**c. THIS PAGE**			King, Paul I.
U	**U**	**U**	**UU**	127	**19b. TELEPHONE NUMBER** *(Include area code)* (937) 255-3636 x4628 (paul.king@afit.edu)

Standard Form 298 (Rev. 8-98)
Prescribed by ANSI Std. Z39-18